Veljko Lipovac, BSc

Real-time Control of open Multibody Systems with discontinuous data

MASTER'S THESIS

to achieve the university degree of

Diplom-Ingenieur

Master's degree programme: Mathematics

submitted to

Graz University of Technology

Supervisor

Prof. Dr. O. Steinbach

Institute of Applied Mathematics

Graz, July 2020

Preface

This master's thesis was written in cooperation with the company *Magna Steyr* and the *Institute for Applied Mathematics* at *Graz University for Technology*, in order to provide insight on the simulation of actuated multibody systems with poor actuation signals and to provide means for modelling and simulating such systems within a framework used in the preproduction process at *Magna Steyr*. While the framework and use cases for the company are clear and specific, I was aiming for a more general thesis, such that the processed knowledge out of the literature and from several numerical tests is applicable to a wider range of tasks. Several steps are explained to a degree, where it should be a manageable objective to translate them for another setting. The rest is up to the reader.

I want to say thank you to the company and to the team I was working in, primarily to Markus Salchner and Severin Stadler who supported this topic as representatives of Magna Steyr, both financially and as colleagues.

Furthermore I want to express my deepest gratefulness to my parents, Radenko and Biljana, who guided me on the path of studying from the early beginning and who supported my choice to go to Graz. The bond to one's parents is an obvious one, but it is always worth mentioning and showing gratitude.

Finally I also want to record my appreciation to Professor Steinbach, who as my supervisor accompanied the development of this thesis and gave motivating and directive input when the work ground to a hold from time to time.

With all being said there is to say, I finally hope the reader will find this thesis interesting and furnishing for further engagement with the matter.

Veljko Lipovac
July 2020 Graz, Austria

Abstract

In this work a method to exert control with discontinuous signal functions onto bodies within multibody systems is deduced and the results of some numerical experiments are presented. The control cannot be applied in the form of servo constraints due to discontinuities and jumps in the signal, since this would deteriorate the regularity of the resulting DAE system. By generalizing the signal to be (at least) a L^2-function, the domain of standard multibody simulation techniques, namely the solution or approximative solution of systems of ODEs, is left and only papers dealing with specific multibody systems are published so far. This thesis summarizes the mathematical modelling of multibody systems, uses optimal control theory to reformulate the problem by splitting the servo constraints from the remaining joint constraints and applies a minimization approach to the servo constraint residual. Signal samples were collected out of the software framework of *Autodesk VRED* and a library for modelling and simulation applications was implemented. Numerical algorithms were constructed and tested, which allow control of multibody systems in real time. This renders interactive simulation and visualization of multibody systems possible and the methods were designed for the application inside modern virtual environments, such as *Augmented, Mixed* and *Virtual Reality*, in order to contribute to an efficient preproduction process in the field of virtual product development.

Kurzfassung

Im Rahmen der Arbeit wurde eine Methode hergeleitet, um Mehrkörpersysteme mit unstetigen Signalen zu steuern, und die Resultate numerischer Experimente werden vorgestellt. Die Steuerung kann nicht in Form von Servo-Zwangsbedingungen durchgeführt werden, da aufgrund der Unstetigkeitsstellen und Sprünge im Signal sich die Regularität der resultierenden Systeme von differential-algebraischen Gleichungen verschlechtern würde. Durch Verallgemeinerung und Annahme, dass das Signal (zumindest) eine L^2-Funktion ist, wird das Gebiet der Standardmethoden für Mehrkörpersimulationen, nämlich das Lösen und Approximieren von Lösungen von gewöhnlichen Differentialgleichungssystemen, verlassen und die Publikationen in diesem Bereich befassen sich soweit nur mit sehr spezifischen Mehrkörpersystemen. Diese Diplomarbeit fasst das mathematische Modellieren von Mehrkörpersystemen zusammen, verwendet die Theorie der optimalen Kontrolle um das Problem neu zu formulieren, indem Servo-Zwangsbedingungen von den restlichen Zwangsbedingungen getrennt werden, und wendet ein Minimierungsverfahren auf das Servo-Residuum an. Es wurden Signalproben aus der Software-Umgebung von *Autodesk VRED* entnommen und ein Programm zur Modellierung und Simulation entworfen. Es wurden diverse numerische Verfahren konstruiert und getestet, welche eine Steuerung von Mehrkörpersystem in Echtzeit ermöglichen. Das wiederum ermöglicht einen interaktiven Simulations- und Visualisierungsprozess und die Methoden wurden so gestaltet, dass eine Anwendung in modernen Gebieten wie *Augmented*, *Mixed* und *Virtual Reality* möglich ist und damit der Vorentwicklungsprozess im Bereich der virtuellen Produktentwicklung effizienter gestaltet werden kann.

Contents

Introduction

Motivation and goal

The importance of simulations of multibody systems has already been recognized in industry and science. Its applications are numerous and new use cases are found regularly. The automotive and robotics industry rely on this field and put great effort into real-time simulations for in-the-loop development and other preproduction processes. Within manufactures within the automotive industry are investing heavily in order to virtualize the whole preproduction and development process. Modern technologies as *Augmented, Mixed* and *Virtual Reality*, collectively abbreviated by *xR*, are being used to shorten the preproduction, especially the feedback and visual assessment process. Not only are matters of design in question, but also the assessment of kinematics. Examples for this are the movement of wheel suspensions, the bodywork reactions to angular moments, which are applied to driving wheels, and the visual evaluation of space between fenders, mudguards and wheels in all kinematically possible positions, to mention a few. While it is possible to calculate motion sequences in advance and to animate the movement, a far more interesting goal is to implement real-time simulations within a virtual environment itself and to provide a certain interactivity. This will shorten the whole preproduction process even more since one immediately gets output for applied input.
This interactivity can be realized by controllers and similar electronic gadgets for commercial xR software. The signals provided by these gadgets can be used for the actuation of multibody systems, which are modelled beforehand. While every commercial software provides means for extracting the position and orientation of a controller, the signal quality and usability pose an obstacle when aiming for physically accurate simulations. As an example, the *Autodesk VRED* software provides Virtual Reality functionalities, but the user can not influence how often the software registers the controller movement. One can access the currently cached position and orientation via various programming interfaces. This software itself relies on *Steam VR*, created by the VALVE Corporation, in order to create a 3D-scene. It is compatible with controllers and trackers sold by *VIVE* and all three in combination enable the user to create geometries, manipulate them and interact with them.

Figure 0.1.: A VR tracker and controller from *VIVE*.[1]

There is no need to discuss compatible versions and specify gadgets, build numbers, etc. Solely the fact of having so many factors involved and having to move within a

[1] 2011-2020 HTC Corporation, accessed 4th February 2020, `https://www.vive.com/de/accessory/`.

preset framework gives rise to many problems. On the one hand the microelectronic elements inside gadgets, on the other hand the implementations, which finally provide position and orientation in the form of vectors, are factors which deteriorate the signal quality.

In this thesis, in collaboration with the industrial partner, the goal is to implement a multibody simulator and visualize vehicle kinematics within a virtual environment. Interactivity is provided by allowing the user to move single bodies with a controller. This movement is more generally called *actuation* and has to be treated from a mechanical point of view. Since the concept of movement is not restricted to controllers, but can also be extended to gestures in other xR applications. The virtual environment used here is not a restriction. It is only used exemplarily.

Contact problems and elasticity are not taken into account. The thesis is restricted to rigid bodies and their movement under specified types of constraints. The objective is in its most simple form, the approximation of position and velocity of the rigid bodies. The solution to this objective has to fulfil several criteria:

- **Real-time simulation**
  In order to gain a feeling of immersion into the VR environment, the simulation has to keep up with the visual perception of the user. This gives rise to a need for fast numerical algorithms and approaches. The exerted actuation is also based on the real time scale. Hence if the simulation is slower, the dynamics do not display the correct response to the actuation.
- **Accuracy**
  While the gaming industry provides several so-called *physics engines* for the real-time visualization of movement, their physical correctness and accuracy can hardly be comprehended and an insight is not provided. This thesis however, aims for a solution applicable to real industrial needs and development and production processes. Physical correctness has to be guaranteed. Since there are already several excellent approaches which have proven to be sufficiently accurate, this criterion can be fulfilled, but has to be balanced with the first criterion. The well-known conflict between accuracy and efficiency gets a new, aggravated aspect: accuracy against real-time perception.
- **Generality**
  The solution must not be tied to a given framework. While the modelling and solving of unactuated multibody systems is general and can be found in any basic literature on mechanics, the actuation depends on the framework. Therefore several different types of actuation are taken into account and generalized to an extent, which does not depend on the framework and its implementation. While the simulation of multibody systems is already a well-researched field, the generality of the actuation signals is a rather new consideration.

Keeping these criteria in mind this thesis will introduce the topic from a rigorous, mathematical point of view. The connections to the introduced framework will be explained, such that the necessity of sometimes abstract conditions is underlined and can be related to the source.

Thesis overview

The simulation of multibody systems requires a wide range of preparations to be made. It starts with defining the model and the quantities of interest. The first chapters are based on standard literature on mechanics and ordinary differential equations (ODEs) and summarize the topic to an extent which is sufficient for this thesis [11, 15, 18, 20].

In Chapter 1 the rigid body model and the relevant kinematic and kinetic quantities representing and influencing the *kinematic state* of such a body are introduced. These quantities are the position, orientation, velocity and angular velocity. The modelling of joints and actuation is achieved by stating algebraic equations, which set the kinematic quantities into relation to each other [17, 20]. A deeper understanding for these constraints is provided by changing the perspective to a geometrical one [10, 19]. Finally a short glance at an object-oriented approach for a computer-aided modelling process is given [10].

In order to obtain a solvable system of ODEs, the Newton-Euler approach is used in Chapter 2 to formulate a set of equations of motion. The algebraic equations from Chapter 1 are used as constraints on the set of admissible solutions. The general approach to solve differential-algebraic equations (DAEs) is introduced [9] and applied to the multibody setting. Various forms of resulting DAEs are presented and related to constraints treated by this thesis. Additionally, means of stabilizing the system [3] are also presented and applied.

Chapter 3 deals with the numerical approximation of the solution, since the ODEs gained in multibody dynamics are only in simpler cases analytically solvable. At first the requirements of the application are stated. The class of linear-implicit solvers is then introduced and applied to the model elaborated in Chapter 2. At the end of this chapter a comparison of results for actuation signals of different nature is presented.

In Chapter 4 the problem of actuated multibody systems is considered from another perspective. Optimal Control Theory is applied and a single-stage approach is used in order to minimize the residual of actuation. Algorithms based on the preliminaries in Chapter 3 are derived in order to solve the newly obtained system of ODEs. Regularizations with two different norms are applied and tested.

Finally some conclusions are drawn, which summarize the results of this thesis. Appendix A contains exemplarily the modelling of three different joints. Appendix B presents the approximation of the solution of the one-dimensional *Yukawa* equation with a finite element approach. This equation appears in Chapter 4 when considering a certain type of regularization.

1. Modelling of multibody systems

In this chapter the mathematical modelling of rigid bodies, forces and different types of constraints is treated, where a closer look onto joints and actuation is taken. At the end, an idea is given of how to implement the modelling process with an object oriented approach. It serves mainly for introducing mathematical assumptions on which this work is based, the notation and to relate to underlying literature [11, 15, 16, 19, 20]. A rigorous derivation of all mentioned physical terms is found in the cited literature.

1.1. Kinematics and kinetics of rigid bodies

The object of interest is a set of rigid bodies $\{\mathcal{K}_i\}_{i=1}^{n_K}$, $n_K \in \mathbb{N}$, which move through space. Each element has two constant physical properties, *mass* and *inertia*, associated with it. In order to describe the space $\mathbb{R}^3$, the canonical base and xyz- notation are used.

Definition 1.1 (Rigid Body)
Let $\mathcal{K}_i = \mathcal{K}_i(t) \subset \mathbb{R}^3$ be a compact region at time t. Let further $m_i \in (0, \infty)$ denote the mass and $\Theta_i \in \mathbb{R}^{3\times 3}$ the inertia tensor, where Θ_i is positive definite. For every point $P \in \mathcal{K}_i$, let $\underline{x}_P(t)$ denote the position at time t.
If

$$\|\underline{x}_{P_1}(t) - \underline{x}_{P_2}(t)\|_2 = c(P_1, P_2) \ , \ \forall t \geq 0,$$

holds for each pair of points P_1, $P_2 \in \mathcal{K}_i$ with a constant $c(P_1, P_2) \geq 0$, then $\mathcal{K}_i$ is called a *rigid body.* $\|\cdot\|_2$ denotes the Euclidean norm for vectors in space.

The condition in Definition 1.1 implies that there is no relative movement between points of a rigid body. Hence it is sufficient to consider only a single point of $\mathcal{K}_i$ and the orientation of all remaining points with respect to this specific one. For simplicity reasons consider the centre of gravity and denote its position with a $\mathcal{C}^2$-regular function

$$\underline{x}_{\mathbf{t},i} : \mathbb{R}_{\geq 0} \to \mathbb{R}^3 \ .$$

There are several ways to describe the orientation of a body. The probably most illustrative one is the *Kardan* formalism [20, Sec. 3.6]. It is based on the assumption, that each rotation in space can be decomposed into "three, plain, elementary rotations around defined coordinate axes" [16, P. 38]:

1. rotation: around the x-axis with angle α_i.
2. rotation: around the *resulting* y-axis with angle β_i.
3. rotation: around the z-axis, resulting after the previous rotations, with angle γ_i.

α_i, β_i and γ_i are functions of time and $\mathcal{C}^2$-regularity is assumed again. The range of the angles is

$$\begin{aligned} \alpha_i(t),\ \gamma_i(t) \ &\in \ [\,0, 2\pi\,) \ , \\ \beta_i(t) \ &\in \ \left[-\tfrac{\pi}{2}, \tfrac{\pi}{2}\right] \ . \end{aligned}$$

The *vector of angles* $\underline{w}_i(t)$ is defined by concatenating these quantities into a function

$$\begin{array}{rcl} \underline{w}_i : \mathbb{R}_{\geq 0} & \to & \mathbb{R}^3 \ , \\ t & \to & \begin{bmatrix} \alpha_i(t) \\ \beta_i(t) \\ \gamma_i(t) \end{bmatrix} \ . \end{array}$$

Assuming that the position of each point $P \in \mathcal{K}_i$ is given relative to the centre of gravity by a (constant) vector $\hat{\underline{x}}_P$, its movement through space is hence given by

$$\underline{x}_P(t) = \underline{x}_{\mathbf{t},i}(t) + R_i(t)\hat{\underline{x}}_P \ , \tag{1.1}$$

where $R_i(t)$ is a rotation matrix. It holds

$$\det\left(R_i(t)\right) = 1 \ , \ R_i^\top(t)R_i(t) = I \ , \ \forall t \ ,$$

where I is the identity. Instructions on how to construct the rotation matrix out of angles can be found in [16, Chap 2.5] and [20, Chap. 3.6]. Note that R_i depends on time only by the dependency on the angles. For readability reasons only t is denoted.

The velocity of a point is obtained by total differentiation of the position with respect to time. This operation is denoted by a dot above the differentiated quantity. For a point P it is

$$\dot{\underline{x}}_P(t) = \dot{\underline{x}}_{\mathbf{t},i}(t) + \dot{R}_i(t)\hat{\underline{x}}_P \ .$$

The term

$$\underline{v}_{\mathbf{t},i}(t) := \dot{\underline{x}}_{\mathbf{t},i}(t) \tag{1.2}$$

is called *translational velocity* and represents the velocity of the centre of gravity. The derivative of the matrix introduces a new quantity. Since it equals

$$\begin{array}{rcl} R_i^\top R_i & = & I \ , \\ \dot{R}_i^\top R_i + R_i^\top \dot{R}_i & = & 0 \ , \\ \dot{R}_i^\top R_i = -R_i^\top \dot{R}_i & = & -\left(\dot{R}_i^\top R_i\right)^\top \ , \end{array}$$

it holds that $\dot{R}_i^\top R_i$ is a skew-symmetric matrix. Hence there exists a vector $\underline{\omega}_i$ such that

$$\dot{R}_i R_i^\top \ \underline{x} = \underline{\omega}_i \times \underline{x} \ , \ \forall \underline{x} \in \mathbb{R}^3 \ .$$

It further holds that

$$\dot{R}_i = -R_i \dot{R}_i^\top R_i = \dot{R}_i R_i^\top R_i \ .$$

Hence the velocity of a point P can be written as

$$\underline{v}_p(t) := \dot{\underline{x}}_P(t) = \underline{v}_{\mathbf{t},i}(t) + \underline{\omega}_i(t) \times \left[R_i(t)\hat{\underline{x}}_P\right] \ . \tag{1.3}$$

The vector $\underline{\omega}_i$ is called *angular velocity* of the rigid body with respect to the centre of gravity, since the orientation is also given with respect to this point. The following relation holds for the angular velocity and the Kardan angles:

Lemma 1.2 (Kinematic Kardan Equation, [16, Eqn. 2.87])
For a rigid body $\mathcal{K}_i$, its angular velocity $\underline{\omega}_i$ and its vector of angles $\underline{w}_i$ there exists a singular linear mapping $K_i(\underline{w}_i)$ such that

$$\dot{\underline{w}}_i(t) = K_i(\underline{w}_i) \ \underline{\omega}_i(t) \ . \tag{1.4}$$

It is singular for all configurations with $\beta_i = \pm\frac{\pi}{2}$.

This singularity does not pose a huge obstacle in most cases. Even when simulating multibody systems with large finite rotations, singular configurations result rarely due to numerical inaccuracy. However it cannot be excluded and in order to avoid it one has to introduce a different formalism, e.g., unit quaternion based rotation. Unit quaternions introduce more parameters (an axis and an angle instead of three angles), but they have no singularities. As a matter of fact, there exists an orthonormal mapping between the angular velocity and the derivative of a quaternion with respect to time (see [20, Sec. 3.7]).

In summary the *kinematic state* of a rigid body $\mathcal{K}_i$ is given by the four vectorial quantities

$$\underline{x}_{\mathbf{t},i}(t),\ \underline{w}_i(t),\ \underline{v}_{\mathbf{t},i}(t) \text{ and } \underline{\omega}_i(t)\ .$$

A system of n_K rigid bodies has the total degree of freedom of $6n_K$. The unknowns are the position and the orientation, whereas the velocities are derivable quantities.

There are differential relations between these functions and other, vectorial functions

$$\underline{f}_i(t)\ ,\ \underline{m}_i(t)\ ,$$

which represent the vectors of acting forces and moments in a mechanical sense. They are in general assumed to be given by, e.g., gravity, spring and damper force laws and may depend on the kinematic states of multiple rigid bodies (springs and dampers connecting two bodies for example). All together they represent the *kinetic state* of a rigid body $\mathcal{K}_i$. The relation between the kinematic and kinetic state will be presented in Chapter 2 in the form of ordinary differential equations.

1.2. Constraints

In mechanical terms, constraints are imposed by introducing joints between rigid bodies. These joints constrain the movement of respective bodies relative to each other. In mathematical terms, constraints introduce algebraic equations containing the functions $\underline{x}_{\mathbf{t},i}(t)$ and $\underline{w}_i(t)$ for various $i \in \{1, \dots, n_K\}$. There are also constraints containing the derivatives $\underline{v}_{\mathbf{t},i}$ and $\underline{\omega}_i$ which are, and this is the crucial difference, not integrable to algebraic equations. Constraints of this type are called *non-holonomic* [15, Sec. 2.3]. This thesis covers only holonomic constraints or those, which have a purely algebraic form. Furthermore only constraints involving two rigid bodies $\mathcal{K}_{i_1}$ and $\mathcal{K}_{i_2}$ are considered. Involving more bodies does not change anything in the methods elaborated in this work and is for simplicity reasons omitted.

In sum, implicit algebraic equations

$$\Phi_j(\underline{x}_{\mathbf{t},i_1}, \underline{w}_{i_1}, \underline{x}_{\mathbf{t},i_2}, \underline{w}_{i_2}, t) = 0\ , \tag{1.5}$$

are considered, where

$$\Phi_j\ : \mathbb{R}^3 \times \mathbb{R}^3 \times \mathbb{R}^3 \times \mathbb{R}^3 \times \mathbb{R} \to \mathbb{R}^{n_{B_j}}$$

is at least twice continuously differentiable with respect to time. The dependency on time of various functions is not noted, when said functions are used as arguments for mappings. In total $n_B = \sum n_{B_j}$ algebraic equations are considered, where

$0 < n_B < 6n_K$. If there are as many independent constraints as total degrees of freedom, the multibody system is kinetically defined and the simulation is reduced to solving a system of algebraic equations.

Depending on whether Equation (1.5) contains the time t explicitly or not, the constraints are called rheonomic or scleronomic, respectively. A pendulum of varying length is a standard example for rheonomic constraints (see [15, Examp. 2.8]).

This thesis covers two classes of constraints.

Joints, i.e. equations of type

$$\Phi_j(\underline{x}_{\mathbf{t},i_1}, \underline{w}_{i_1}, \underline{x}_{\mathbf{t},i_2}, \underline{w}_{i_2}) = 0 \ , \tag{1.6}$$

which are holonomic and scleronomic, and *actuations*, i.e. holonomic and rheonomic constraints

$$\Psi_k(\underline{x}_{\mathbf{t},i_k}, \underline{w}_{i_k}, t) = 0 \ , \tag{1.7}$$

where

$$\Psi_k : \mathbb{R}^3 \times \mathbb{R}^3 \times \mathbb{R} \to \mathbb{R}^{n_{A_k}} \ .$$

General regularity assumptions are not imposed on the Ψ_k. Only the amount of equations is assumed to be limited. The number of joint equations n_B and the number of actuation equations $n_A = \sum n_{A_k}$ must not exceed the total degrees of freedom, which means

$$0 < n_B + n_A < 6n_K \ .$$

Actuation can have various forms. Exemplarily a simple form is given by

$$\Psi_k(\underline{x}_{\mathbf{t},i_k}, \underline{w}_{i_k}, t) = \underline{x}_{\mathbf{t},i_k} - \underline{h}_k(t) = 0 \ , \tag{1.8}$$

where $\underline{h}_k(t)$ is a given function in time. This actuation constrains the movement of the centre of gravity to a curve in space given by $\underline{h}_k(t)$ and imposes 3 algebraic equations onto the system. This special type of constraint is often referred to as *servo constraint* [1, 4].

The modelling of joints and the underlying mathematical equations are explained in Appendix A.

1.3. A geometric interpretation of multibody systems

In this section the previously introduced degrees of freedom are understood as functions, more precisely parametrized curves in space. Without any constraints, all possible configurations cover the whole space, i.e. for each body $\mathcal{K}_i$ the vector $\underline{x}_{\mathbf{t},i}(t)$ can point to any point in space.

Consider two bodies, $\mathcal{K}_{i_1}$ and $\mathcal{K}_{i_2}$, and constraints of the form

$$\underline{\Phi}(\underline{x}_{\mathbf{t},i_1}, \underline{x}_{\mathbf{t},i_2}) = 0 \ . \tag{1.9}$$

Assuming Equations (1.9) can be explicitly solved for $\underline{x}_{\mathbf{t},i_2}$, a representation of the position

$$\underline{x}_{\mathbf{t},i_2}(t, \underline{\widetilde{y}}) = \underline{\widetilde{\Phi}}(\underline{x}_{\mathbf{t},i_1}, \underline{\widetilde{y}}) \tag{1.10}$$

for the second body can be obtained. A necessary condition for this conversion is the independency of the Equations (1.9). $\underline{\widetilde{y}}$ is a set of parameters necessary to describe the relative movement between the two bodies. The number of necessary parameters equals the number of degrees of freedom of the joint, which is represented by $\underline{\Phi}$. In general the parameters also depend on time. This dependency is sometimes omitted for readability reasons.

The possible configurations for the second body are now restrained to the ones fulfilling Equation (1.10). The union of all possible configurations form a manifold within $\mathbb{R}^3$ and for an arbitrary but fixed time t a parametrization is given by Equation (1.10). Its dimension equals the number of parameters necessary to form the explicit representation. A rigorous form of this statement will be given in Subsection 1.3.1.

Differentiation with respect to time shows an affine linear relation between the translational velocities of the bodies

$$\underline{v}_{\mathbf{t},i_2}(t, \underline{\widetilde{y}}) = \frac{\partial}{\partial \underline{x}_{\mathbf{t},i_1}} \underline{\widetilde{\Phi}}(\underline{x}_{\mathbf{t},i_1}, \underline{\widetilde{y}}) \ \underline{v}_{\mathbf{t},i_1}(t) + \frac{\partial}{\partial \underline{\widetilde{y}}} \underline{\widetilde{\Phi}}(\underline{x}_{\mathbf{t},i_1}, \underline{\widetilde{y}}) \ \dot{\underline{\widetilde{y}}} \ . \tag{1.11}$$

More general this is a relation between the tangential spaces of the parameter and image space, called *push-forward*, a term originating from the field of differential geometry.

Example 1.3 (Spatial mass point pendulum)
Consider two mass points and their respective position in space, $\underline{x}_1(t)$ and $\underline{x}_2(t)$. A pendulum of constant length 1 is formulated by the single constraint

$$\underline{\Phi}(\underline{x}_1, \underline{x}_2) = \|\underline{x}_1 - \underline{x}_2\|_2^2 - 1 = 0 \ .$$

Any spatial rotation relative to the other mass point is allowed and a constant distance of 1 is kept. On the other hand an explicit representation of $\underline{x}_2(t)$ can be achieved by introducing spherical coordinates $(r = 1, \theta, \phi)$ and stating

$$\underline{x}_2(t) = \underline{x}_1(t) + \begin{bmatrix} \sin(\theta)\cos(\phi) \\ \sin(\theta)\sin(\phi) \\ \cos(\theta) \end{bmatrix} = \widetilde{\Phi}(\underline{x}_1, \underline{\widetilde{y}}) \ ,$$

where $\underline{\widetilde{y}} = [\theta, \phi]^\top$. For an arbitrary but fixed time t, $\underline{x}_1$ is given and the pair (θ, ϕ) parametrizes a spherical surface around the first mass point, which is a 2-dimensional manifold in $\mathbb{R}^3$.

The problem of finding two curves in space can be transformed into a problem of finding a parametrized curve in $\mathbb{R}^6$. By denoting

$$\underline{x}(t) = \begin{bmatrix} \underline{x}_{\mathbf{t},i_1}(t) \\ \underline{x}_{\mathbf{t},i_2}(t) \end{bmatrix}$$

and considering constraints

$$\underline{\Phi}(\underline{x}) = \underline{0} \ ,$$

one can obtain an explicit representation

$$\underline{x}(t) = \begin{bmatrix} \underline{x}_{\mathbf{t},i_1}(t) \\ \underline{x}_{\mathbf{t},i_2}(t) \end{bmatrix} = \begin{bmatrix} \underline{x}_{\mathbf{t},i_1}(t) \\ \underline{\widetilde{\Phi}}(\underline{x}_{\mathbf{t},i_1}, \underline{\widetilde{y}}) \end{bmatrix} = \underline{\hat{\Phi}}(\underline{y}(t)) \ , \tag{1.12}$$

where the set of parameters is chosen as

$$\underline{y}(t) = \begin{bmatrix} \underline{x}_{\mathbf{t},i_1}(t) \\ \underline{\widetilde{y}} \end{bmatrix} .$$

The choice of this set is not unique, but it is minimal in a sense that it is the least amount of parameters necessary to parametrize the generalized curve in $\mathbb{R}^6$. This set of coordinates is commonly referred to as *generalized coordinates* in mechanics' literature. The amount of parameters, especially contained in $\underline{\widetilde{y}}$, depends on the modelled joint and its degree of freedom. This concept can easily be extended to the orientational degrees of freedom, namely the angles $\underline{w}_i(t)$. Considering two rigid bodies with 6 degrees of freedom each, the explicit representation of a single body using the constraints can contain up to 6 additional parameters.

1.3.1. The state manifold

The idea to consider the problem of finding the kinematic curves of multiple rigid bodies as a problem in a higher dimensional space is stated by C. Lanczos in [11].

Consider n_K rigid bodies and their kinematic quantities $\underline{x}_{\mathbf{t},i}(t), \underline{w}_i(t)$, which are 6 unknown scalar functions in total. Define the *global position vector* $\underline{x}(t)$ by concatenating the kinematic quantities in a manner deemed to be convenient

$$\underline{x}(t) = \begin{bmatrix} \underline{x}_{\mathbf{t},1}(t) \\ \underline{w}_1(t) \\ \vdots \\ \underline{x}_{\mathbf{t},n_K}(t) \\ \underline{w}_{n_K}(t) \end{bmatrix} . \tag{1.13}$$

For reasons of simplicity the translational and orientational quantities of a rigid body are kept next to each other in the global form. Methods on how to number and order different rigid bodies are given in Section 1.4. By the same means define the *global velocity vector* $\underline{v}(t)$ and the *global force vector* $\underline{f}(t)$ as

$$\underline{v}(t) = \begin{bmatrix} \underline{v}_{\mathbf{t},1}(t) \\ \underline{\omega}_1(t) \\ \vdots \\ \underline{v}_{\mathbf{t},n_K}(t) \\ \underline{\omega}_{n_K}(t) \end{bmatrix} , \ \underline{f}(t) = \begin{bmatrix} \underline{f}_1(t) \\ \underline{m}_1(t) \\ \vdots \\ \underline{f}_{n_K}(t) \\ \underline{m}_{n_K}(t) \end{bmatrix} . \tag{1.14}$$

All possible configurations of the multibody system are now elements of the higher dimensional "configuration space" $\mathbb{R}^{6n_K}$ [11, Chap. 1], where a single point represents all translational and orientational quantities.

Again by a manner one deems to be convenient, all holonomic constraints in implicit form can be assembled to

$$\underline{\Phi}(\underline{x}, t) = \underline{0} \ , \tag{1.15}$$

where

$$\underline{\Phi} \ : \mathbb{R}^{6n_K} \times \mathbb{R} \to \mathbb{R}^{n_B} \ , \ 0 < n_B < 6n_K \ ,$$

is a function of sufficient smoothness. Extend the assumption of independent equations to the new, global constraint vector. The following theorem will be used for describing the set of admissible states and can be found in any standard literature on higher analysis and differential geometry. It can be proved to be a consequence of the *implicit function theorem.*

Theorem 1.4 (Regular Value Theorem, [19, Part II, Prop. 2.1.25])
Let $n, m \in \mathbb{N}$ be such that $n \geq m$ and let $F : \mathbb{R}^n \to \mathbb{R}^m$ be a differentiable function. Let $\underline{a} \in \mathbb{R}^m$ be a regular value *of F, i.e.*

$$\mathrm{rank}(DF(\underline{x})) = m, \ \ \forall \underline{x} \in F^{-1}(\underline{a}) \ ,$$

where DF denotes the Jacobian of F.

Then the equation

$$F(\underline{x}) = \underline{a}$$

defines a $(n - m)$-dimensional sub-manifold $M \subset \mathbb{R}^n$ and it holds

$$T_{\underline{x}}M = \ker(DF(\underline{x})) \ ,$$

where $T_{\underline{x}}M$ denotes the tangential space of M at $\underline{x}$.

By the assumption of independent equations, it holds that the Jacobian of $\underline{\Phi}$ from Equation (1.15) has full rank, i.e.

$$\mathrm{rank}(DF(\underline{\Phi})) = n_B \ .$$

Therefore, the algebraic constraints define a $6n_K - n_B$ - dimensional manifold within the configuration space $\mathbb{R}^{6n_K}$.

Definition 1.5 (State manifold)
Let $\{\mathcal{K}_i\}_{i=1}^{n_K}$ be a multibody system with n_B independent algebraic constraints. The sub-manifold of the configuration space implicitly defined by $\underline{\Phi}(\underline{x}, t) = 0$ is called *state manifold* and denoted by $\mathcal{S}$. It represents a set of all kinematically admissible states of the system.

The constraints reduce the set of all kinematically possible configurations to $\mathcal{S}$ and the unknown global position vector $\underline{x}(t)$ is a parametrized curve lying on this manifold. The quantity

$$n_f f := 6n_K - n_B$$

is commonly referred to as *absolute degree of freedom* and is important when investigating algorithms for simulating multibody systems.

Since the dimension of $\mathcal{S}$ is n_f, a set of generalized coordinates $\underline{y}$ for an explicit parametrization of $\underline{x}(t)$ as a subset of the $\mathcal{S}$, i.e.

$$\underline{x} = \underline{x}(\underline{y}, t) \ , \tag{1.16}$$

is an element of $\mathbb{R}^{n_f}$, $\underline{y} = [y_1, \ldots, y_f]^\top$. Equation (1.12) showed how $\underline{y}$ can be chosen for two bodies.

One can compute the basis of the tangential space by differentiating the parametrization with respect to time

$$\underline{v}(\underline{y}, t) = J(\underline{y}, t)\ \dot{\underline{y}} + \bar{\underline{v}}(\underline{y}, t) \ , \tag{1.17}$$

where

$$\begin{aligned} J(\underline{y}, t) &:= \frac{\partial}{\partial \underline{y}} \underline{x}(\underline{y}, t) \ , \\ \bar{\underline{v}}(\underline{y}, t) &:= \frac{\partial}{\partial t} \underline{x}(\underline{y}, t) \ . \end{aligned} \tag{1.18}$$

The time t in Equation (1.16) and the vector $\bar{\underline{v}}$ appear only when considering rheonomic constraints. The term $\dot{\underline{y}}$ is commonly referred to as *generalized velocities* (see [20, Sec. 5.2]). The tangential space of the state manifold at a certain point is spanned by the columns of $J(\underline{y}, t)$ and, if applicable, by $\bar{\underline{v}}(\underline{y}, t)$,

$$T_{\underline{x}(t)} := \operatorname{span}\left\{ \frac{\partial}{\partial y_1} \underline{x}(\underline{y}, t), \ldots, \frac{\partial}{\partial y_f} \underline{x}(\underline{y}, t), \bar{\underline{v}}(\underline{y}, t) \right\} \ .$$

By Equation (1.17) the global velocity vector $\underline{v}(t)$ $(= \underline{v}(\underline{y}, t))$ is an element of $T_{\underline{x}(t)}$.

1.3.2. Restraining forces and the cotangent space

In Newtonian mechanics the change of the impulse depends on the sum of all acting forces, i.e. the change of the velocity vector of a rigid body with constant mass is equal to the forces acting on it. Equation (1.17) shows that the velocity is an element of the tangential space. Therefore one can assume the existence of forces and moments, which cancel out every change of the velocity in all directions perpendicular to the tangential space. For an arbitrary but fixed time t, this narrows down the space in which these *restraining* forces and moments exist to a manifold implicitly defined as the orthogonal complement of $T_{\underline{x}(t)}$. This observation is also a consequence of the mechanical *principle of D'Alembert* [15, Sec. 4.2], which states that the work done by the restraining forces must be zero for infinitesimal variations of the position in tangential direction.

These variations are associable with velocities and since work is the scalar product of force and changes in position, the zero value of the scalar product corresponds with the geometrical interpretation stated here. Figure 1.1 visualizes this relation exemplarily for a pendulum.

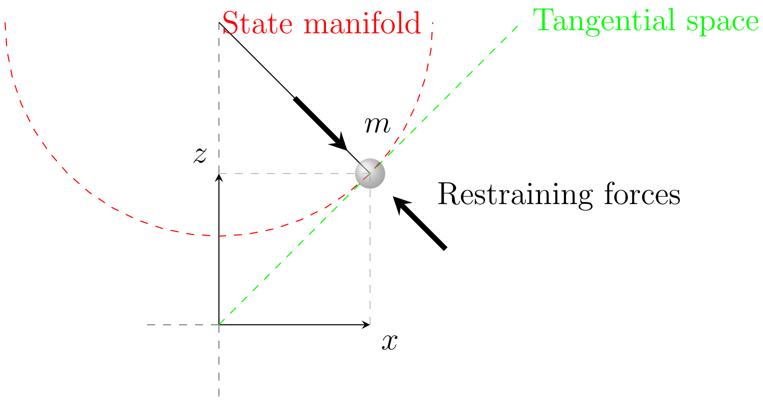

Figure 1.1.: Tangential space and restraining forces of a pendulum at a fixed time.

Let from now on

$$\underline{f}^r(t)$$

denote the restraining forces and moments. The kinetic state is split into two parts [15, Subsec. 3.1.2]

$$\underline{f}(t) = \underline{f}^e(t) + \underline{f}^r(t) \ , \tag{1.19}$$

where the super-script e denotes *external* forces and moments applied by objects like springs and dampers.

In order to obtain a representation of the orthogonal complement, consider the implicit constraints

$$\underline{\Phi}(\underline{x}, t) = \underline{0}, \tag{1.20}$$

and differentiate them with respect to time

$$\frac{\mathrm{d}}{\mathrm{dt}}\underline{\Phi}(t) = \frac{\partial}{\partial \underline{x}}\underline{\Phi}(\underline{x}, t)\ \underline{v}(t) + \frac{\partial}{\partial t}\underline{\Phi}(\underline{x}, t) := G(\underline{x}, t)\ \underline{v}(t) + \underline{\bar{\varphi}}(t) = \underline{0}\ . \tag{1.21}$$

$G = G(\underline{x}(t), t)$ is called *implicit constraint matrix* and the vector $\underline{\bar{\varphi}}$ occurs only when considering rheonomic constraints. Substituting the velocity term by its explicit representation from Equation (1.17) yields

$$G(\underline{x}, t)\ J(\underline{y}, t)\ \underline{\dot{y}} + G(\underline{x}, t)\ \underline{\bar{v}}(\underline{y}, t) + \underline{\bar{\varphi}}(t) = 0\ . \tag{1.22}$$

Equation (1.22) holds for arbitrary, independent values of the generalized coordinates and velocities, $\underline{y}$ and $\underline{\dot{y}}$. Hence each of the terms

$$\begin{aligned} G(\underline{x}, t)\ J(\underline{y}, t) &= \underline{0}\ , \\ G(\underline{x}, t)\ \underline{\bar{v}}(\underline{y}, t) + \underline{\bar{\varphi}}(t) &= \underline{0} \end{aligned} \tag{1.23}$$

must be zero. The following can be observed now:
For each time t, the rows of G are orthogonal to any vector spanned by the columns of J. Since the columns span the tangential space, the rows of G span therefore a subspace of the orthogonal complement. Since furthermore the dimension of the tangential space is $6n_K - n_B$ and G has n_B independent rows, the rows of G span the whole orthogonal complement within the configuration space $\mathbb{R}^{6n_K}$.

By this observation, the global vector of restraining forces $\underline{f}^r(t)$ has an explicit representation

$$\underline{f}^r(t) = G^\top(\underline{x}, t)\ \underline{\rho}\ , \tag{1.24}$$

where $\underline{\rho} \in \mathbb{R}^{n_B}$ is a Lagrangian multiplier (see Chapter 2). $\underline{\rho}$ also depends on time in general.

Remark 1.1
The dual space

$$T^*_{\underline{x}(t)} := \left(T_{\underline{x}(t)}\right)^*$$

is commonly referred to as *cotangent space*.

If the row vectors of $G(\underline{x}, t)$ are seen as Riesz-representatives of elements of $T^*_{\underline{x}(t)}$ at time t , one obtains a n_B-dimensional subspace of $T^*_{\underline{x}(t)}$, which is orthogonal to the n_f-dimensional subspace $T_{\underline{x}(t)}$. Since $n_f = 6n_K - n_B$ they are also the orthogonal complement to each other. Due to this, the rows of $G(\underline{x}, t)$ span the whole *annihilator* of $T_{\underline{x}(t)}$, who is defined as

$$T^\circ_{\underline{x}(t)} = \{l^* \in T^*_{\underline{x}(t)} \mid l^*(\underline{v}) = 0\ \forall \underline{v} \in T_{\underline{x}(t)}\}\ .$$

Restraining forces are therefore functionals, which are zero for all variations of the position in tangential direction, which do not leave the state manifold.

1.4. Computer-based modelling

In order to model and create multibody systems (MBS) computer-aided, an object-oriented approach in *Python* was chosen. Abstract MBS elements were implemented and connected to a graphic user interface callable by *Autodesk VRED* in a second step. A. Kecskemethy [10] describes a very abstract way of how to model MBS by introducing the term *transfer element*. Such elements transfer velocities in one direction, as seen in Section 1.3, and restraining forces in the other. A single rigid body can be a transfer element, as well as a closed cluster of bodies. This notion is especially useful when considering large, strongly connected and closed systems, a class of MBS which is not treated in this thesis. Only (relatively) small and *open* MBS are taken into account. The term *open* will be introduced in Subsection 1.4.1 and is an expression of the connectedness of the system.

The general simulation and modelling process can be split into three layers, which are building on each other:

1. **Element layer**
   This layer contains all elemental objects which appear in a MBS. Rigid bodies, joints, springs, dampers and gravity are represented by respective classes, which have attributes and provide methods characteristic for the respective element. Four different types of elements were implemented in total.

   The first group are rigid bodies, which have all relevant physical quantities as attributes. A single instance has the non-settable attributes mass and inertia, which can be passed during instantiation. Further, it has settable attributes, such as position, angles, velocity, angular velocity, external forces and external moments, and it has dependent attributes, which are calculated from the settable attributes. The most important ones here are the rotation matrix and the Kardan matrix from Lemma 1.2.

   The second group is formed by joints. These elements have references to the rigid bodies they connect and provide the components of the implicit constraint vector $\underline{\Phi}(\underline{x}(t), t)$, the implicit constraint matrix $G(\underline{x}(t), t)$ and other quantities associated with the constraints based on the kinematic states. Instances of joints have a single, non-settable attribute, which is the degree of freedom they provide. In Appendix A, the revolute, prismatic and spherical joint are presented and their constraint quantities are derived.

   The third group consists of active elements, such as springs, dampers and the gravity. Instances of this type also have a reference to all bodies affected by them and manipulate their attributes representing the kinetic state. They exert forces and moments according to their force laws.

   The fourth and last group are the actuators, which again can be split into two types. Kinetic actuators, very much like active elements, exert forces or moments onto rigid bodies they are assigned to. Kinematic actuators on the other hand, can be treated like joints. They constrain the movement to a given path. Therefore they also have to provide components of the constraint matrix and vector. They further have attributes representing the current kinematic state of the actuator, such as velocity and acceleration.

2. **System layer**
   The multibody system itself can be implemented as a class, which provides means of managing base layer elements. Elements of all types can be added and removed. The MBS instance provides topological data based on all the elements it has a reference to (see Subsection 1.4.1).

3. **Solver layer**
   The solver layer is represented by either algorithms or classes, which take a MBS instance and a time stepping scheme and start updating the kinematic states of the rigid bodies, according to the numerical algorithm they represent.

Figure 1.2 summarizes the modelling process and provides on overview on mentioned layers and elements.

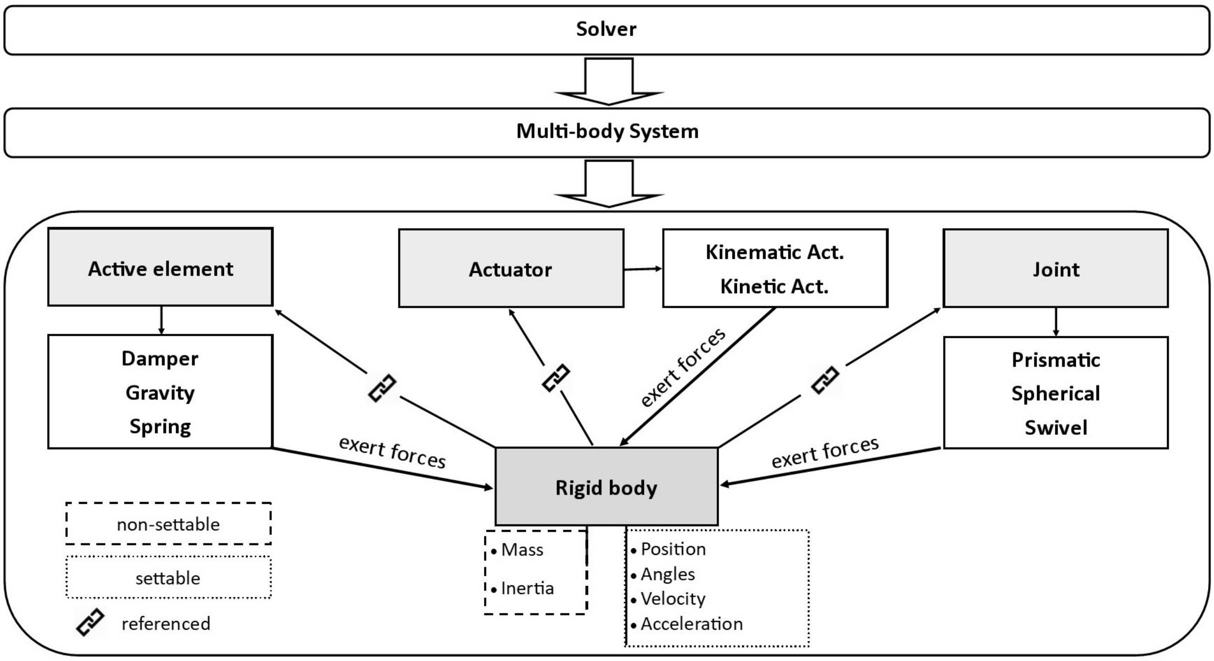

Figure 1.2.: Class structure chart for the modelling process.

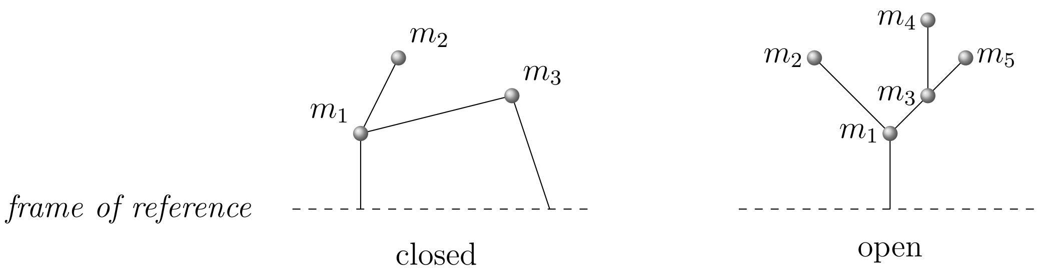

Figure 1.3.: The graph of a closed and an open multibody system.

1.4.1. The topological index

Many ways of categorizing multibody systems into different classes are found in the literature [10, 15, 16, 17, 20]. Two frequently occurring notions are those of *closed* and *open* systems. They are based on yet another notion, the *topology* of a multibody system.

Consider a system given by n_K rigid bodies and n_B algebraic equations imposed by joints. When visualizing this system as a graph, let the bodies represent the nodes and the joints the edges. Further, let there be a frame of reference, which represents the absolute coordinate system. The bodies are allowed to be connected to this frame via joints.

If the graph is a tree in a graph-theoretical sense, the multibody system is called *open*. If there is a loop, involving the frame of reference or not, the system is called *closed*.

In closed systems the problem appears that algebraic equations representing the joints are no longer independent, hence the matrix G does not have a full rank any more. Further treatment of the equations is necessary, which is quite technical and will not be covered in this thesis. W. Schiehlen [15] provides some insight into a project, which deals with constructing independent equations out of closed systems.

Loops, various trees, bodies and joints are all topological elements of a multibody system and account for the notion of topology in this field. By considering and treating the topology, more efficient simulation algorithms can be obtained in general. Consider exemplarily the open system given in Figure 1.3. The rigid bodies have indices assigned to them in a certain manner.

Definition 1.6 (Topological index)
Let $\{\mathcal{K}_i\}$ and $\{\Phi_j\}$ represent rigid bodies and joints modelled by the equations Φ_j. Consider the topological graph of this multibody system.

1. If there exists a node which is connected to the frame of reference via a joint, let it be the root node. If there is no such node, choose an arbitrary one.
2. Assign the index 1 to this node.
3. Assign the next natural numbers to all adjacent nodes in increasing order.
4. Continue this assignment in each subset of nodes with increasing distance to the root, until all leaves have an index assigned to them.
5. Assign the indices j to the sets of joint equations, such that they correspond to the assignment of i, i.e. the joint connecting the root to the frame of reference (if it exists) gets $j = 1$, the joint between root ($i = 1$) and the adjacent node with $i = 2$ gets $j = 2$, etc. ...

The indices created by this algorithm are called *topological indices*.

This approach can be found in [20, Sec. 7.1] in a more generalized form, where path and incidence matrices are defined in order to represent the connectedness of the multibody system.

The advantage gained through this indexing is evident, when applying it to the assembly of the global quantities given in Equations (1.13), (1.14) and (1.15).

If this index is used, one can obtain a lower block diagonal form of the matrix $G(\underline{x}(t), t)$. Since it equals

$$\frac{\partial}{\partial \underline{x}} \Phi_j = G_{j,1} \; \dot{\underline{x}}_1 + \cdots + G_{j,n_k} \; \dot{\underline{x}}_{n_k} \; , \; G_{j,i} = \frac{\partial}{\partial \underline{x}_i} \Phi_j \; , \tag{1.25}$$

all blocks $G_{i,j}$ become zero for $i > j$, due to the choice of the index. It will be shown in Chapter 3 that the numerical treatment involves the inversion of terms containing G or $G^\top$. More efficient procedures can be used when keeping the structure in mind. Also more efficient data structures become an option, such as sparse matrices.

Remark 1.2
The choice of the root node requires more dedication when implementing an automatized generation of equations. If there are bodies connected to the frame of reference, their choice as the root is beneficial, since the respective joint equations depend only on the kinematic state of a single body. If there are kinematic actuators present in the system, the actuated elements can also be set as roots. The choice between multiple nodes, which are actuated or connected to the frame, can be a matter of preference, but also of simplicity of the structure of G, if one takes into account how many degrees of freedom are being actuated or bound to the frame of reference.

2. Resulting systems of ordinary differential-algebraic equations

In the second chapter the equations of motion, a set of ordinary differential equations (ODEs) describing the movement of rigid bodies, are introduced. This set, or rather the motion, is augmented by an additional set of algebraic equations imposed by joints and actuators and shifts the task of finding a solution into the field of the so-called *differential-algebraic* equations, or DAEs. An approach to solving such systems is introduced and remarks on the solvability and uniqueness are given [5, 8, 9]. Finally the stabilization method according to Baumgarte [3] is introduced for those cases, where the algebraic part of the equations is violated.

2.1. The Newton-Euler approach

Newton's Second Law is a principle commonly used to obtain the equations of motion for a mass point. Applied to the centre of gravity of a rigid body $\mathcal{K}_i$ it states

$$m_i \dot{\underline{v}}_{\mathrm{t},i}(t) = \underline{f}_i(\underline{x}, \underline{v}, t) \ . \tag{2.1}$$

The force vector on the right-hand side depends in general on the kinematic state of the whole system.

This principle yields 3 scalar equations for each body, whereas 6 are necessary since each rigid body has 6 degrees of freedom. Euler's equations for rigid body rotations are introduced in order to obtain a solvable system of ordinary differential equations

$$\Theta_i \ \dot{\underline{\omega}}_i(t) = \underline{m}_i(\underline{x}, \underline{v}, t) - \underline{\omega}_i \times (\Theta_i \ \underline{\omega}_i) \ . \tag{2.2}$$

Θ_i denotes the inertia tensor of body $\mathcal{K}_i$. Like the force vector the vector of acting moments $\underline{m}_i$ also depends in general on the global kinematic state. The constant scalar m_i, which must not to be confused with the vector $\underline{m}_i$, represents the mass. The second term on the right-hand side is the vector of the Coriolis force. This simple form of the Equations (2.1) and (2.2) only holds when formulated with respect to the centre of gravity, which is assumed to be known. For formulations with respect to arbitrary points additional terms are necessary, see e.g. [15].

These six scalar equations describe the movement of a rigid body completely

$$\begin{bmatrix} m_i I & \\ & \Theta_i \end{bmatrix} \begin{bmatrix} \dot{\underline{v}}_{\mathrm{t},i}(t) \\ \dot{\underline{\omega}}_i(t) \end{bmatrix} = \begin{bmatrix} \underline{f}_i(\underline{x}, \underline{v}, t) \\ \underline{m}_i(\underline{x}, \underline{v}, t) \end{bmatrix} + \begin{bmatrix} \underline{0} \\ -\underline{\omega}_i \times (\Theta_i \ \underline{\omega}_i) \end{bmatrix} \ . \tag{2.3}$$

Using the indexing introduced in Subsection 1.4.1, a global, solvable system of ODEs can be obtained by

$$\begin{bmatrix} m_1 I & & & & \\ & \Theta_1 & & & \\ & & \ddots & & \\ & & & m_{n_K} I & \\ & & & & \Theta_{n_K} \end{bmatrix} \begin{bmatrix} \dot{\underline{v}}_{\mathrm{t},1}(t) \\ \dot{\underline{\omega}}_1(t) \\ \vdots \\ \dot{\underline{v}}_{\mathrm{t},n_K}(t) \\ \dot{\underline{\omega}}_{n_K}(t) \end{bmatrix} = \begin{bmatrix} \underline{f}_1(\underline{x},\underline{v},t) \\ \underline{m}_1(\underline{x},\underline{v},t) \\ \vdots \\ \underline{f}_{n_K}(\underline{x},\underline{v},t) \\ \underline{m}_{n_K}(\underline{x},\underline{v},t) \end{bmatrix} + \begin{bmatrix} \underline{0} \\ -\underline{\omega}_i \times (\Theta_i\ \underline{\omega}_i) \\ \vdots \\ \underline{0} \\ -\underline{\omega}_{n_K} \times \left(\Theta_{n_K}\ \underline{\omega}_{n_K}\right) \end{bmatrix} . \tag{2.4}$$

From left to right, above terms are denoted as

$$M\ \dot{\underline{v}}(t) = \underline{f}(\underline{x},\underline{v},t) + \underline{f}^c(\underline{v}) \ . \tag{2.5}$$

M is called *mass matrix* and represents a block diagonal matrix. It is assumed to be symmetric and positive definite, hence invertible. $\underline{f}^c$ is the global vector of Coriolis forces.

System (2.5) is a second order system with $6n_K$ unknown functions. Using the Dynamic Kardan Equation from Lemma 1.2 a larger, first order system can be obtained. It holds that

$$\dot{\underline{x}}(t) = \begin{bmatrix} I & & & & \\ & K_1(\underline{w}_1) & & & \\ & & \ddots & & \\ & & & I & \\ & & & & K_{n_K}(\underline{w}_{n_K}) \end{bmatrix} \underline{v}(t) =: K(\underline{x})\ \underline{v}(t) \ . \tag{2.6}$$

This yields finally the first order system of ODEs

$$\begin{aligned} \dot{\underline{x}}(t) &= K(\underline{x})\ \underline{v}(t) \ , \\ M\ \dot{\underline{v}}(t) &= \underline{f}(\underline{x},\underline{v},t) + \underline{f}^c(\underline{v}) \ , \end{aligned} \tag{2.7}$$

with $2\cdot 6n_K$ unknown functions. Note that contrary to Chapter 1, Equation (2.6) holds here and not $\dot{\underline{x}}(t) = \underline{v}(t)$. This is due to the additional rotational degrees of freedom. When applying the Kardan formalism and defining the global quantities as in (1.13) and (1.14), the position vector contains the Kardan angles and the velocity vector the angular velocity. Their differential relation is not obtained by total differentiation with respect to time, but by Lemma 1.2.

2.2. Overview on the treatment of differential-algebraic equations

As discussed in Sections 1.2 and 1.3, System (2.7) is augmented by a set of n_B algebraic equations

$$\underline{\Phi}(\underline{x}, t) = \underline{0}. \tag{2.8}$$

They reduce the set of admissible solutions of the system to a manifold implicitly defined by $\underline{\Phi}$. It is assumed, that $\underline{\Phi}$ is at least twice continuously differentiable with respect to time and that $\underline{0}$ is a regular value, i.e. the equations are independent and the Jacobian has full rank n_B.

Let $\underline{y}(t) = \left[\underline{x}^\top(t), \underline{v}^\top(t)\right]^\top$ denote the unknown vectorial functions as a mapping

$$\underline{y} \ : \ \mathbb{R} \to \mathbb{R}^{12n_K} \ .$$

After inverting the mass matrix M, System (2.7) is essentially a system of ODEs of the form

$$\underline{\dot{y}}(t) = \tilde{F}(\underline{y}, t) \ , \tag{2.9}$$

where $\tilde{F}$ is sufficiently often continuously differentiable with respect to time. With initial conditions $\underline{y}(0) = \underline{y}_0$ it represents a class of commonly known and well investigated initial value problems [18]. The dependency of the algebraic equation can be changed likewise to $\underline{y}$. Summarized the following system of differential-algebraic equations is considered

$$\begin{aligned} \underline{\dot{y}}(t) &= \tilde{F}(\underline{y}, t) \ , \\ \underline{\Phi}(\underline{y}, t) &= \underline{0} \ , \end{aligned} \tag{2.10}$$

with initial values $\underline{y}(0) = \underline{y}_0$.

In terms of solvability, firstly it is noted that the algebraic part of System (2.10) also restricts the initial values to an admissible manifold

$$\Upsilon = \{\underline{\tilde{y}} \in \mathbb{R}^{12n_K} \ \mid \ \underline{\Phi}(\underline{\tilde{y}}, 0) = 0\} \ . \tag{2.11}$$

If $\underline{y}_0 \notin \Upsilon$, a solution does not exist. When approximating the solution numerically, larger imprecision due to ,e.g., noise or accuracy constraints can lead to instability of the numerical algorithm. Therefore $\underline{y}_0 \in \Upsilon$ is always assumed, or at least inside a sufficiently small neighbourhood.

The general idea of solving differential-algebraic systems involves the manipulation of both equations in (2.10). This includes coordinate transformations, algebraic manipulation and most frequently differentiation. The common goal is to obtain a solvable system of ordinary differential equations. The term *index* appears throughout the literature on DAEs [5, 8, 9]. For various classes of DAE systems the index is defined differently. It is a quantity, which describes the complexity and the necessary effort to solve it in an abstract way. In general, a higher index implies a more difficult system. Also "from the point of view of the numerical solution, it is desirable for the DAE to have an index which is as small as possible" (Brenan, [5, P. 36]). This thesis utilizes the definition of Brenan in order to describe the influence of the algebraic part of the equations.

Definition 2.1 (Differential index, [5, Def. 2.2.2])
For a differential-algebraic system

$$\begin{aligned} \dot{\underline{y}}(t) &= \tilde{F}(\underline{y}, t) \ , \\ \underline{\Phi}(\underline{y}, t) &= \underline{0} \ , \end{aligned}$$

the *differential index* is the minimum number of times that the algebraic part $\underline{\Phi}$ has to be differentiated with respect to time, such that a system of ordinary differential equations

$$\dot{\underline{y}}(t) = F(\underline{y}, t)$$

can be obtained.

Remark 2.1
The obtainment of such a system involves aforementioned manipulation of the equations. In general, special care has to be taken of the regularity of $\underline{\Phi}$. Most solution strategies involve an insertion of differentiated terms of $\underline{\Phi}$ into the right-hand side of the differential equation. This can deteriorate the regularity of the new right-hand side, namely F. In the case of open multibody systems involving only joints, $\mathcal{C}^2$-regularity is given for $\underline{\Phi}$. If servo constraints are involved, the regularity depends on the quality of the signals. It is sufficient to have piecewise constant actuation signals to deteriorate the regularity of F such that it is not continuous any more (see Chapter 3). Solvability and stability of standard numerical algorithms can not be guaranteed in this case.

The approach to differentiate the algebraic constraints sufficiently often is called *index reduction method* [5, Subsec. 2.5.3]. In order to force the solution of (2.9) to fulfil the algebraic part (2.8), a Lagrangian multiplier

$$\underline{\rho} \ : \ \mathbb{R} \rightarrow \mathbb{R}^{n_B}$$

is introduced and Equation (2.9) is augmented such that

$$\dot{\underline{y}}(t) = \tilde{F}(\underline{y}, t) + G(\underline{y}, t)^\top \underline{\rho} \ , \tag{2.12}$$

where $G(\underline{y}, t)$ is as in (1.21). According to the assumptions for (2.8), G is a $n_B \times (12 n_K)$-matrix with full rank n_B.

Theorem 2.2
Let

$$\begin{aligned} \dot{\underline{y}}(t) &= \tilde{F}(\underline{y}, t) + G(\underline{y}, t)^\top \underline{\rho} \ , \\ \underline{\Phi}(\underline{y}, t) &= \underline{0} \ , \end{aligned} \tag{2.13}$$

be an augmented DAE system with a Lagrangian multiplier $\underline{\rho}$. Let $\tilde{F}$ be continuous and $\underline{\Phi}$ at least continuously differentiable. Let further G have full rank.

A tuple $\big(\underline{y}, \underline{\rho}\big)$ is a solution to the augmented System (2.13) if and only if $\underline{\rho} = \underline{0}$ and $\underline{y}$ is a solution to System (2.10).

Proof. Analogous to [5, Proof of Thm. 2.5.1]. □

The existence and the uniqueness of a solution is mostly guaranteed by the unique solvability of the unrestrained System (2.9). The *Theorem of Picard-Lindelöf* or

Theorem of Peano can be applied as for any standard problem in the theory of ordinary differential equation. The only difference is that two new assumptions have to be made in order to assure unique solvability:

1. The initial value $\underline{y}_0$ has to be an element of the admissible manifold of initial values Υ, as defined in (2.11) (or inside a sufficiently small neighbourhood).
2. The augmentation of the ODEs and the differentiation of the algebraic part must not deteriorate the regularity of the right-hand side (see Remark 2.1) to such a degree, that the assumptions of the two mentioned theorems are violated, i.e. F has to be continuous.

Example 2.3 (Index reduction for a constrained multibody system)
As seen in Chapter 1 and Section 2.1, the dynamics of a multibody system are modelled by

$$\begin{aligned} \dot{\underline{x}}(t) &= K(\underline{x})\ \underline{v}(t)\ , \\ M\ \dot{\underline{v}}(t) &= \underline{f}(\underline{x},\underline{v},t) + \underline{f}^c(\underline{v})\ , \end{aligned}$$

or

$$\dot{\underline{y}}(t) = \tilde{F}(\underline{y},t) = \begin{bmatrix} K(\underline{x})\ \underline{v}(t) \\ M^{-1}\left[\underline{f}(\underline{x},\underline{v},t) + \underline{f}^c(\underline{v})\right] \end{bmatrix}\ ,$$

where

$$\underline{y}(t) = \begin{bmatrix} \underline{x}(t) \\ \underline{v}(t) \end{bmatrix}\ .$$

In Subsection 1.3.2 it was shown that scleronomic constraints in the form of

$$\underline{\Phi}(\underline{x}) = \underline{0} \tag{2.14}$$

introduce restraining forces of type $\underline{f}^r(t) = G^\top(\underline{x})\ \underline{\rho}$, i.e.

$$\dot{\underline{y}}(t) = \begin{bmatrix} K(\underline{x})\ \underline{v}(t) \\ M^{-1}\left[\underline{f}(\underline{x},\underline{v},t) + \underline{f}^c(\underline{v}) + G^\top(\underline{x})\ \underline{\rho}\right] \end{bmatrix}\ .$$

The coupling by Lagrangian multipliers appears here naturally due to the mechanical nature.

A first differentiation of (2.14) leads to the DAE System

$$\begin{aligned} \begin{bmatrix} \dot{\underline{x}}(t) \\ \dot{\underline{v}}(t) \end{bmatrix} &= \begin{bmatrix} K(\underline{x})\ \underline{v}(t) \\ M^{-1}\left[\underline{f}(\underline{x},\underline{v},t) + \underline{f}^c(\underline{v}) + G^\top(\underline{x})\ \underline{\rho}\right] \end{bmatrix}\ , \\ G(\underline{x})\ \underline{v}(t) &= \underline{0}\ . \end{aligned} \tag{2.15}$$

This already yields a solvable system of equations, as shown in Subsection 3.1.1.
A second differentiation leads to constraints in the form of

$$G(\underline{x})\ \dot{\underline{v}}(t) + \dot{G}(\underline{x})\ \underline{v}(t) =: G(\underline{x})\ \dot{\underline{v}}(t) + \underline{\hat{\varphi}}(t)\ ,$$

where $\underline{\hat{\varphi}}(t)$ represents the second order terms. The resulting system is now

$$\begin{bmatrix} I & & \\ & M & -G^\top(\underline{x}) \\ & -G(\underline{x}) & \end{bmatrix} \begin{bmatrix} \dot{\underline{x}}(t) \\ \dot{\underline{v}}(t) \\ \underline{\rho} \end{bmatrix} = \begin{bmatrix} K(\underline{x})\ \underline{v}(t) \\ \underline{f}(\underline{x},\underline{v},t) + \underline{f}^c(\underline{v}) \\ \underline{\hat{\varphi}}(t) \end{bmatrix}\ . \tag{2.16}$$

Even though this system already poses a solvable system of ODEs, it can be simplified further. Taking the second row of (2.16) and inverting the mass matrix M yields

$$\dot{\underline{v}}(t) = M^{-1}\left[\underline{f}(\underline{x},\underline{v},t) + \underline{f}^c(\underline{v}) + G^\top(\underline{x})\ \underline{\rho}\right]\ .$$

Inserting this representation of $\dot{\underline{v}}(t)$ into the third row of (2.16) yields

$$\begin{aligned} -G(\underline{x})M^{-1}\left[\underline{f}(\underline{x},\underline{v},t) + \underline{f}^c(\underline{v}) + G^\top(\underline{x})\ \underline{\rho}\right] &= \hat{\underline{\varphi}}(t)\ , \\ -G(\underline{x})M^{-1}G^\top(\underline{x})\ \underline{\rho} - G(\underline{x})M^{-1}\left[\underline{f}(\underline{x},\underline{v},t) + \underline{f}^c(\underline{v})\right] &= \hat{\underline{\varphi}}(t)\ . \end{aligned}$$

Since G has full rank by assumption, the matrix $GM^{-1}G^\top$ is invertible. Therefore an explicit representation of the Lagrangian multiplier $\underline{\rho}$ can be obtained

$$\underline{\rho} = \underline{\rho}(\underline{x},\underline{v},t) = -\left[G(\underline{x})M^{-1}G^\top(\underline{x})\right]^{-1}\left[\hat{\underline{\varphi}}(t) + G(\underline{x})M^{-1}\left[\underline{f}(\underline{x},\underline{v},t) + \underline{f}^c(\underline{v})\right]\right]\ . \qquad (2.17)$$

Inserting this representation into the second row of the vector equation in (2.15) leads to the elimination of $\underline{\rho}$. By doing so, an explicit system for $\underline{y}(t)$ is obtained

$$\begin{bmatrix} \dot{\underline{x}}(t) \\ \dot{\underline{v}}(t) \end{bmatrix} = \dot{\underline{y}}(t) = F(\underline{y},t) = \begin{bmatrix} K(\underline{x})\ \underline{v}(t) \\ M^{-1}\left[\underline{f}(\underline{x},\underline{v},t) + \underline{f}^c(\underline{v}) + G^\top(\underline{x})\ \underline{\rho}(\underline{x},\underline{v},t)\right] \end{bmatrix}\ . \qquad (2.18)$$

According to Definition 2.1 a constrained multibody system is therefore a *index-2*-system of differential-algebraic equations. (2.15) is called an *index-1-reduced* system, (2.16) and (2.18) are called *index-2-reduced* systems. The regularity of the right-hand side in both cases is not deteriorated, if the constraints originate from joints according to Appendix A. These elemental joints are modelled by $\mathcal{C}^\infty$-functions and G and $\underline{\rho}$ are accordingly smooth.

Example 2.4 (Index reduction for an actuated multibody system)
Additionally to the scleronomic constraints as treated in Example 2.3, servo constraints of the form

$$\underline{\Psi}(\underline{x},t) = P\underline{x}(t) - \underline{h}(t) = \underline{0} \qquad (2.19)$$

are introduced. P is the canonical projection onto the n_A components of $\underline{x}(t)$, which are restrained to a curve defined by the signal function $\underline{h}(t)$. The procedure remains the same as in the previous example. The only difference now is, that additional restraining forces are introduced,

$$\underline{f}^d = P^\top\underline{\mu},$$

where $\underline{\mu} \in \mathbb{R}^{n_A}$ is another Lagrangian multiplier comparable to $\underline{\rho}$.

The index-1-reduced system is now

$$\begin{aligned} \begin{bmatrix} \dot{\underline{x}}(t) \\ \dot{\underline{v}}(t) \end{bmatrix} &= \begin{bmatrix} K(\underline{x})\ \underline{v}(t) \\ M^{-1}\left[\underline{f}(\underline{x},\underline{v},t) + \underline{f}^c(\underline{v}) + G^\top(\underline{x})\ \underline{\rho} + P^\top\underline{\mu}\right] \end{bmatrix}\ , \\ G(\underline{x})\ \underline{v}(t) &= \underline{0}\ , \\ P\underline{v}(t) &= \dot{\underline{h}}(t)\ . \end{aligned} \qquad (2.20)$$

At this point there are multiple ways of how to tackle the system further. One does not necessarily have to reduce the index of both types of constraints. If the regularity of $\underline{h}(t)$ is very low, even an index-1-reduction of the scleronomic constraints might not be possible, since $\dot{\underline{h}}(t)$ might not be defined for all t in the classical sense.

Consider a partially reduced system

$$\begin{aligned} \begin{bmatrix} \dot{\underline{x}}(t) \\ \dot{\underline{v}}(t) \end{bmatrix} &= \begin{bmatrix} K(\underline{x})\ \underline{v}(t) \\ M^{-1}\left[\underline{f}(\underline{x},\underline{v},t) + \underline{f}^c(\underline{v}) + G^\top(\underline{x})\ \underline{\rho} + P^\top \underline{\mu}\right] \end{bmatrix} , \\ -G(\underline{x})\ \dot{\underline{v}}(t) &= \hat{\underline{\varphi}}(t) \ , \\ P\underline{x}(t) - \underline{h}(t) &= \underline{0}, \end{aligned} \tag{2.21}$$

where the rheonomic constraints $\underline{\Psi}$ remain unchanged and the Newton-Euler equations are augmented by both types of restraining forces. As seen in Equation (2.17), the multiplier $\underline{\rho}$ has an explicit representation. This representation now includes a dependency on $\underline{\mu}$, i.e

$$\underline{\rho}(\underline{x},\underline{v},\underline{\mu},t) = -\left[G(\underline{x})M^{-1}G^\top(\underline{x})\right]^{-1}\left[\hat{\underline{\varphi}}(t) + G(\underline{x})M^{-1}\left[\underline{f}(\underline{x},\underline{v},t) + \underline{f}^c(\underline{v}) + P^\top \underline{\mu}\right]\right] \ .$$

The dependency is linear though and can be separated such that

$$\underline{\rho}(\underline{x},\underline{v},\underline{\mu},t) = \underline{\rho}(\underline{x},\underline{v},t) - \left[G(\underline{x})M^{-1}G^\top(\underline{x})\right]^{-1} G(\underline{x})M^{-1}P^\top \underline{\mu} \ , \tag{2.22}$$

where $\underline{\rho}(\underline{x},\underline{v},t)$ is as in Equation (2.17).
Define

$$\tilde{P}(\underline{x}) := \left[I - \left[G(\underline{x})M^{-1}G^\top(\underline{x})\right]^{-1} G(\underline{x})M^{-1}\right] P^\top \tag{2.23}$$

and eliminate the scleronomic constraints by an index-2-reduction and explicit representation of $\underline{\rho}$. The obtained system is of the form

$$\begin{aligned} \begin{bmatrix} \dot{\underline{x}}(t) \\ \dot{\underline{v}}(t) \end{bmatrix} &= \begin{bmatrix} K(\underline{x})\ \underline{v}(t) \\ M^{-1}\left[\underline{f}(\underline{x},\underline{v},t) + \underline{f}^c(\underline{v}) + G^\top(\underline{x})\ \underline{\rho}(\underline{x},\underline{v},t)\right] \end{bmatrix} + \begin{bmatrix} \underline{0} \\ M^{-1}\tilde{P}(\underline{x})\underline{\mu} \end{bmatrix} , \\ P\underline{x}(t) - \underline{h}(t) &= \underline{0}, \end{aligned}$$

or more compactly using $\underline{y}(t)$

$$\begin{aligned} \dot{\underline{y}}(t) &= F(\underline{y},t) + \hat{P}(\underline{y})\underline{\mu} \ , \\ P\underline{y}(t) - \underline{h}(t) &= \underline{0} \ , \end{aligned} \tag{2.24}$$

where P is extended by accordingly many zero columns.

System (2.24) is a partially reduced, index-2 system of differential-algebraic equations. Its treatment will be the topic of Chapters 3 and 4. In Chapter 3 the rheonomic constraints will be index-1-reduced the same way it was done for the scleronomic constraints and the effects of signal functions of various smoothness will be investigated. In Chapter 4 a different approach to approximating the solution of (2.24) will be introduced, without reducing the rheonomic constraints at all. The domain of DAE theory will be left and the problem will be reformulated as an *optimal control problem*, where the multipliers $\underline{\mu}$ serve as a control function.

2.3. The *Baumgarte* stabilization method

Index reduction methods as presented in Section 2.2 have a significant disadvantage, the so-called *drift-off phenomenon* [9, P. 468], which appears frequently. This term encloses all situations, where the approximated solution of the index-reduced system leaves the state manifold implicitly defined by

$$\underline{\Phi}(\underline{x},t) = \underline{0}\ . \tag{2.25}$$

When differentiating the implicit constraints they become *constraints on velocity level* [20, Subsec. 5.2.6]. The equation

$$\dot{\underline{\Phi}}(\underline{x},t) = G(\underline{x},t)\ \underline{v}(t) + \bar{\underline{\varphi}}(t) = \underline{0} \tag{2.26}$$

describes only the tangential space of a manifold at time t and its relation to the global velocity. There are infinitely many manifolds whose tangential space is described by (2.26). This loss of information is comparable to the loss of constants when differentiating. Without a fixed point and the respective value, the integral yields a family of solutions. Since all numerical schemes deliver an approximation to a certain order, the approximated solution is designed to leave the state manifold and the drift-off effect occurs due to approximative inaccuracy.

Depending on how often the index has been reduced, three different equations appear. The constraints on positional level (2.25), the constraints on velocity level (2.26) and the *constraints on acceleration level* (see again [20, Subsec. 5.2.6])

$$\ddot{\underline{\Phi}}(\underline{x},t) = G(\underline{x},t)\ \dot{\underline{v}}(t) + \dot{G}(\underline{x},t)\underline{v}(t) + \dot{\bar{\underline{\varphi}}}(t) = \underline{0}\ . \tag{2.27}$$

All second-order terms are again denoted by the vector

$$\hat{\underline{\varphi}}(t) := \dot{G}(\underline{x},t)\underline{v}(t) + \dot{\bar{\underline{\varphi}}}(t)\ .$$

In order to nevertheless enforce the constraints on all levels, independent of the index-reduction, Baumgarte [3] suggests a linear combination of all three equations, namely

$$\ddot{\underline{\Phi}}(\underline{x},t) + 2\alpha\dot{\underline{\Phi}}(\underline{x},t) + \beta\underline{\Phi}(\underline{x},t) = \underline{0}\ . \tag{2.28}$$

The parameters α and β are named *Baumgarte parameters*, after their inventor. Equation (2.28) is designed to represent the damped harmonic oscillator equation for $\underline{\Phi}$. The Baumgarte parameters are chosen such that the damping goes on to the aperiodic borderline case, i.e. both eigenvalues $-\alpha \pm \sqrt{\alpha^2 - \beta}$ of Equation (2.28) have negative real parts (see [2, P. 8]).

When using only an index-1-reduction, Arnold [2] proposes a linear combination of the form

$$\dot{\underline{\Phi}}(\underline{x},t) + \widetilde{\alpha}\underline{\Phi}(\underline{x},t) = \underline{0}\ . \tag{2.29}$$

The choice of $\widetilde{\alpha}$ is such that ”the error in the position constraint after one time step [...] has the magnitude of $\mathcal{O}(h^2)$” [2, Sec. 3.2, P. 9]. Arnold argues though, that one should not choose the full optimal parameter, since this can ”introduce additional stiffness [...] and a large error”. The optimal parameter is $\widetilde{\alpha} = \dfrac{1}{h}$, where h is the time step size of the numerical algorithm. The stabilization can be controlled by using a parameter α, where

$$\alpha = \varepsilon\widetilde{\alpha},\ \ \varepsilon \in (0,1)\,. \tag{2.30}$$

The choice of ε is mostly based on empirical references.

3. Numerical approximations using time stepping schemes

During preliminary work for this thesis, numerical simulations have already been conducted in [12, 13] for unactuated, open multibody systems. In this section the gained insights are used and a new, suitable solver is introduced. After discussing the requirements, the time stepping scheme for a partitioned linear-implicit Euler approach is presented for general multibody systems. This scheme is then applied to three differently actuated, simple single-body systems and the results are analysed. Starting point are index-1-reduced systems as seen in Section 2.2, where the scleronomic joint constraints and the rheonomic servo constraints are treated the same.

3.1. Requirements for the application

Since the application is a real-time simulation inside a virtual environment, fast solvers are necessary. This excludes fully implicit algorithms, which often require an iterative approach in each time step. It also excludes multistep methods of high order, since the repeated evaluation of the right-hand side of the system can by very expensive for complex multibody systems. The memory access and writing time in the case of multistep methods can also influence the performance.

On the other side, multibody systems are very *stiff* in terms of dynamic behaviour. It is sufficient to build in springs and dampers with constants of different decimal power in order to introduce such behaviour. And it is further well known that in these cases explicit solvers fail to converge to the real solution [18, Part II], [9].

Hence a compromise is necessary between efficiency and stability. This compromise can be found in the class of *linear-implicit* methods.

3.1.1. A partitioned linear-implicit Euler algorithm

Explicit solvers need a drastic reduction of time step size when dealing with stiff systems, which is not ideal for a real-time application. Implicit solvers handle stiff behaviour better in terms of convergence, but iterations are also undesirable. The idea of only calculating a single iteration of the implicit algorithm, leads to the class of linear-implicit algorithms and has already been proven to be a suitable approach to real-time simulation in the automotive industry [2, 7]. Since higher order algorithms also lead to losses in efficiency, the restriction to first order Runge-Kutta methods was made, namely the Euler algorithm.

Consider the system of DAEs

$$\begin{array}{rcl} \dot{\underline{x}}(t) &=& K(\underline{x})\ \underline{v}(t)\ , \\ M\ \dot{\underline{v}}(t) &=& \underline{f}(\underline{x},\underline{v})\ , \\ \underline{\Phi}(\underline{x},t) &=& \underline{0}\ , \end{array}$$

where $\underline{f}$ and K are continuous and $\underline{\Phi}$ is assumed to be at least continuously differentiable. An index-1-reduction as seen in Section 2.2 and Subsection 1.3.2, leads to

$$\begin{array}{rcl} \dot{\underline{x}}(t) &=& K(\underline{x})\ \underline{v}(t)\ , \\ M\ \dot{\underline{v}}(t) - G^\top(\underline{x},t)\underline{\rho} &=& \underline{f}(\underline{x},\underline{v})\ , \\ G(\underline{x},t)\ \underline{v}(t) + \underline{\bar{\varphi}}(t) &=& \underline{0}\ . \end{array}$$

Due to the index reduction, a drift-off effect might occur and stabilization according Baumgarte is introduced

$$\begin{array}{rcl} \dot{\underline{x}}(t) &=& K(\underline{x})\ \underline{v}(t)\ , \\ M\ \dot{\underline{v}}(t) - G^\top(\underline{x},t)\underline{\rho} &=& \underline{f}(\underline{x},\underline{v})\ , \\ G(\underline{x},t)\ \underline{v}(t) + \underline{\bar{\varphi}}(t) + \alpha\underline{\Phi}(\underline{x}) &=& \underline{0}\ . \end{array} \tag{3.1}$$

The first equation in System (3.1) does not contain the possibly stiff behaviour of a multibody system, since it represents only the differential relation between position and velocity. The second and the third equation can though, since various force laws and constraints influence the dynamics at this point. Therefore a partitioning can be made, in order to gain a more efficient algorithm.

An explicit Euler algorithm is applied to the first equation. The result is then used in a linear-implicit Euler scheme to update solely the velocity in the second and third equation.

Let $\{t_k\}_{k\in\mathbb{N}}$ be the time grid used by the numerical approximation algorithm and let $\underline{x}_k$ and $\underline{v}_k$ be the respective values of the approximating curves. A discretization of $\underline{\rho}$ is not considered, since force analysis is omitted. The involvement of the Lagrangian multiplier is now purely for obtaining a solvable system. The partitioning leads to the following finite difference algorithm:

1. Position update:
$$\frac{1}{h}\left(\underline{x}_{k+1} - \underline{x}_k\right) = K(\underline{x}_k)\ \underline{v}_k\ .$$
2. Velocity update, where $\underline{x}_{k+1}$ from step 1 is used:

$$\begin{array}{rcl} M\ \dfrac{1}{h}\left(\underline{v}_{k+1} - \underline{v}_k\right) - G^\top(\underline{x}_{k+1},t_{k+1})\underline{\rho} &=& \underline{f}(\underline{x}_{k+1},\underline{v}_{k+1})\ , \\ G(\underline{x}_{k+1},t_{k+1})\ \underline{v}_{k+1} &=& -\underline{\bar{\varphi}}(t_{k+1}) - \alpha\underline{\Phi}(\underline{x}_{k+1})\ . \end{array} \tag{3.2}$$

$\underline{f}(\underline{x}_{k+1},\underline{v}_{k+1})$ is unknown due to the implicit approach. A first-order approximation can be obtained by the first two terms of the Taylor expansion with respect to $\underline{v}$

$$\underline{f}(\underline{x}_{k+1},\underline{v}_{k+1}) = \underline{f}(\underline{x}_{k+1},\underline{v}_k) + \underline{f}_{\underline{v}}(\underline{x}_{k+1},\underline{v}_k)\left(\underline{v}_{k+1} - \underline{v}_k\right) + \mathcal{O}(h^2),$$

where $\underline{f}_{\underline{v}}(\underline{x}_{k+1},\underline{v}_k) := \dfrac{\partial}{\partial\underline{v}}\underline{f}(\underline{x},\underline{v})\Big|_{\underline{x}=\underline{x}_{k+1},\ \underline{v}=\underline{v}_k}$.

Inserting this into (3.2) leads finally to the time stepping scheme

1. Position update:
$$\underline{x}_{k+1} = \underline{x}_k + h\ K(\underline{x}_k)\ \underline{v}_k\ . \tag{3.3}$$
2. Velocity update:
$$\begin{bmatrix} M - h\ \underline{f}_{\underline{v}}(\underline{x}_{k+1}, \underline{v}_k) & -h\ G^\top(\underline{x}_{k+1}, t_{k+1}) \\ G(\underline{x}_{i+1}, t_{k+1}) & \end{bmatrix} \begin{bmatrix} \underline{v}_{k+1} - \underline{v}_k \\ \underline{\rho} \end{bmatrix} = \begin{bmatrix} h\ \underline{f}(\underline{x}_{k+1}, \underline{v}_k) \\ -G(\underline{x}_{k+1}, t_{k+1})\underline{v}_k - \underline{\bar{\varphi}}(t_{k+1}) - \alpha\underline{\Phi}(\underline{x}_{i+1}) \end{bmatrix} . \tag{3.4}$$

According to Equations (3.3) and (3.4) it is necessary to update the $6n_K$ values in the global position vector $\underline{x}$, solve a quadratic system of $6n_K + n_B$ linear equations and finally update the $6n_K$ values of the global velocity vector $\underline{v}$. Thus, instead of having to solve iteratively for $\underline{v}_{k+1}$, a single matrix inversion has to be made. This reduces the expenses significantly and additionally introduces stabilizing properties of an implicit algorithm.

3.2. Examples of actuation signals

Subsequently, three different actuation signals are given and the numerical method from Section 3.1.1 is applied. In each example the systems consist of a single unit sphere with mass $m = 1$ and inertia $\Theta = I\frac{2}{5}m$, where I is the unit tensor. The position $\underline{x}_{\mathbf{t}}(t)$ is actuated by providing a curve $\underline{h} : \mathbb{R} \to \mathbb{R}^3$ and constraining it by setting

$$\Phi(\underline{x}, t) = \underline{x}_{\mathbf{t}}(t) - \underline{h}(t) = \underline{0}\ .$$

Differentiation with respect to time yields implicit constraints on velocity level in the form of

$$\underline{v}_{\mathbf{t}}(t) - \dot{\underline{h}}(t) = \underline{0}\ ,$$

or

$$[I, O] \begin{bmatrix} \underline{v}_{\mathbf{t}}(t) \\ \underline{\omega}(t) \end{bmatrix} - \dot{\underline{h}}(t) = \underline{0}$$

when including the angular velocity in order to obtain a global formulation of the implicit constraints. O is a 3×3 zero matrix. Orientational quantities and angular velocities are not considered in this section. The matrix $[I, O]$ corresponds to the matrix $G(\underline{x}_{k+1}, t_{k+1})$ from Equation (3.4) and is constant in this case. The vector $\underline{\bar{\varphi}}(t_{k+1})$ is given by $\dot{\underline{h}}(t_{k+1})$ in each time step.

The first example is a smooth actuation and convergence of order 1 can be shown. The second and third example consider piece-wise constant curves and two different ways of approximating $\dot{\underline{h}}(t)$. The piece-wise constant curves represent real samples of position signals of a *VIVE* controller and the following notation is used:

$$\begin{aligned} \text{Controller position: } \underline{p}^c(t) &:= \underline{h}(t)\ , \\ \text{Controller velocity: } \underline{v}^c(t) &:= \dot{\underline{h}}(t)\ . \end{aligned}$$

3.2.1. Smooth actuation

Let a sphere be at the initial position $\underline{x}_{\mathrm{t}}(0) = [1,0,1]^\top$ and the actuation be given by

$$\begin{aligned} \underline{h}(t) &= \begin{bmatrix} \cos(\omega t) \\ \sin(\omega t) \\ 1 \end{bmatrix} , \\ \dot{\underline{h}}(t) &= \begin{bmatrix} -\sin(\omega t) \\ \cos(\omega t) \\ 0 \end{bmatrix} \omega . \end{aligned} \tag{3.5}$$

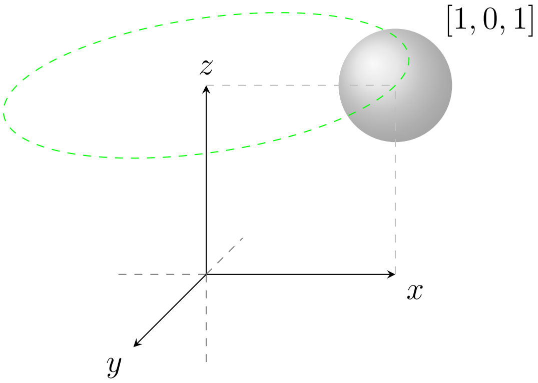

Figure 3.1.: Setup for smooth actuation.

Figure 3.1 shows the sphere in grey and the state manifold in green. The sphere moves along the green curve in anti-clockwise direction and a frequency $\omega = \frac{\pi}{4}$ was chosen. It is supposed to pass a quarter circle every 2 seconds. The point-wise error is analysed exemplarily for the x-components of both, position and velocity. The results remain the same for the other components.

The algorithm from Section 3.1.1 was applied with a constant time step size $h = 0.001$. The parameter was uniformly refined by $h = 0.001 \cdot 2^{-n}$, $n \in \{0,1,2\}$. Figure 3.2 shows linear convergence for the point-wise error of the position approximation. For the velocity, an exact approximation is evident, as pointed out in [2].

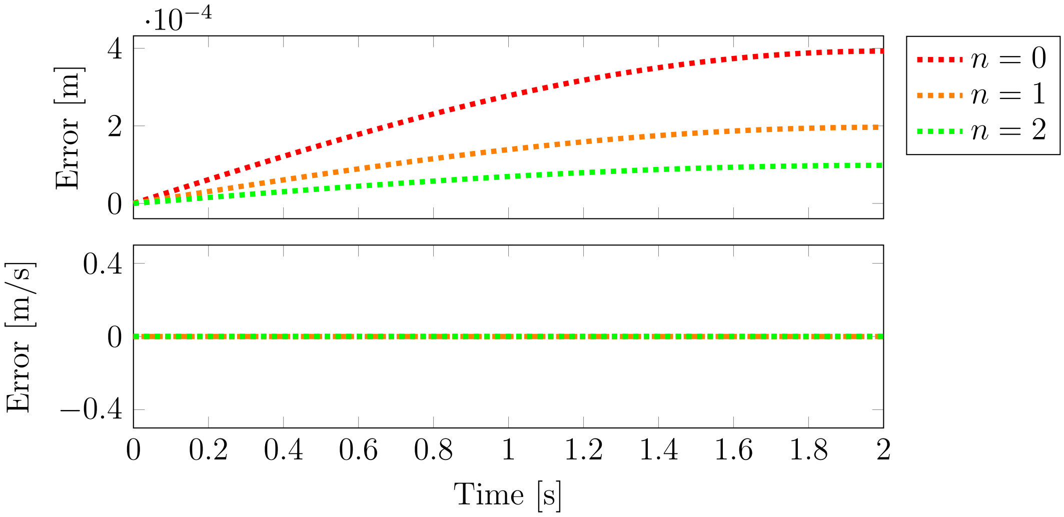

Figure 3.2.: Point-wise error for the x-component approximations.

3.2.2. Piecewise constant actuation

In Figure 3.3 a sample of an actuation signal is shown, which was extracted from *Autodesk VRED* using a *VIVE* controller. The initial values are

$$\underline{p}^c(0) = \underline{x}_t(0) = \begin{bmatrix} 0,9716 \\ -0,1003 \\ 1,2480 \end{bmatrix} , \ \underline{v}^c(0) = \underline{v}_t(0) = \begin{bmatrix} -0,3151 \\ -0,3398 \\ -1,0652 \end{bmatrix} .$$

In this case the velocity values were approximated by central differences based on grid points, which do not match the grid of the applied partitioned Euler method.

Let $\{\tau_j\}_{j\in\mathbb{N}}$ be a time grid, based on which the software registers a change in position of the controller and the velocity values are approximated. Let further $\{t_k\}_{k\in\mathbb{N}}$ be a finer grid, which represents the time steps of the numerical method and define the velocity values as follows

$$\underline{v}^c(t_k) = \underline{v}^c(\tau_j), \ \forall \ t_k \in [\ \tau_j, \tau_{j+1}\ ),\ j = 1\dots$$

This leads to a piece-wise constant actuation signal on positional and velocity level.

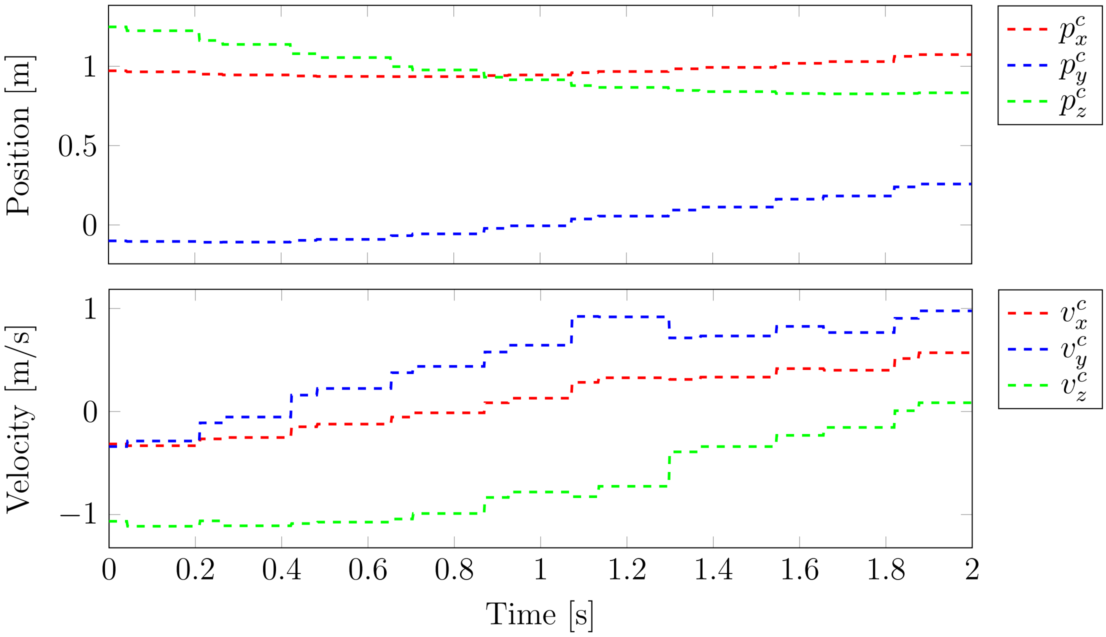

Figure 3.3.: Position and velocity sample for a moving controller.

The same algorithm as in the previous example was applied and tests for convergence with the same time step sizes $h = 0.001 \cdot 2^{-n},\ n \in \{0,1,2\}$, were carried out. Consistency was not achieved, as seen in Figure 3.4. Despite this, an exact approximation of the velocity was again observed, which is at first a surprising result. Since the integration method integrates polynomials up to order 1 exactly, and the velocity signal is a piece-wise constant function, this result is expected at the continuous parts. However, an investigation for larger discontinuities may be necessary. The problem for the position approximation emerges from the fact that the position ought to be the integral of the velocity, a quantity which is discontinuous now. Hence the assumptions the numerical scheme is built on are not fulfilled.

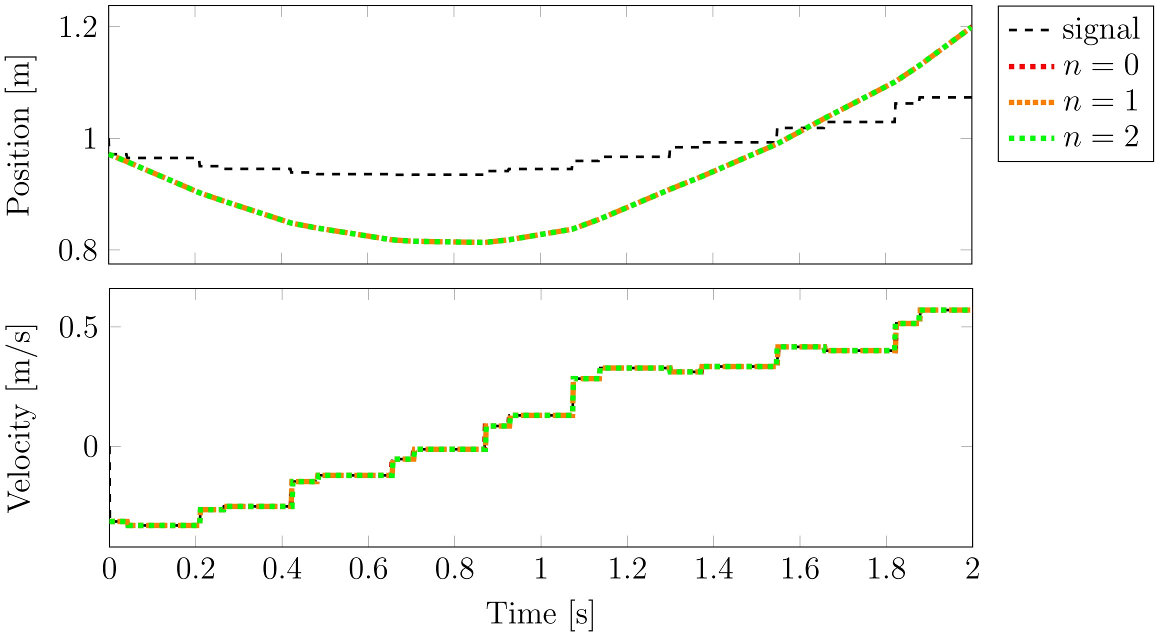

Figure 3.4.: Results for the x-component of position and velocity.

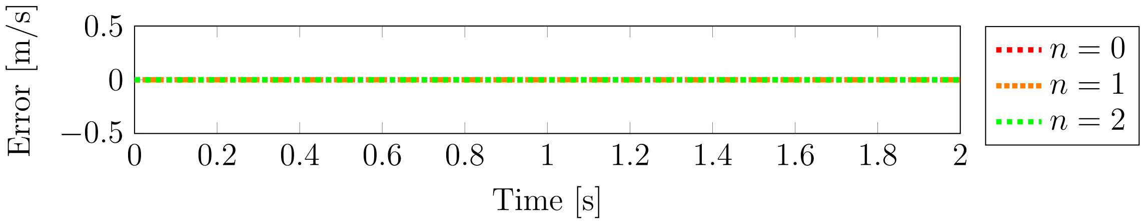

Figure 3.5.: Point-wise error in the x-component of the velocity.

In order to achieve a better result for the position approximation, stabilization according to Baumgarte was applied. A parameter $\alpha = \varepsilon\widetilde{\alpha}$ as introduced in Section 2.3 was defined and inserted into the system of ODEs. A constant time step size of $h = 0.0005$ was chosen and stabilization was introduced for $\varepsilon \in \{0.2, 0.5, 0.8\}$. In Figure 3.6 the results for position and velocity are displayed. While mostly satisfying result were achieved for the position with an increasing stabilization parameter, impulse-like deflections appear in the approximating curves. They appear at the points of discontinuity of the signal, as indicated by the point-wise error in Figure 3.7. The quality of the velocity approximation deteriorates. While it was integrated exactly without stabilization, Figure 3.7 shows errors independent of the size of the stabilization parameter α. When visualizing the movement of a single actuated body, this may not pose a great problem. But in the case of other bodies attached to the actuated one, the effects of these deflection may not be predictable. Joints transfer velocities and therefore this error is also propagated.

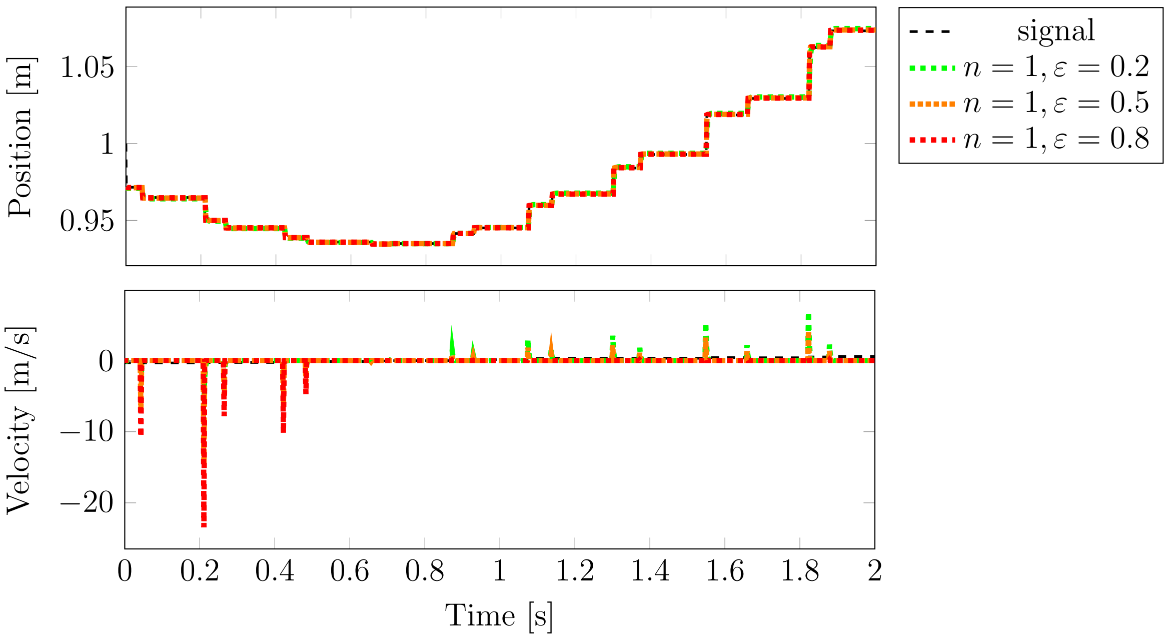

Figure 3.6.: Results for the x-component with Baumgarte stabilization.

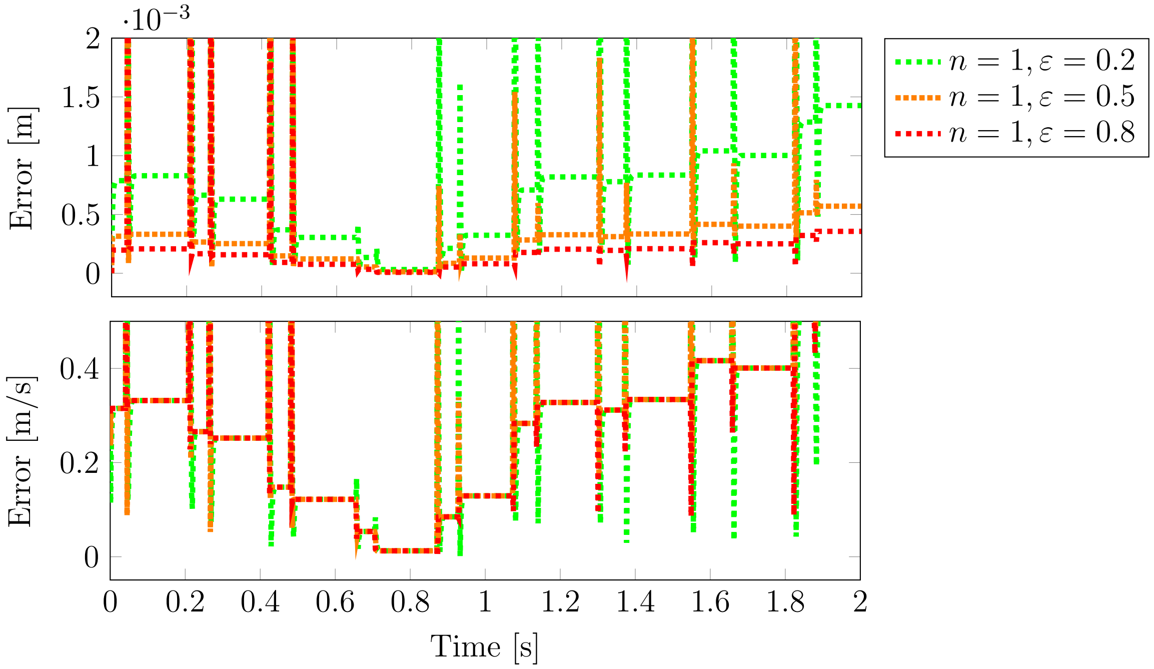

Figure 3.7.: Point-wise error in the x-component with Baumgarte stabilization.

3.2.3. Dirac impulse-like actuation

As in Section 3.2.2, consider a grid $\{\tau_j\}_{j\in\mathbb{N}}$ which represents the times at which a change in the position of the controller is registered and cached. When approximating the velocity on a finer grid $\{t_k\}_{k\in\mathbb{N}}$ by setting

$$\underline{p}^c(t_k) = \underline{p}^c(\tau_j),\ \forall\ t_k \in [\,\tau_j, \tau_{j+1}\,)\,,\ j = 1 \ldots\ ,$$

the velocity becomes zero almost everywhere on the finer grid. Dirac impuls-like changes can be observed for grid points t_{k+1} where there is a j such that

$$t_k \le \tau_j < t_{k+1}\ .$$

This leads to an actuation signal as seen in Figure 3.8.

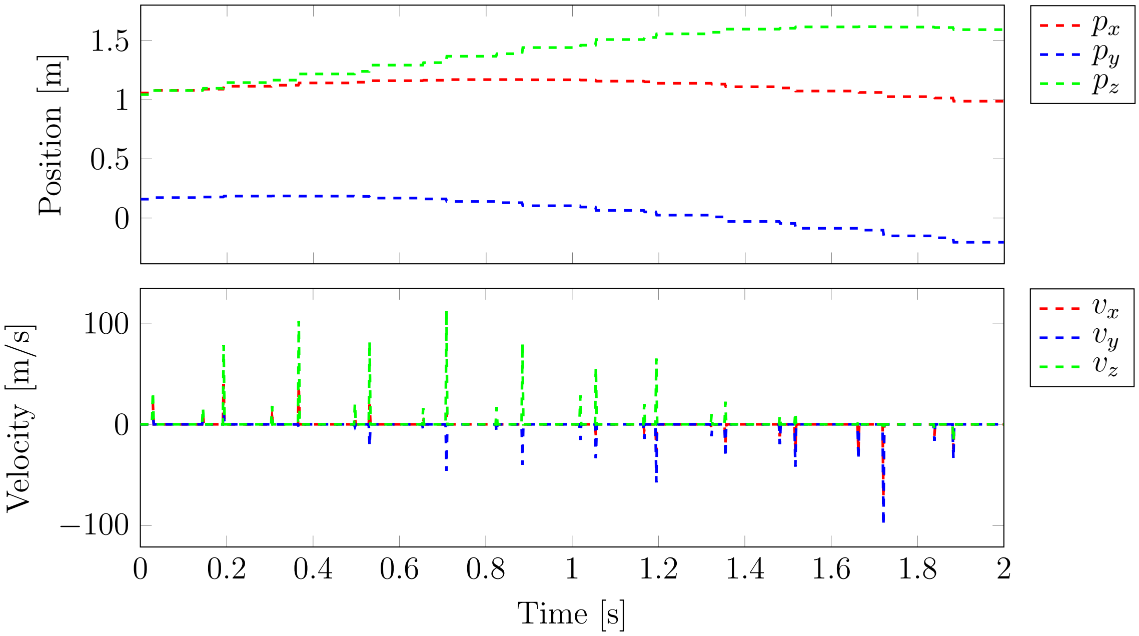

Figure 3.8.: Position and velocity sample for a moving controller.
The velocity is approximated on a finer grid.

Signals of this kind are considered for the following reason: Software like *Autodesk VRED* provides means to conduct calculations at the moments in time, where the controller position is updated. Hence the grid for the central difference approximation of the velocity can be chosen to be the grid of the position updates. This was treated in the previous Section 3.2.2. In order to not rely on this specific software, the velocity approximation was carried out within the numerical integration method for the equations of motion. This results in a Dirac impulse-like velocity profile, since the time grid for this method is in general finer.

Figure 3.9 shows the results for time step sizes $h = 0.001 \cdot 2^{-n}$, $n \in \{0, 1, 2\}$. As in the previous case, consistency can not be shown for the position approximation, but the velocity was integrated exactly. The impulse-like deflection appear in the approximation.

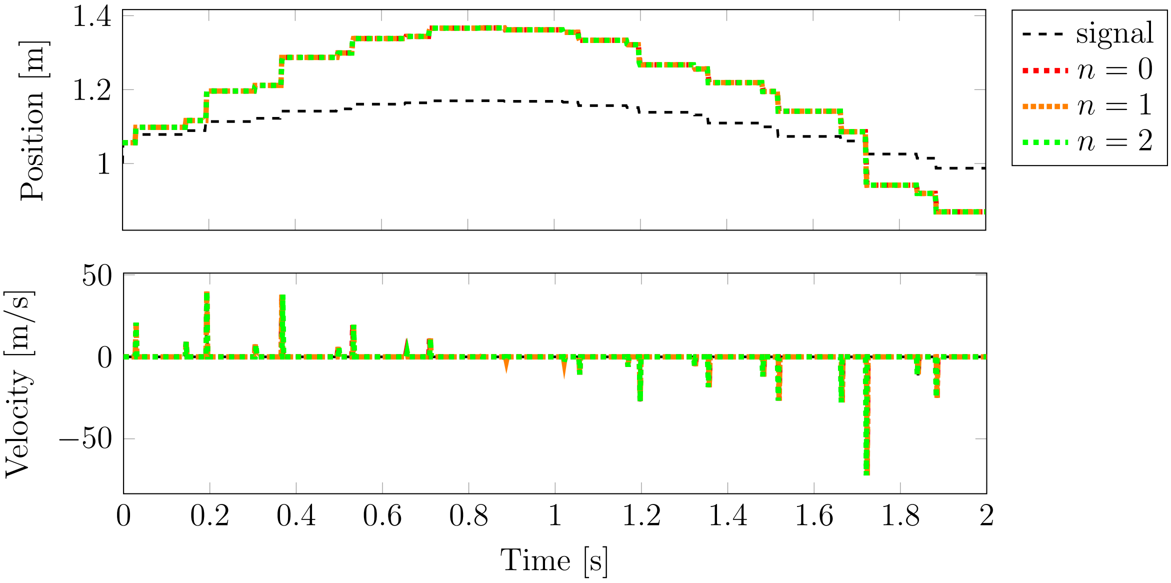

Figure 3.9.: Results for the x-component of position and velocity.

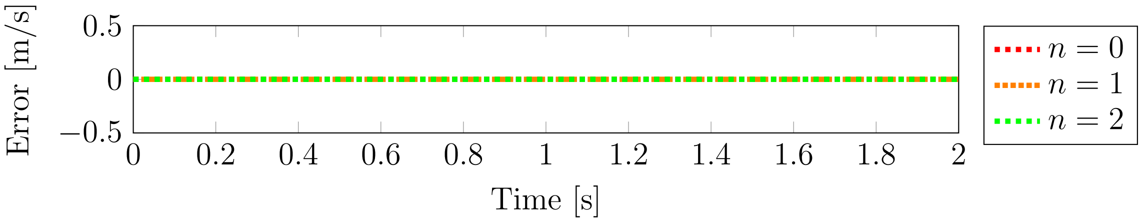

Figure 3.10.: Piece-wise error for the x-component of the velocity.

When applying the stabilization according to Baumgarte, a new behaviour occurs in contrast to Subsection 3.2.2. The phenomena of overshooting is apparent at the points of discontinuity. It is not dominating though and the solution evens out very fast. The velocity approximation worsens again compared to the original problem and shows very high deflections as seen in Figure 3.12.

In both cases of discontinuous actuation, disturbances appear at the points of discontinuity. For the purpose of visualization they are not severe in a single-body setting. The effects of this error profile on other constraints though, especially joint equations, are not controllable and can result in unusually high errors due to error propagation. The reason these problems occur is the breaking of the continuity assumption. Most of the standard numerical algorithms for ODEs are based on it. Therefore a different approach is necessary.

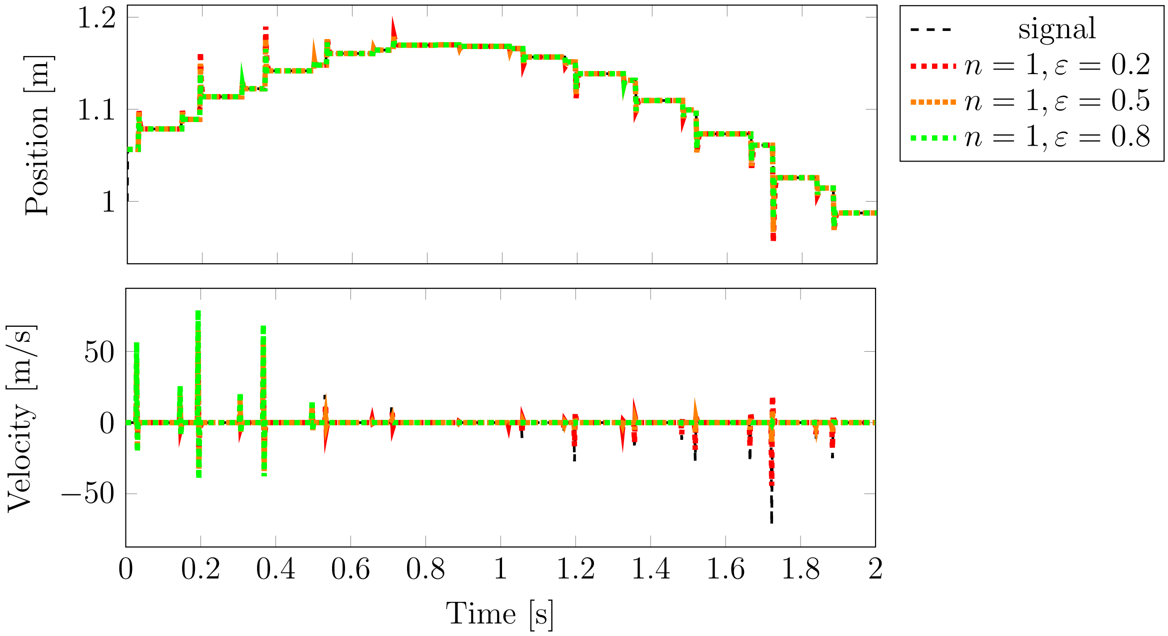

Figure 3.11.: Results for the x-component with Baumgarte stabilization.

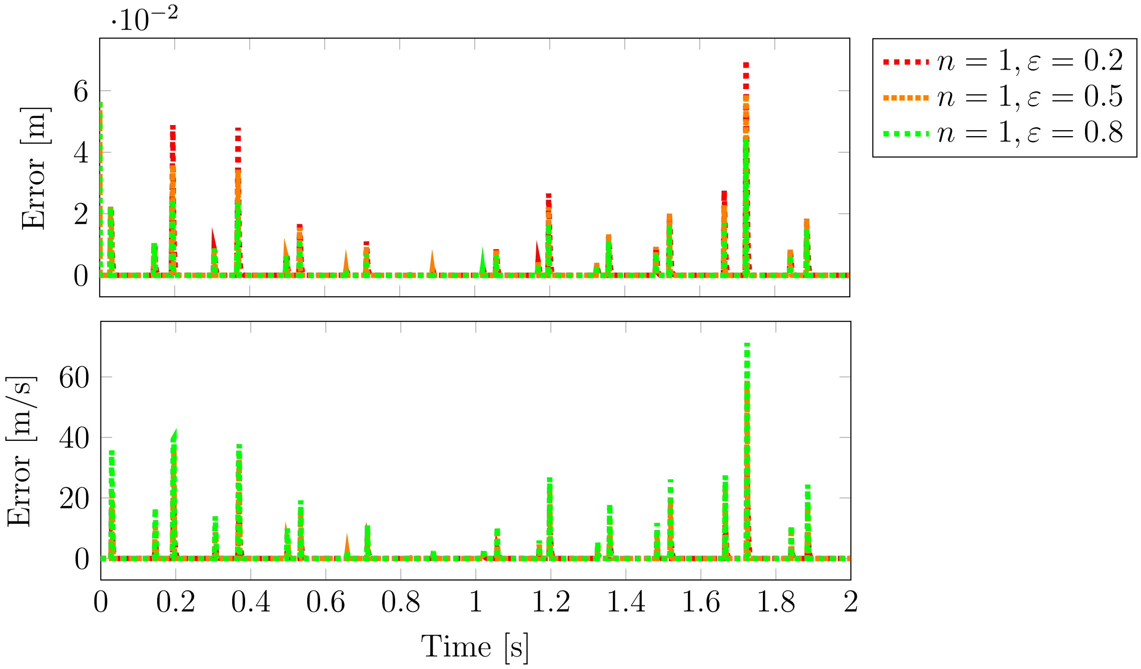

Figure 3.12.: Piece-wise error for the x-component with Baumgarte stabilization.

4. An optimal control problem for actuated multibody systems

It was shown in Chapter 3, that a conventional DAE approach to actuated multibody systems fails to show convergent results in the case of discontinuous actuation signals. It can be stabilized to a somewhat satisfactory level, though the stabilized approximations show inconsistent behaviour around discontinuities. A new approach is introduced here in order to avoid this problem. The restraining forces imposed by an actuation are understood as a control function and the task is reformulated as an *optimal control problem.* A *single-stage* approach [6] is introduced and two different regularizations are applied and tested.

4.1. A single-stage approach with L^2-regularization

In Chapter 2 a constrained, unactuated multibody system was modelled as a system of DAEs of the form

$$\begin{aligned} \dot{\underline{x}}(t) &= K(\underline{x})\underline{v}(t) \\ M\dot{\underline{v}}(t) &= F(\underline{x},\underline{v},\underline{\rho},t) = \underline{f}(\underline{x},\underline{v},t) + G^\top(\underline{x})\underline{\rho}\ , \\ \underline{0} &= \underline{\Phi}(\underline{x})\ , \\ \underline{x}(0) &= \underline{\tilde{x}}_0\ , \\ \underline{v}(0) &= \underline{\tilde{v}}_0\ , \end{aligned} \tag{4.1}$$

where $\underline{\tilde{x}}_0$, $\underline{\tilde{v}}_0$ are known initial values. All functions are sufficiently smooth and if the initial values are consistent with the holonomic constraints, a unique solution exists.

Consider a time interval $E = (0,T)$ and two points in time $t_1 > t_0 \in E$. Consider further a bounded function

$$\begin{aligned} \underline{h} : E &\to \mathbb{R}^{n_A}\ , 0 < n_A < 6n_K - n_B\ , \\ t &\mapsto \underline{h}(t)\ , \end{aligned} \tag{4.2}$$

and servo constraints

$$\underline{\Psi}(\underline{x},t) = P\underline{x}(t) - \underline{h}(t) = \underline{0}\ , \tag{4.3}$$

where P is the canonical projection onto the n_A actuated components, i.e.

$$\begin{aligned} P_{i,j} &\in \{0,1\}\ , \\ \textstyle\sum_{j=1}^{12n_K} P_{i,j} &= 1,\ \forall i = 1\cdots n_A\ , \\ \operatorname{rank}(P) &= n_A\ , \end{aligned}$$

Define discrete servo constraints on the subinterval $[t_0,t_1]$ of the form

$$\underline{\Psi}(t_1) = P\underline{x}(t_1) - \underline{h}(t_1) = \underline{0} \tag{4.4}$$

As stated in Section 2.2, servo constraints introduce restraining forces

$$\underline{f}^d = P^\top \underline{\mu} \ ,$$

where

$$\underline{\mu} \ : \ \mathbb{R} \to \mathbb{R}^{n_A}$$

is in general a vector valued and unknown function in time. They can not be substituted as seen in Example 2.3 without loosing the solvability due to a lack of continuity. By viewing $\underline{\mu}$ as a control function in System (4.1) and assuming the knowledge of $\underline{x}(t_0)$, $\underline{v}(t_0)$, one obtains

$$\begin{aligned} \dot{\underline{x}}(t) &= K(\underline{x})\underline{v}(t) \\ M\dot{\underline{v}}(t) &= F(\underline{x}, \underline{v}, \underline{\rho}, t) = \underline{f}(\underline{x}, \underline{v}, t) + G^\top(\underline{x})\underline{\rho} + P^\top \underline{\mu} \ , \\ \underline{0} &= \underline{\Phi}(\underline{x}) \ , \\ \underline{x}(t_0) &= \underline{x}_0 \ , \\ \underline{v}(t_0) &= \underline{v}_0 \ , \end{aligned} \tag{4.5}$$

and the following *minimization problem*:

Problem 4.1
Find $\underline{x}(t)$ and $\underline{\mu}(t)$ on $[t_0, t_1]$, such that

$$\|P\underline{x}(t_1) - \underline{h}(t_1)\|_\nu^2 \to \min \tag{4.6}$$

subject to the constraints

$$\begin{aligned} \dot{\underline{x}}(t) &= K(\underline{x})\underline{v}(t) \\ M\dot{\underline{v}}(t) &= F(\underline{x}, \underline{v}, \underline{\rho}, t) \\ \underline{0} &= \underline{\Phi}(\underline{x}) \ , \end{aligned}$$

and the initial values

$$\begin{aligned} \underline{x}(t_0) &= \underline{x}_0 \ , \\ \dot{\underline{x}}(t_0) &= \underline{v}_0 \ . \end{aligned}$$

Remark 4.1
1. The minimum is zero and represents a state where the servo constraints are fulfilled at time t_1. This formulation, which is a mix between a discrete and continuous setting, aims for a time stepping scheme where $t_k = t_0$ and $t_{k+1} = t_1$. The values of $\underline{h}$ are extracted in real time, therefore the problem cannot be considered on the whole interval.

2. The regularity and continuity of $\underline{h}$ becomes irrelevant for now, as long as the function is bounded.

3. The norm $\|\cdot\|_\nu$ denotes a suitable norm. In the most cases the Euclidean norm is sufficient. If there are several actuated bodies, it is suggested in [2] to use a weighted norm

$$\|\tilde{\underline{x}}\|_\nu^2 = \|\tilde{\underline{x}}\|_M^2 := \tilde{\underline{x}}^\top PMP^\top \tilde{\underline{x}} \ ,$$

where M is the mass matrix. This way emphasize is given to heavier bodies which are dynamically more critical. If not specified, the subscript is omitted and the Euclidean norm is used.

The new goal now is to minimize the *servo constraint residual*, a functional of the form

$$J_0(\underline{x}) = \frac{1}{2}\|P\underline{x}(t_1) - \underline{h}(t_1)\|^2 \; + \frac{1}{2}\int\limits_{t_0}^{t_1} [P\underline{x}(t) - \underline{h}(t)]^\top [P\underline{x}(t) - \underline{h}(t)] \, \mathrm{dt}. \tag{4.7}$$

It represents the $L^2(t_0, t_1)$-norm of the residual and an additional point-wise evaluation at the target time t_1. This functional is augmented by a regularization

$$J_1(\underline{x}) = J_0(\underline{x}) + \frac{\rho_0}{2} \; \|\underline{\mu}\|^2_{L^2(t_0,t_1)} \; , \tag{4.8}$$

where $0 < \rho_0 \in \mathbb{R}$. The idea is the following:

A piecewise constant actuation is physically not possible in the classical sense. Bodies can not jump instantly and their movement has to be at least continuous. Rapid changes of the velocity occur due to large forces acting. By penalizing the forces imposed by the actuation, namely $\underline{\mu}$, one can smooth out the unphysical actuation signal. Depending on the quality and the sizes of the discontinuities in the signal, a penalty for the derivatives of $\underline{\mu}$ can be introduced in a similar form. This idea is stated in [1] using an energy norm, where a proof of equivalence of the augmented functional is given exemplarily for a simplified two-cars-system.

The system of DAEs, obtained by joints and the Newton-Euler approach, represents a constraint on the set of admissible functions and can be embedded into the functional by Lagrangian multipliers $\underline{\lambda}_p(t)$, $\underline{\lambda}_v(t)$ and $\underline{\kappa}(t)$ [6, Sec. 2.3]. This leads to a new functional

$$\begin{aligned} J_2(\underline{x}) \;&=\; J_1(\underline{x}) \\ &+\; \int\limits_{t_0}^{t_1} \left\{\underline{\lambda}_p^\top(t)\,[K(\underline{x}) - \dot{\underline{x}}(t)] + \underline{\lambda}_v^\top(t)\,\left[F(\underline{x}, \underline{v}, \underline{\rho}, \underline{\mu}, t) - M\dot{\underline{v}}(t)\right] + \underline{\kappa}^\top \Phi(\underline{x})\right\} \mathrm{dt} \end{aligned} \tag{4.9}$$

$\underline{\lambda}_p$ and $\underline{\lambda}_v$ couple the differential parts and $\underline{\kappa}$ the holonomic constraints. Defining the *Hamiltonian function*

$$\begin{aligned} H \;&=\; H(\underline{x}, \dot{\underline{x}}, \underline{\rho}, \underline{\mu}, \underline{\lambda}_p, \underline{\lambda}_v, \underline{\kappa}, t) \\ &=\; \frac{1}{2}\,[P\underline{x}(t) - \underline{h}(t)]^\top\,[P\underline{x}(t) - \underline{h}(t)] + \frac{\rho_0}{2}\;\underline{\mu}^\top(t)\underline{\mu}(t) \\ &+\; \underline{\lambda}_p^\top(t)K(\underline{x})\underline{v}(t) + \underline{\lambda}_v^\top(t)F(\underline{x}, \underline{v}, \underline{\rho}, \underline{\mu}, t) + \underline{\kappa}^\top \Phi(\underline{x}) \end{aligned} \tag{4.10}$$

and inserting it into (4.9) yields

$$J(\underline{x}) := J_2(\underline{x}) = \frac{1}{2}\|P\underline{x}(t_1) - \underline{h}(t_1)\|^2 + \int\limits_{t_0}^{t_1} \left[H - \underline{\lambda}_p^\top(t)\dot{\underline{x}}(t) - \underline{\lambda}_v^\top(t)M\dot{\underline{v}}(t)\right] \mathrm{dt}\;.$$

Integration by parts of the terms containing $\underline{\lambda}_p$ and $\underline{\lambda}_v$ leads to

$$\begin{aligned} J(\underline{x}) \;&=\; \tfrac{1}{2}\|P\underline{x}(t_1) - \underline{h}(t_1)\|^2 - \left[\underline{\lambda}_p^\top(t)\underline{x}(t)\right]_{t_0}^{t_1} - \left[\underline{\lambda}_v^\top(t)M\underline{v}(t)\right]_{t_0}^{t_1} \\ &+\; \int\limits_{t_0}^{t_1} \left[H + \dot{\underline{\lambda}}_p^\top(t)\underline{x}(t) + \dot{\underline{\lambda}}_v^\top(t)M\underline{v}(t)\right] \mathrm{dt}\;. \end{aligned} \tag{4.11}$$

By [11, Sec. II] a *necessary* condition for this functional to reach the minimum over all possible control functions is, that the *first variation* δJ with respect to $\underline{\mu}$ becomes zero.

Remark 4.2
1. By introducing $\underline{\mu}$ as generalized restraining forces, $\underline{x}$ and $\underline{v}$ depend on $\underline{\mu}$. There are several attempts on how to construct a mapping

$$\underline{\mu} \mapsto \underline{x} \ ,$$

but they depend highly on the structure of the considered dynamical system and the function spaces, where $\underline{x}$ and $\underline{\mu}$ are considered to be in. An overview is provided in [4] and its underlying literature.

2. $\underline{\rho}$ also depends on $\underline{\mu}$. This dependency is derived in Example 2.4, Equation (2.22).

3. *Sufficient* conditions for the functional to reach a minimum is, that the *second variation* $\delta^2 J$ with respect to $\underline{\mu}$ is *greater than* zero and that the Hamiltonian H is convex with respect to $\underline{\mu}$.

The variation of the point-wise term in (4.7) is

$$\begin{aligned}
\delta\frac{1}{2}\|P\underline{x}(t_1) - \underline{h}(t_1)\|^2 &= \delta\frac{1}{2}\left[\underline{x}^\top(t_1)P^\top P\underline{x}(t_1) - 2\underline{x}^\top(t_1)P^\top\underline{h}(t_1) + \underline{h}^\top(t_1)\underline{h}(t_1)\right] \\
&= \left[P^\top P\underline{x}(t_1)\right]^\top \delta\underline{x}(t_1) - \left[P^\top\underline{h}(t_1)\right]^\top \delta\underline{x}(t_1) \\
&= \left[P^\top P\underline{x}(t_1) - P^\top\underline{h}(t_1)\right]^\top \delta\underline{x}(t_1) \ . \qquad (4.12)
\end{aligned}$$

The variation of the second term in the right-hand side of (4.11) is simply

$$-\,\delta\left[\underline{\lambda}_p^\top(t)\underline{x}(t)\right]_{t_0}^{t_1} = -\underline{\lambda}_p^\top(t_1)\delta\underline{x}(t_1) \ , \qquad (4.13)$$

since $\underline{x}(t_0)$ is assumed to be known and constant in all components. This can by achieved by using only test functions, which are zero on the left-hand side of the interval.

The same holds for the third term

$$-\,\delta\left[\underline{\lambda}_v^\top(t)M\underline{v}(t)\right]_{t_0}^{t_1} = -\underline{\lambda}_v^\top(t_1)M\delta\underline{v}(t_1) \ , \qquad (4.14)$$

since $\underline{v}(t_0)$ is assumed to be known.

The variation of the integral term includes the partial derivatives

$$\begin{aligned}
H_x &= \frac{\partial}{\partial\underline{x}}H(\underline{x},\dot{\underline{x}},\underline{\rho},\underline{\mu},\underline{\lambda}_p,\underline{\lambda}_v,\underline{\kappa},t) \ , \\
H_v &= \frac{\partial}{\partial\underline{v}}H(\underline{x},\dot{\underline{x}},\underline{\rho},\underline{\mu},\underline{\lambda}_p,\underline{\lambda}_v,\underline{\kappa},t) \ , \\
H_\rho &= \frac{\partial}{\partial\underline{\rho}}H(\underline{x},\dot{\underline{x}},\underline{\rho},\underline{\mu},\underline{\lambda}_p,\underline{\lambda}_v,\underline{\kappa},t) \ , \\
H_\mu &= \frac{\partial}{\partial\underline{\mu}}H(\underline{x},\dot{\underline{x}},\underline{\rho},\underline{\mu},\underline{\lambda}_p,\underline{\lambda}_v,\underline{\kappa},t) \ .
\end{aligned}$$

It holds

$$\begin{aligned}
&\delta \int\limits_{t_0}^{t_1} \left[H + \underline{\dot{\lambda}}_p^\top(t)\underline{x}(t) + \underline{\dot{\lambda}}_v^\top(t)M\underline{v}(t)\right] \,\mathrm{dt} \\
&= \int\limits_{t_0}^{t_1} \left[H_x\delta\underline{x}(t) + H_v\delta\underline{v}(t) + H_\rho\delta\underline{\rho} + H_\mu\delta\underline{\mu} + \underline{\dot{\lambda}}_p^\top(t)\delta\underline{x}(t) + \underline{\dot{\lambda}}_v^\top(t)M\delta\underline{v}(t)\right] \mathrm{dt} \\
&= \int\limits_{t_0}^{t_1} \left[\left[H_x + \underline{\dot{\lambda}}_p^\top(t)\right]\delta\underline{x}(t) + \left[H_v + \underline{\dot{\lambda}}_v^\top(t)\right]\delta\underline{v}(t) + H_\rho\delta\underline{\rho} + H_\mu\delta\underline{\mu}\right] \mathrm{dt}\ .
\end{aligned} \tag{4.15}$$

By the necessary condition

$$0 \overset{!}{=} \delta J\ , \tag{4.16}$$

Equations (4.12) and (4.13) lead to

$$\left[P^\top P\underline{x}(t_1) - P^\top\underline{h}(t_1) - \underline{\lambda}_p(t_1)\right]^\top \delta\underline{x}(t_1) \overset{!}{=} 0$$

for arbitrary, admissible variations $\delta\underline{x}(t_1)$, which in return leads to the terminal value

$$\underline{\lambda}_p(t_1) = P^\top P\underline{x}(t_1) - P^\top\underline{h}(t_1)\ .$$

Analogously, Equation (4.14) leads to

$$\underline{\lambda}_v(t_1) = \underline{0}\ ,$$

since M is injective. For the variations in (4.15) to be zero, each non-variational term has to become zero, i.e.

$$\begin{aligned}
\underline{\dot{\lambda}}_p(t) &= -H_x^\top \\
M^\top\underline{\dot{\lambda}}_v(t) &= -H_v^\top \\
\underline{0} &= H_\rho = \underline{\lambda}_v^\top(t)\frac{\partial}{\partial\underline{\rho}}F(\underline{x},\underline{v},\underline{\rho},\underline{\mu},t) = \underline{\lambda}_v^\top(t)G^\top(\underline{x}) = G(\underline{x})\underline{\lambda}_v(t)\ , \\
\underline{0} &= H_\mu = \rho_0\ \underline{\mu}(t) + \underline{\lambda}_v^\top(t)\frac{\partial}{\partial\underline{\mu}}F(\underline{x},\underline{v},\underline{\rho},\underline{\mu},t) = \rho_0\ \underline{\mu}(t) + P\underline{\lambda}_v(t)
\end{aligned} \tag{4.17}$$

Together with the constrained Newton-Euler system and by recalling the definition of

H and F, a solvable second-order system of differential-algebraic equations is obtained

$$\begin{aligned}
\underline{\dot{x}}(t) &= K(\underline{x})\underline{v}(t) \\
M\underline{\dot{v}}(t) &= \underline{f}(\underline{x},\underline{v},t) + G^\top(\underline{x})\underline{\rho} + P^\top \underline{\mu} \ , \\
\underline{0} &= \underline{\Phi}(\underline{x}) \ , \\
\underline{\dot{\lambda}}_p(t) &= -\left[\frac{\partial}{\partial \underline{x}} K(\underline{x})\underline{v}(t)\right]^\top \underline{\lambda}_p(t) - \left[\frac{\partial}{\partial \underline{x}}\underline{f}(\underline{x},\underline{v},t) + \frac{\partial}{\partial \underline{x}} G^\top(\underline{x})\underline{\rho}\right]^\top \underline{\lambda}_v(t) \\
&- P^\top P\underline{x}(t) + P^\top \underline{h}(t) - G^\top(\underline{x})\underline{\kappa} \qquad (4.18) \\
M^\top \underline{\dot{\lambda}}_v(t) &= -K^\top(\underline{x})\underline{\lambda}_p(t) - \left[\frac{\partial}{\partial \underline{v}}\underline{f}(\underline{x},\underline{v},t)\right]^\top \underline{\lambda}_v(t) \\
\underline{0} &= G(\underline{x})\underline{\lambda}_v(t) \ .
\end{aligned}$$

Since

$$\left[\frac{\partial}{\partial \underline{x}}\left(K(\underline{x})\underline{v}(t)\right)\right]^\top \underline{\lambda}_p(t) = \left[\frac{\partial}{\partial \underline{x}}\underline{\dot{x}}(t)\right]^\top \underline{\lambda}_p(t) = \underline{0} \quad ,$$

the fourth equation can be simplified further to

$$\underline{\dot{\lambda}}_p(t) = -\left[\frac{\partial}{\partial \underline{x}}\underline{f}(\underline{x},\underline{v},t) + \frac{\partial}{\partial \underline{x}} G^\top(\underline{x})\underline{\rho}\right]^\top \underline{\lambda}_v(t) - P^\top P\underline{x}(t) + P^\top \underline{h}(t) - G^\top(\underline{x})\underline{\kappa}$$

System (4.18) is called *optimality system.* Together with the initial and terminal conditions

$$\begin{aligned}
\underline{x}(t_0) = \underline{x}_0 \quad &, \quad \underline{\dot{x}}(t_0) = \underline{v}_0 \ , \\
\underline{\lambda}_p(t_1) = P^\top \left[P\underline{x}(t_1) - \underline{h}(t_1)\right] \quad &, \quad \underline{\lambda}_v(t_1) = \underline{0} \ ,
\end{aligned} \qquad (4.19)$$

this forms a *forward-backward coupled system.* The control function, which represents the restraining forces due to the actuation, is obtained by the last equation in (4.17), i.e.

$$\underline{\mu}(t) = -\frac{1}{\rho_0} P \ \underline{\lambda}_v(t) \ . \qquad (4.20)$$

This equation will be referred to as *control equation.*

Remark 4.3
The holonomic constraints on the dual variable $\underline{\lambda}$, namely

$$\underline{0} = G(\underline{x})\underline{\lambda}_v(t) \ ,$$

disappear completely in the unrestrained case.

If there are no holonomic constraints on the primal variable $\underline{x}$, the Hamiltonian function (4.10) has no dependency on $\underline{\rho}$ and its variation with respect to $\underline{\rho}$ vanishes. .

4.1.1. Example: A single-body drive

Consider the single-body system from Chapter 3 and the piece-wise constant actuation signal from Subsection 3.2.2. No external forces are present, except the constant gravitational force denoted by $\underline{g}$. Furthermore no joints in form of scleronomic constraints are considered. The optimality system, which was deduced in the previous section, is then reduced to

$$\begin{aligned} \dot{\underline{x}}(t) &= K(\underline{x})\underline{v}(t), && (4.21)\\ M\dot{\underline{v}}(t) &= \underline{g} + P^\top \underline{\mu}\ , && (4.22)\\ \dot{\underline{\lambda}}_p(t) &= -P^\top P\underline{x}(t) + P^\top \underline{h}(t), && (4.23)\\ M^\top \dot{\underline{\lambda}}_v(t) &= -K^\top(\underline{x})\underline{\lambda}_p(t), && (4.24)\\ \rho_0\ \underline{\mu}(t) &= -P\ \underline{\lambda}_v(t)\ . && (4.25) \end{aligned}$$

The adjoint system is

$$\begin{aligned} \dot{\underline{\lambda}}_p(t) &= -P^\top P\underline{x}(t) + P^\top \underline{h}(t),\\ M^\top \dot{\underline{\lambda}}_v(t) &= -K^\top(\underline{x})\underline{\lambda}_p(t)\ , \end{aligned}$$

with terminal conditions

$$\underline{\lambda}_p(t_1) = P^\top \left[P\underline{x}(t_1) - \underline{h}(t_1)\right]\ ,\ \ \underline{\lambda}_v(t_1) = \underline{0}\ .$$

A time stepping scheme as seen in Subsection 3.1.1, only backwards in time, leads to

$$\begin{aligned} \frac{1}{h}\left[\underline{\lambda}_p(t_{k+1}) - \underline{\lambda}_p(t_k)\right] &= -P^\top \left[P\underline{x}(t_k) - \underline{h}(t_k)\right]\ ,\\ M^\top \frac{1}{h}\left[\underline{\lambda}_v(t_{k+1}) - \underline{\lambda}_v(t_k)\right] &= -K^\top(\underline{x}(t_k))\underline{\lambda}_p(t_k)\ . \end{aligned}$$

Inserting the the terminal conditions for the time interval $[t_k, t_{k+1}]$, namely

$$\underline{\lambda}_p(t_{k+1}) = P^\top \left[P\underline{x}(t_{k+1}) - \underline{h}(t_{k+1})\right]\ , \underline{\lambda}_v(t_{k+1}) = \underline{0}\ ,$$

leads to

$$\underline{\lambda}_p(t_k) = P^\top \left[P\underline{x}(t_{k+1}) - \underline{h}(t_{k+1})\right] + h\ P^\top \left[P\underline{x}(t_k) - \underline{h}(t_k)\right]\ , \tag{4.26}$$

and

$$\begin{aligned} \underline{\lambda}_v(t_k) &= h\ M^{-\top}K^\top(\underline{x}(t_k))\underline{\lambda}_p(t_k)\\ \underline{\lambda}_v(t_k) &= h\ M^{-\top}K^\top(\underline{x}(t_k))P^\top \left[P\underline{x}(t_{k+1}) - \underline{h}(t_{k+1}) + h\ \left[P\underline{x}(t_k) - \underline{h}(t_k)\right]\right] && (4.27) \end{aligned}$$

Using Equation (4.25), the generalized actuation forces at t_k can be calculated as follows

$$\begin{aligned} \rho_0\ \underline{\mu}(t_k) &= -P\ \underline{\lambda}_v(t_k) && (4.28)\\ \underline{\mu}(t_k) &= -\frac{h}{\rho_0}PM^{-\top}K^\top(\underline{x}(t_k))P^\top \left[P\underline{x}(t_{k+1}) - \underline{h}(t_{k+1}) + h\ \left[P\underline{x}(t_k) - \underline{h}(t_k)\right]\right]\ . \end{aligned}$$

With this approximation of $\underline{\mu}$ at time t_k, the primary system

$$\begin{aligned} \underline{\dot{x}}(t) &= K(\underline{x})\underline{v}(t), \\ M\underline{\dot{v}}(t) &= \underline{g} + P^\top \underline{\mu}\ , \end{aligned} \tag{4.29}$$

can now be solved with the partitioned linear-implicit Euler algorithm from Subsection 3.1.1.

4.1.2. Numerical results

Numerical experiments were carried out in order to approximate the curve given in Figure 3.3. A constant time step size $h = 0.001$ was used, combined with an uniform refinement $\frac{h}{2^n}, n \in \{0, 1, 2\}$.

The only force applied was the gravitation in the negative direction of the third, translative component.

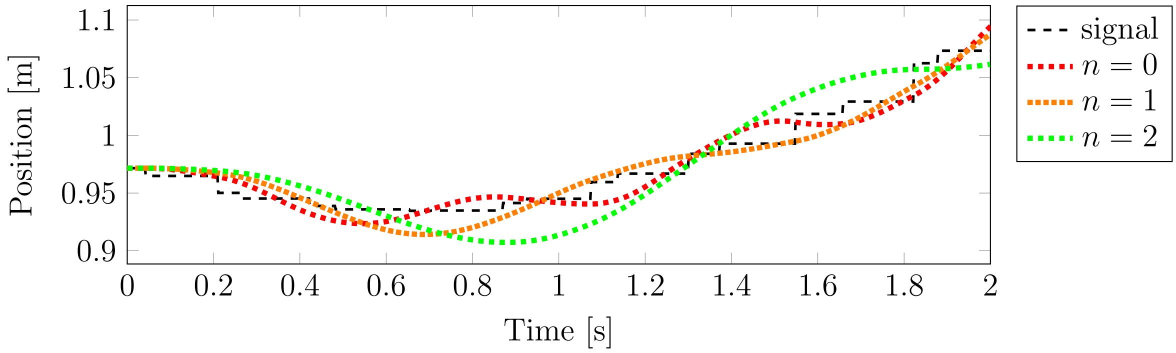

Figure 4.1.: Results for the x-component of the position. $\rho_0 = 1\mathrm{e} - 5$.

Figure 4.1 shows the results for the first translative component, with a regularization $\rho_0 = 1\mathrm{e} - 5$ and increasing refinement. Higher refinement leads to a smoother curve. This is more evident when inspecting the velocity profile in Figure 4.2. But it leads to cancellations of the order of the regularization, according to Equation (4.28). A finer time step size demands a finer regularization parameter.

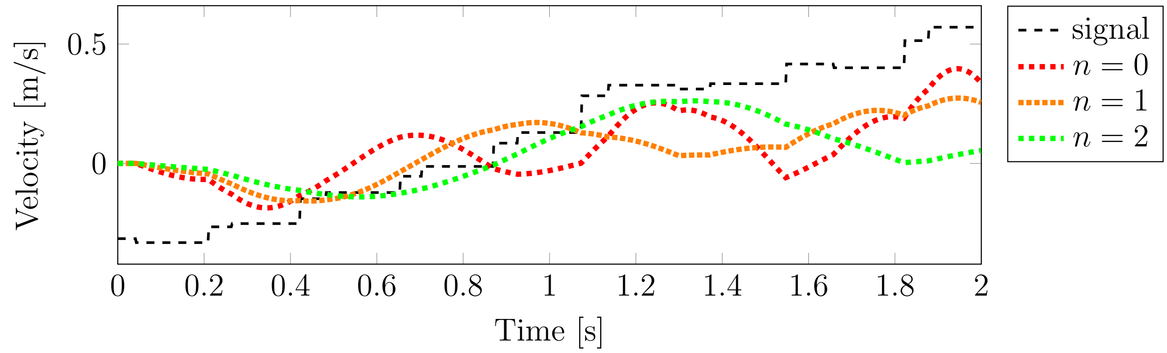

Figure 4.2.: Results for the x-component of the velocity. $\rho_0 = 1\mathrm{e} - 5$.

The body is at rest at time $t = 0$, i.e. $\underline{v}_0 = \underline{0}$. The controller velocity was approximated on the coarser grid representing the moments in time the position was updated.

Since the optimal control approach does not strictly restrain the solution to a manifold defined by the actuation

$$\underline{\Psi}(\underline{x},t) = P\underline{x}(t) - \underline{h}(t) = \underline{0} \ ,$$

the discrepancy between the initial velocity values is not essential. The presented optimal control approach in general effects solely the positional level, since the derivatives of the rheonomic constraint equation do not appear. Figure 4.2 serves for comparisons.

Figure 4.3 shows a conflict between the gravitational force and the actuation force. The regularisation parameter can be refined further, as seen in Figure 4.4. Too small regularization parameters cause an oscillatory behaviour though.

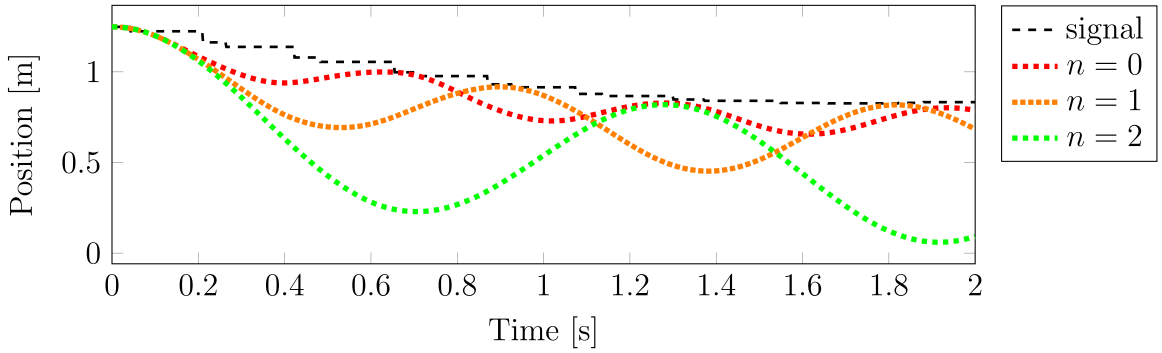

Figure 4.3.: Results for the z-component of the position. $\rho_0 = 1\mathrm{e} - 5$.

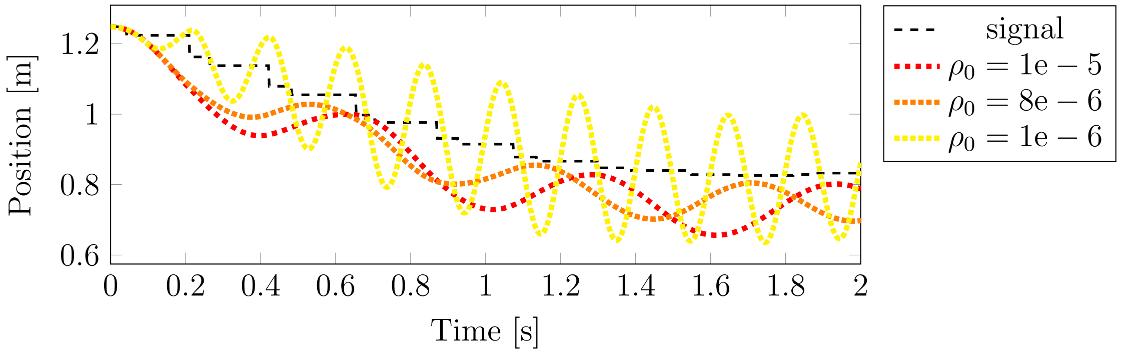

Figure 4.4.: Results for the z-component of the position. $n = 0$.

The current approach has the following three issues:

Firstly, the minimization process for each time interval $[t_k, t_{k+1}]$ is almost completely decoupled. Only the initial conditions $\underline{x}(t_k)$ and $\underline{v}(t_k)$, which are the results from the previous time step, are used. Especially for $\underline{\mu}$ this results in the discrepancy, that $\underline{\mu}(t_k)$ has different values, depending on the considered interval, $[t_{k-1}, t_k]$ or $[t_k, t_{k+1}]$. The control parameters $\underline{\mu}$ are therefore globally discontinuous in time. This leads to $\underline{v}$ being the integral of a globally discontinuous function.

Secondly, a linear-implicit algorithm according Section 3.1.1 can strictly speaking not be applied. It holds

$$\underline{\mu}(t_{k+1}) = -\frac{1}{\rho_0} P \ \underline{\lambda}_v(t_{k+1}) = \underline{0}$$

in each time step. In a correct algorithm, there would be no actuation forces in the discrete finite difference scheme, where the right-hand side is evaluated at t_{k+1}. Therefore a mixed scheme has to be applied, where $\underline{\mu}(t_k)$ instead of $\underline{\mu}(t_{k+1})$ is used.

Thirdly and finally, there is a conflict between actuation forces obtained by the adjoint variable and both constant and solely time dependent forces. The right-hand side of the adjoint system consists of partial derivatives of the Hamiltonian with respect to $\underline{x}$ and $\underline{v}$ of the right-hand side of the primal system. This completely cancels out the effects of constant and time dependent forces onto the adjoint system. Additional treatment is necessary.

4.2. $\mathcal{H}^1$-regularization

In order to tackle some of the problems mentioned at the end of Subsection 4.1.2, another kind of actuation is introduced. Recall Equation (4.8)

$$J_1(\underline{x}) = J_0(\underline{x}) + \frac{\rho_0}{2} \, \|\underline{\mu}\|^2_{L^2(t_0,t_1)} \ ,$$

and add an additional penalization for the derivative of $\underline{\mu}$, i.e.

$$J_1(\underline{x}) = J_0(\underline{x}) + \frac{\rho_0}{2} \, \|\underline{\mu}\|^2_{L^2(t_0,t_1)} + \frac{\rho_1}{2} \, \|\underline{\dot{\mu}}\|^2_{L^2(t_0,t_1)} \ . \tag{4.30}$$

This represents a regularization using a weighted *Sobolev* norm including derivatives up to order 1, namely the $\mathcal{H}^1$-norm. The last term can be integrated by parts and leads to

$$J_1(\underline{x}) = J_0(\underline{x}) + \int\limits_{t_0}^{t_1} \frac{\rho_0}{2} \, \underline{\mu}^\top(t)\underline{\mu}(t)\mathrm{dt} + \left[\frac{\rho_1}{2} \, \underline{\dot{\mu}}^\top(t)\underline{\mu}(t)\right]_{t_0}^{t_1} - \int\limits_{t_0}^{t_1} \frac{\rho_1}{2} \, \underline{\ddot{\mu}}^\top(t)\underline{\mu}(t)\mathrm{dt} \ . \tag{4.31}$$

Performing the same steps as in Section 4.1 yields the new control equation

$$-\rho_1\underline{\ddot{\mu}}(t) + \rho_0\underline{\mu}(t) = -P\underline{\lambda}_v(t) \ , \tag{4.32}$$

which is a second-order ODE also known as the one-dimensional *Yukawa equation.*

There are two ways to choose the boundary condition.

One can demand homogeneous Neumann boundary conditions

$$\underline{\dot{\mu}}(t_0) = \underline{\dot{\mu}}(t_1) = \underline{0} \ , \tag{4.33}$$

which will cancel out the boundary term in (4.31).

Since $[t_0, t_1]$ represents the interval of a time stepping scheme, one can also use the approximation of the previous time step at the right interval end for a Dirichlet boundary condition on the left interval end of the current time step. This results in mixed boundary conditions of the form

$$\underline{\mu}(t_0) = \underline{\tilde{\mu}} \ , \quad \underline{\dot{\mu}}(t_1) = \underline{0} \ . \tag{4.34}$$

Both approaches eliminate the problem of having to rely on a hybrid time stepping scheme, since $\underline{\mu}(t_1)$ is not automatically zero and can be evaluated after solving (4.32).

The later one with mixed boundary conditions assures further, that $\underline{\mu}$ is a globally continuous function.

The solution to both types of problems can be approximated with a *Finite-Element approach*. This is shown in Appendix B. For each component of $\underline{\mu}$ a small FE system is derived and has to be solved. Since at each time step the value for $-P\underline{\lambda}_v(t)$ is given only at the interval ends, they have to be interpolated in order to gain a right-hand side for (4.32). A linear interpolation yields the function

$$\underline{f}(t) = -P\underline{\lambda}_v(t_0) + \frac{P\underline{\lambda}_v(t_0)}{t_1 - t_0}\,(t - t_0)\ . \tag{4.35}$$

Here the terminal condition $P\underline{\lambda}_v(t_1) = \underline{0}$ has already been used.

4.2.1. Control equation with homogeneous Neumann boundary conditions

On a time interval $E_k = [t_k, t_{k+1}]$, each component of $\underline{\mu}$ can be obtained by solving

$$\begin{aligned} -\rho_1 \ddot{\mu}_l + \rho_0 \mu_l &= f_l(t)\ ,\ l = 1, \dots, n_A\ , \\ \dot{\mu}_l(t_k) = \dot{\mu}_l(t_{k+1}) &= 0\ , \end{aligned} \tag{4.36}$$

where $f_l(t)$ represents a component of the vector valued function in (4.35). In Section B.2 the following FE system on a transformed interval was constructed

$$\left(\rho_1 \frac{1}{h_k}\ B + \rho_0\ h_k\ C\right) \underline{\mu}_l = \underline{f}_{l;h_k}\ , \tag{4.37}$$

Each component of the right-hand side is calculated as follows

$$f_{l,i;h_k} = F(S_{i,2;h_k}) = \int_{\frac{h_k}{4}}^{\frac{5h_k}{4}} f_l(\widetilde{t})\ S_{i,2;h_k}(\widetilde{t})\ \mathrm{d}\widetilde{t}\ ,\ i = 0, \dots, 5\ . \tag{4.38}$$

The values of the right-hand side can be simplified further, since $f_l(t)$ is a known linear function

$$f_l(t) = f_l(t_k) - \frac{f_l(t_k)}{h_k}\left(t - \frac{h_k}{4}\right)$$

. By integration by substitution and by (B.9) it holds for $\widetilde{t} = h_k t$

$$\begin{aligned} f_{l,i;h_k} &= \int_{\frac{h_k}{4}}^{\frac{5h_k}{4}} \left(f_l(t_k) - \frac{f_l(t_k)}{h_k}\left(\widetilde{t} - \frac{h_k}{4}\right)\right)\ S_{i,2;h_k}(\widetilde{t})\ \mathrm{d}\widetilde{t} \\ &= \int_{\frac{1}{4}}^{\frac{5}{4}} \left(f_l(t_k) - \frac{f_l(t_k)}{h_k}\left(h_k t - \frac{h_k}{4}\right)\right)\ S_{i,2;h_k}(h_k t)\ h_k \mathrm{d}t \\ &= f_l(t_k)\ h_k\ \left(\frac{5}{4}\int_{\frac{1}{4}}^{\frac{5}{4}} S_{i,2}(t)\ \mathrm{d}t - \int_{\frac{1}{4}}^{\frac{5}{4}} t\ S_{i,2}(t)\ \mathrm{d}t\right) \end{aligned}$$

The right-hand side for each FE system can therefore be simply computed by

$$\underline{f}_{l;h_k} = f_l(t_k)\; h_k\; \underline{d}\;, \;\; l = 1, \dots, n_A, \tag{4.39}$$

where $\underline{d}$ is a constant vector independent of h_k and with components

$$d_i = \frac{5}{4} \int\limits_{\frac{1}{4}}^{\frac{5}{4}} S_{i,2}(t)\; \mathrm{d}t - \int\limits_{\frac{1}{4}}^{\frac{5}{4}} t\; S_{i,2}(t)\; \mathrm{d}t\;,\;\; i = 0, \dots, 5\;.$$

The stiffness matrix in (4.37) has to be computed and inverted only once per time step. Similar to the circumstance described in Subsection 4.1.2, the regularization parameters have to be chosen very small. Especially ρ_1, since the factor $\frac{1}{h_k}$ cancels out orders of the parameter for $0 < h_k \ll 1$.

This regularization approach was applied to the example in Subsection 4.1.1 and the results are presented in the following. The time step size was again set to be constantly $h = 1\mathrm{e}-3$.

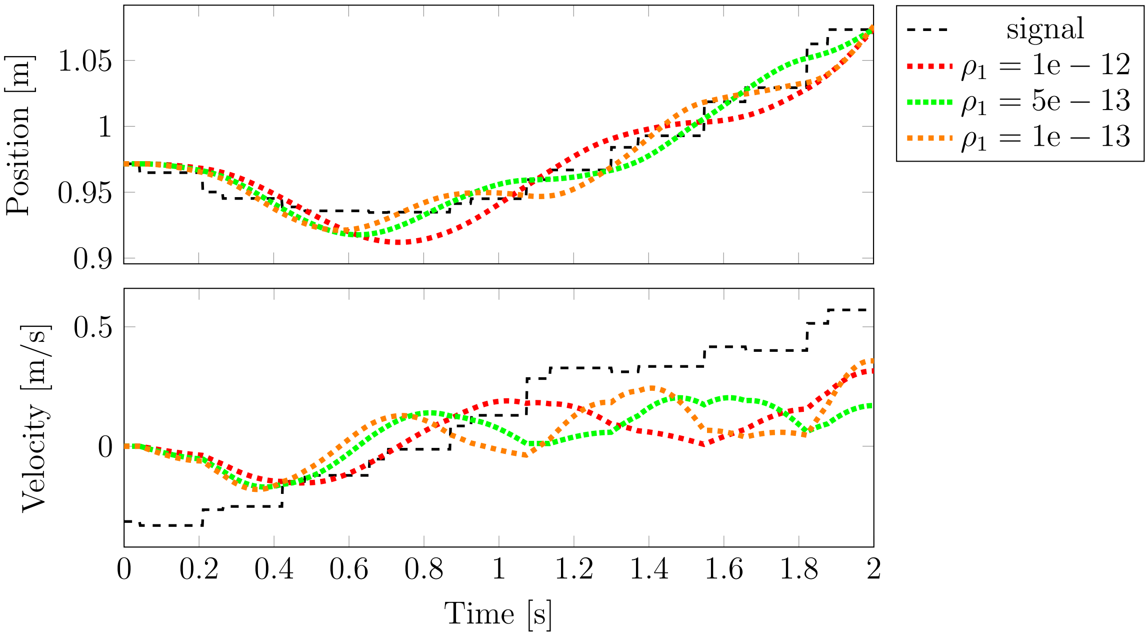

Figure 4.5.: Results for the x-component with one fixed regularization parameter $\rho_0 = 1\mathrm{e}-6$ and constant time step size $h = 1\mathrm{e}-3$.

Figure 4.5 shows the results for varying ρ_1 and fixed ρ_0. In terms of smoothness, the choice $\rho_1 = 5\mathrm{e}-13$ showed visually the best result. For Figure 4.6 ρ_1 was fixed and ρ_0 varied. It is interesting to observe, that for $\rho_0 = 1\mathrm{e}-5$ the best approximating curve was obtained. The quality deteriorates when downsizing to $5\mathrm{e}-6$, but recovers when taking an even smaller parameter. This indicates that there is an optimal choice of the parameter, which does not necessarily have to be small. As in every case so far, the velocity profile becomes less smooth when the position approximates the signal the best.

In Figure 4.7 it is evident, that decreasing ρ_0 beyond a point does not change the result noticeably. Then the parts containing ρ_1 become more dominant. It is different, when ρ_0 is fixed and ρ_1 is reduced consecutively. In this case the quality of the approximation only deteriorates further, as seen in Figure 4.8

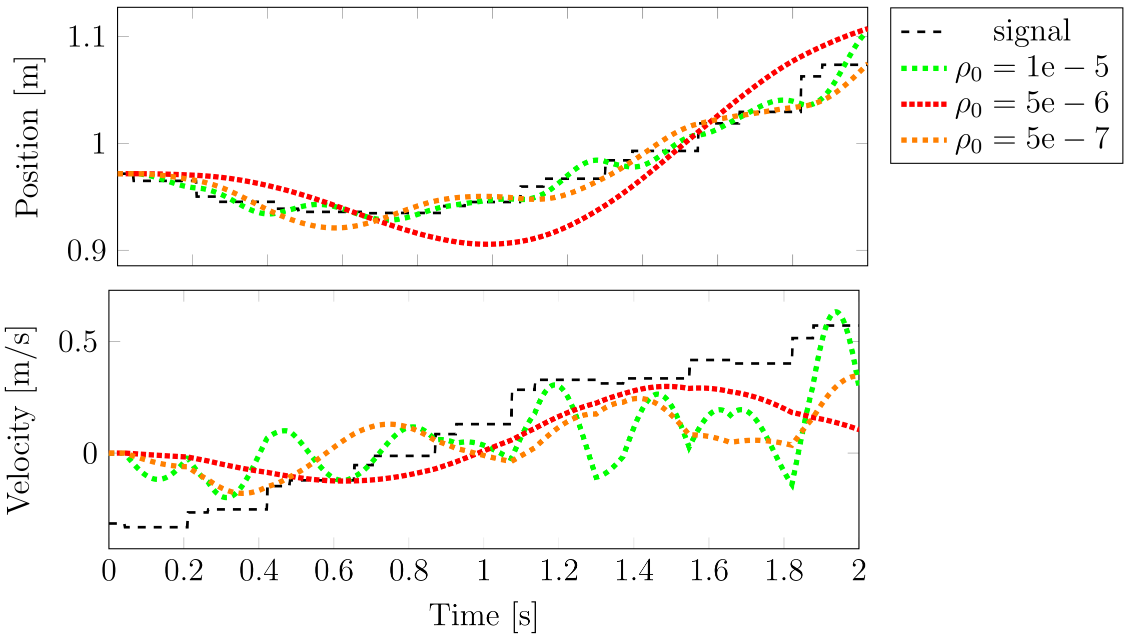

Figure 4.6.: Results for the x-component. $\rho_1 = 5e-13$. $h = 1e-3$.

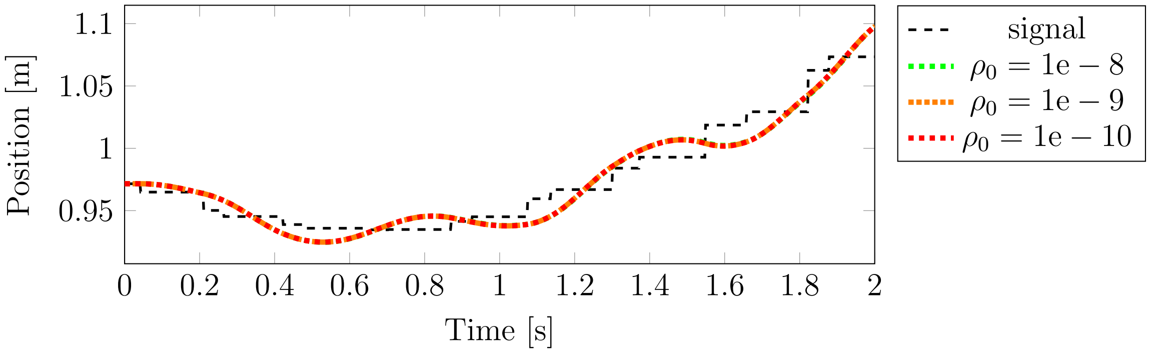

Figure 4.7.: Results for the x-component. $\rho_1 = 5e-13$. $h = 1e-3$.

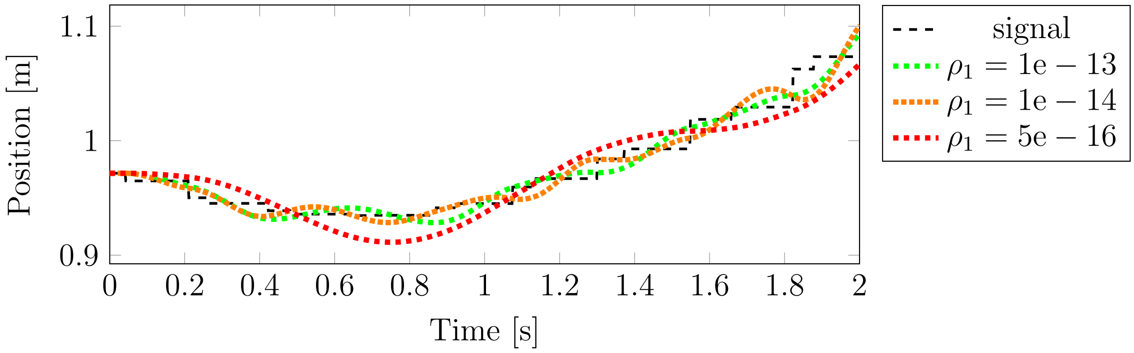

Figure 4.8.: Results for the x-component. $\rho_0 = 5e-7$. $h = 1e-3$.

4.2.2. Control equation with mixed boundary conditions

The time stepping scheme, which extracts the signal value at a new time, namely the controller position, is an overlaying method. In each time step and therefore on each time step interval, the control equation has to be solved separately. Since it is globally one simulation and since globally the velocity is an integral of the generalized actuation force $\underline{\mu}$, (Lipschitz-) continuity assumptions for $\underline{\mu}$ have to be made. By using the approximation calculated on the previous time step interval, the possibility to use this data for the current time step pops up. Let $\underline{\mu}_k$ be the approximation of $\underline{\mu}$ on the time interval $E_k = [t_k, t_{k+1}]$. Evaluating $\underline{\mu}_{k-1}(t_k)$ leads to the opportunity to require

$$\underline{\mu}_k(t_k) = \underline{\mu}_{k-1}(t_k)$$

for the next time step. Now the boundary term in (4.31) can be eliminated by setting mixed boundary conditions in the form of

$$\underline{\mu}_k(t_k) = \underline{\mu}_{k-1}(t_k)\ ,\ \ \dot{\underline{\mu}}_k(t_{k+1}) = \underline{0}\ , \tag{4.40}$$

for the control equation on E_k. The task now is to solve

$$\begin{aligned} -\rho_1 \ddot{\mu}_l + \rho_0 \mu_l &= f_l(t)\ ,\ l = 1, \ldots, n_A\ , \\ \mu_l(t_k) = \tilde{\mu}_l\ ,\ \ \dot{\mu}_l(t_{k+1}) &= 0\ , \end{aligned} \tag{4.41}$$

for each component μ_l of $\underline{\mu}$. In Section B.3 a way to construct a fitting FE system using the Neumann case is shown. It leads to a FE system of the form

$$\left[\rho_1 \frac{1}{h_k}\ \tilde{B} + \rho_0\ h_k\ \tilde{C}\right] \underline{\mu}_l = f_l(t_k)\ h_k\ \underline{\tilde{d}} - \tilde{\mu}_l \left[\tilde{c}\left[\rho_1 \frac{1}{h_k}\ \underline{b}_0 + \rho_0\ h_k\ \underline{c}_0\right] + \rho_1 \frac{1}{h_k}\ \underline{b}_1 + \rho_0\ h_k\ \underline{c}_1\right].$$

The vector

$$\underline{a}_D := \left[\tilde{c}\left[\rho_1 \frac{1}{h_k}\ \underline{b}_0 + \rho_0\ h_k\ \underline{c}_0\right] + \rho_1 \frac{1}{h_k}\ \underline{b}_1 + \rho_0\ h_k\ \underline{c}_1\right]$$

needs to be calculated only once per time step and represents the Dirichlet extension onto E_k. The calculation of $\underline{b}_0, \underline{b}_1, \underline{c}_0$, and $\underline{c}_1$ is shown in Equation (B.37) and following. The matrices $\tilde{B}$, $\tilde{C}$ and the vector $\underline{\tilde{d}}$ represent the remaining components of B, C and $\underline{d}$ from the previous section, after the elements containing the first two splines were excluded. These two splines were used for the Dirichlet extension in $\underline{a}_D$. The mixed boundaries FE system

$$\left(\rho_1 \frac{1}{h_k}\ \tilde{B} + \rho_0\ h_k\ \tilde{C}\right) \underline{\mu}_l = f_l(t_k)\ h_k\ \underline{\tilde{d}} - \tilde{\mu}_l\ \underline{a}_D \tag{4.42}$$

is a solvable system of 4 linear equations.

Figure 4.9 shows the results for fixed ρ_1 and varying ρ_0. Fitting parameters for the mixed problem were found to be up to two orders bigger than for the Neumann problem. The curves are in general visually smoother. Figures 4.10 and 4.11 indicate though, that the tolerance towards the choice of parameters is smaller compared to the Neumann problem. Independent of the direction in which the parameters are varied, the quality of the approximation deteriorates.

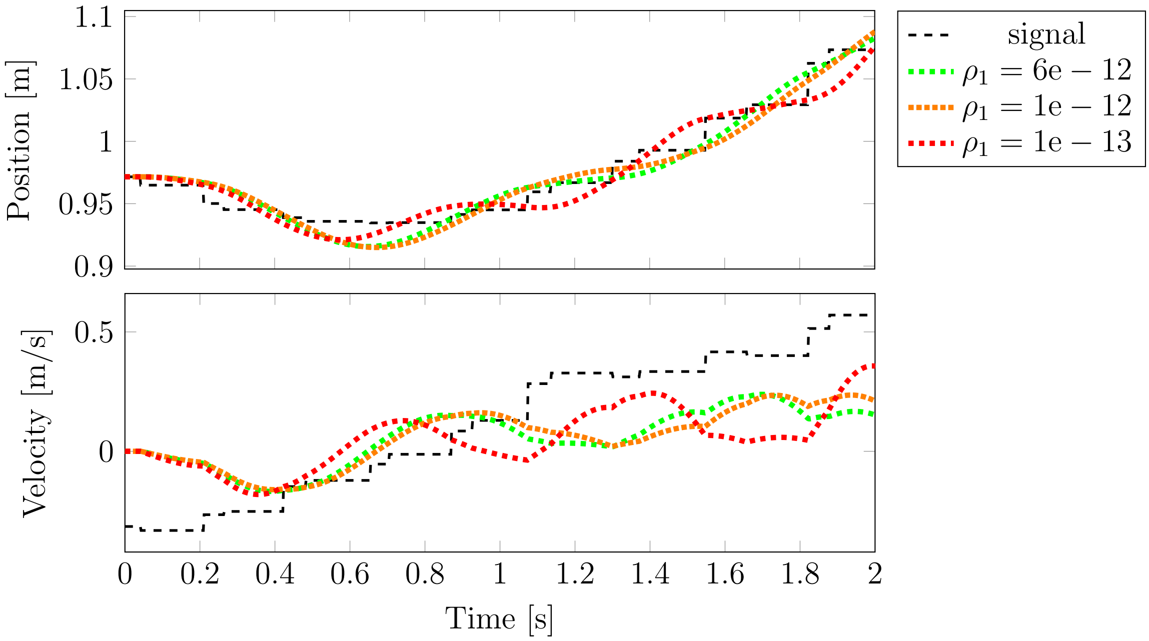

Figure 4.9.: Results for the x-component. $\rho_0 = 5e - 6$. $h = 1e - 3$.

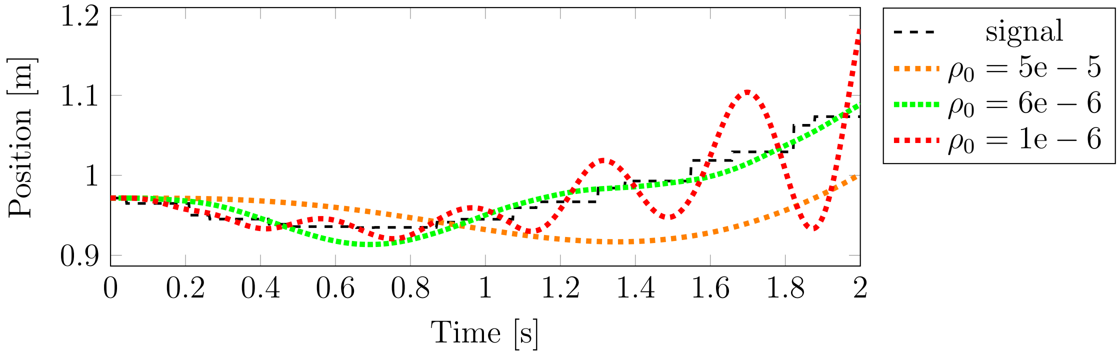

Figure 4.10.: Results for the x-component. $\rho_1 = 6e - 12$. $h = 1e - 3$.

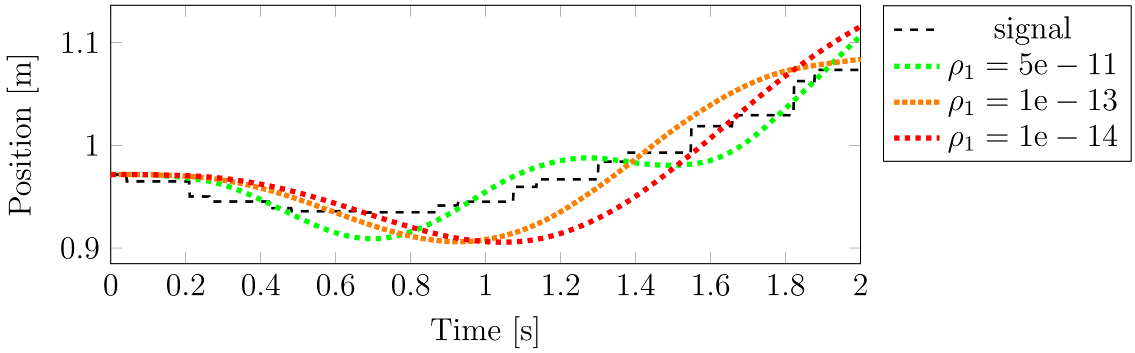

Figure 4.11.: Results for the x-component. $\rho_0 = 6e - 6$. $h = 1e - 3$.

4.3. Treatment of constant and time-dependent forces

The Neumann problem avoids the circumstance of having to use a not strictly linear-implicit algorithm. The mixed approach additionally assures globally continuous actuation forces and smoother results, but shows less stability in terms of regularization parameters and their choice. Both approaches though are still incompatible with constant and time-dependent forces, e.g., the gravity (see Figure 4.12).

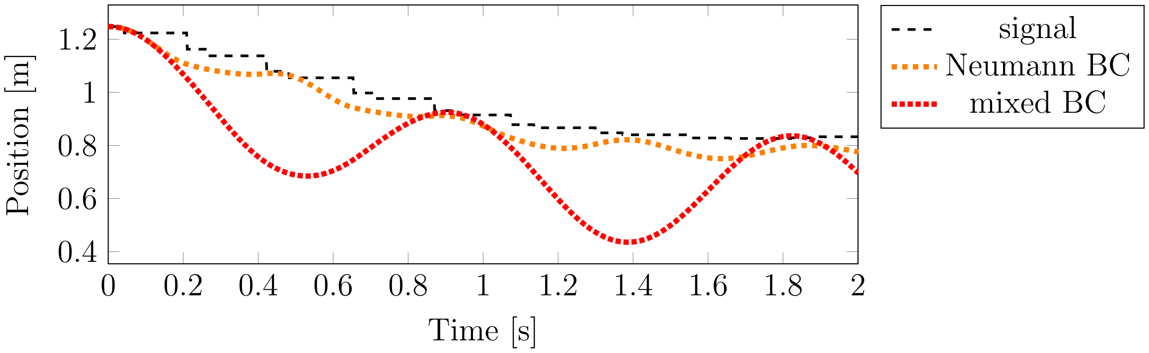

Figure 4.12.: Results for the z-component. Gravity causes large oscillations.

Consider the Newton-Euler equation

$$M\underline{\dot{v}}(t) = \underline{f}(\underline{x},\underline{v}) + \underline{\hat{f}}(t) + P^\top \underline{\mu} \; . \tag{4.43}$$

$\underline{\hat{f}}(t)$ contains all forces which are either constant or solely time-dependent. These forces do not appear in the adjoint system, since the partial derivatives of the Hamiltonian H cancel out all terms not related to $\underline{x}$ or $\underline{v}$. From a mechanical point of view it is clear, that the actuating forces applied to a body have to cancel out all other forces and additionally push towards the desired state. The idea now is to add zero to Equation (4.43) in the form of

$$M\underline{\dot{v}}(t) = \underline{f}(\underline{x},\underline{v}) + \underline{\hat{f}}(t) \pm P^\top P\underline{\hat{f}}(t) + P^\top \underline{\mu} \; . \tag{4.44}$$

Using the transformation

$$\underline{\hat{\mu}} = \underline{\mu} + P\underline{\hat{f}}(t) \; , \tag{4.45}$$

Equation (4.44) can be rewritten as

$$M\underline{\dot{v}}(t) = \underline{f}(\underline{x},\underline{v}) + \underline{\hat{f}}(t) - P^\top P\underline{\hat{f}}(t) + P^\top \underline{\hat{\mu}} \; . \tag{4.46}$$

Applying all steps and regularizations as discussed so far leads to a control equation for $\underline{\hat{\mu}}$, namely

$$-\rho_1\underline{\ddot{\hat{\mu}}}(t) + \rho_0\underline{\hat{\mu}}(t) = -P\underline{\lambda}_v(t) \; . \tag{4.47}$$

Inserting transformation (4.45) leads to a perturbed control equation for the original actuation forces

$$-\rho_1\underline{\ddot{\mu}}(t) + \rho_0\underline{\mu}(t) = -P\underline{\lambda}_v(t) + \rho_1\; P\underline{\ddot{\hat{f}}}(t) - \rho_0\; P\underline{\hat{f}}(t) \; . \tag{4.48}$$

The boundary conditions also change due to the transformation.

$$\dot{\hat{\underline{\mu}}}(t_k) = 0 \quad \Leftrightarrow \quad \dot{\underline{\mu}}(t_k) = -P\dot{\hat{\underline{f}}}(t_k) \ ,$$

$$\hat{\underline{\mu}}(t_k) = \underline{\mu}_D \quad \Leftrightarrow \quad \underline{\mu}(t_k) = \underline{\mu}_D - P\hat{\underline{f}}(t_k) \ .$$

If $\hat{\underline{f}}(t)$ is constant and represents only the gravitational forces f.e., the Neumann problem yields useful results. The perturbation on the right-hand side of (4.48) is sufficiently scaled down due to the regularization parameter, as evident in Figure 4.13. The mixed formulation showed to be unsuitable. Though the approximation does not show drift-offs as in Figure (4.12), the changes in the Dirichlet data cause smaller and more rapid oscillations.

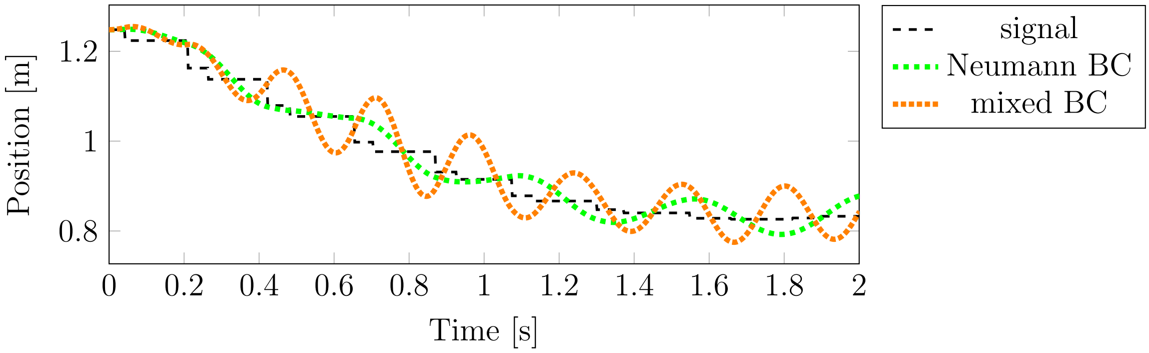

Figure 4.13.: Results for the z-component. Perturbed equation. $\rho_0 = 5\text{e} - 7$. $\rho_1 = 1\text{e} - 13$.

At this point it is clear, that the changes in the right-hand side of the control equation and the boundary conditions can simply be left out. This way the original control equation is solved and the results will be the same as for the other components (x and y). This is equal to only adding $-P^\top P\hat{\underline{f}}(t)$ to Equation (4.43), i.e. simply cancelling all constant and time-dependent forces for all actuated components by adding this term to $P^\top \underline{\mu}$ *after* solving the control equation. Though it is a manipulative interference with the algorithm, it leads to the desired results.

5. Conclusion

In this thesis the modelling process for multibody systems was summarized, as well as how to implement it generally using an object oriented approach. When exerting control onto components of the system, the quality of the signal is crucial. Discontinuous signals lead to non-converging numerical results when applying standard ODE solvers. Despite using stabilization techniques, large errors occur around the points of discontinuity. This problem was solved by introducing an optimal control approach and formulating the servo constraints as a functional, which has to be minimized. Since in this thesis' application the signal is extracted in real time, an overlaying time stepping scheme was constructed and an optimal control algorithm, namely a single stage control, was applied at each step in order to reach the target minimum. Driving forces were introduced into the Newton-Euler system as control functions and regularization was applied using either the L^2-norm or a weighted $\mathcal{H}^1$-norm for the control functions. While satisfying results can be achieved using only the L^2-norm, an extension to $\mathcal{H}^1$ has more benefits. The development of the approximating curve can be regulated more precisely, since the time derivative of the control function also appears in the functional. Visually better results can be achieved. The drawback is a higher computational effort. Finally a way to handle constant and time-dependent disturbance functions, such as gravity, was presented. The forces were cancelled out by adding their complements to the control functions and applying the technique to the transformed control.

By the presented approach, a way to enable simulations in real time was shown. A simple overlaying time stepping scheme ensures a fast progress in time and the optimal control approach in each time step assures a controllable error development. Choosing a fitting time step size and proper regularization parameters can guarantee sufficient overall accuracy. The assumptions for the signal function were reduced to an extent, were boundedness is sufficient. Hence the requirements stated in the thesis introduction can be met.

In terms of regularization parameters, the tests conducted in Chapter 4 imply, that there is an optimal choice of them. Varying the parameters has shown, that imposing stronger regularization is futile beyond a certain point and the choice has to be made specific. This thesis lays a path to further analysis for finding this optimal choice. The possibility to improve the results by using a dynamic and optimal choice of the parameters comes up.

In terms of efficiency, further work can be done too. As stated in the modelling process in Chapter 1, the formulation was conducted in absolute coordinates. Using the parametrization of the state manifold, one can reformulate the problem and reduce thereby the amount of degrees of freedom, which results in smaller systems of ordinary differential equations which have to be solved. When solving the adjoint system presented in Section 4.1, higher order derivatives of the force laws and constraint equations have to be computed. These calculations are cumbersome and expensive. Introducing *algorithmic differentiation* can simplify this process.

Bringing this to a close, there are still open issues around the signal functions. The signal functions appearing in this thesis' application were of piecewise constant nature and the jumps at the points of discontinuity are manageable. Increasing the size of the jumps, i.e. having to deal with a worsening signal, might lead to solvability issues or to oscillatory behaviour in the approximating curve. It is therefore possible, that the requirement of boundedness might not suffice and that a measure of discontinuity or variation gets involved for functions of more general nature. Further analysis is also necessary here.

Taking all these steps will enable simulation engineers to use modern technology for the simulation and assessment process. The Virtual Reality controllers presented here are a first step. Augmented Reality software provides the possibility to use hand gestures in order to interact with the surroundings. Extracting the signal from these gestures, such es positions of fingers or rotation of the hand, is a challenging task on its own. Being able to use these signals for simulations, like applying torque to a beam or in this case manoeuvring multibody systems like robot arms, can be the next step in industrial applications. Tackling this problem is a highly interesting and likely rewarding task.

A. Some models of joints

The modelling of joints can follow different aspects. A. Shabana [17] uses the contact surface between two bodies and its measure to categorize them. Depending on weather the contact surface is two-dimensional, a line, a curve or a point, the complexity can vary. C. Wörnle [20] uses the terminology of *elemental joints*. He introduces for starters 4 elemental types of bindings, which are based solely on geometric concepts. What all categorizations have in common is, that they describe the freedom of movement of the two linked bodies, relative to each other. This aspect is described by the *degree of freedom of the joint*, noted by f_G.

If two rigid bodies are represented by vectors in $\mathbb{R}^6$, $\underline{x}_1$ and $\underline{x}_2$ respectively, a mapping from $\underline{x}_1$ to $\underline{x}_2$ can involve up to 6 additional scalar variables, represented by a vector $\underline{y}$, as seen in Section 1.3, Example 1.3. The minimal amount of *necessary* variables represents the degree of freedom f_G. By Theorem 1.4, $(6 - f_G)$ independent equations are necessary to describe the manifold implicitly, which is parametrized by $\underline{y}$. The respective algebraic constraints therefore are a mapping

$$\begin{aligned} \underline{\Phi} \; : \; \mathbb{R}^{12} &\;\to\; \mathbb{R}^{6-f_G} \;, \\ \underline{x} := \left[\underline{x}_1^\top, \underline{x}_2^\top\right]^\top &\;\mapsto\; \underline{\Phi}(\underline{x}) \;. \end{aligned}$$

Elemental joints represent constraints, which do not change over time, i.e. scleronomic and holonomic constraints. In the following three different elemental joints are introduced. The implicit constraint equations are related to the restriction of movement and the implicit constraint matrices are derived.

A.1. Revolute joint

The revolute joints allows a a single rotational movement between two bodies around a predefined axis [20, Subsec. 6.4.4]. All translational, relative movements are locked and the relative spatial rotation is limited from three to a single axis. This already gives an idea of how the constraint equations are designed: Three equations are necessary in order to lock the translational movement and another two to disable rotations about two axes independent of the joint axis.

Let $\underline{a}(t)$ be the joint axis and let P denote the *point of articulation*. Let further $\underline{x}_{\mathrm{t},i}(t), R_i(t)$ denote the position and orientation of two rigid bodies, where $i \in \{1, 2\}$. The matrices $R_i(t) = R_i(\underline{w}_i(t))$ represent rotation matrices as discussed in Chapter 1. The point P is not necessarily an element of one of the two rigid bodies, it represents the point of reference for the relative movement between them. Let $\underline{x}_P(t)$ denote the position of P in the reference system. Since only rigid bodies are considered, there exist two constant vectors $\underline{p}_1$ and $\underline{p}_2$, where

$$\underline{p}_i = R_i^\top(0) \left[\underline{x}_P(0) - \underline{x}_{\mathrm{t},i}(0)\right] \;, \; i \in \{1, 2\}.$$

They represent the position vector of P at time $t=0$ in the body-fixed frames of reference represented by the body positions and orientations.

The first constraint, which are in fact 3 scalar equations, is the translational lock: There are no translational movements of any body with respect to the point P

$$\underline{x}_{\mathrm{t},1}(t) + R_1(t)\ \underline{p}_1 = \underline{x}_{\mathrm{t},2}(t) + R_2(t)\ \underline{p}_2\ ,\ \forall t \geq 0\ .$$

For the rotational constraints, take any two unit vectors spanning the plain orthogonal to the joint axis $\underline{a}(t)$. Let $\underline{b}(t)$ and $\underline{c}(t)$ denote those vectors. By calculating their coordinates with respect to the body frames given at time $t=0$

$$\begin{array}{rcl} \underline{a}_2 & = & R_2^\top(0)\ \underline{a}(0)\ , \\ \underline{b}_1 & = & R_1^\top(0)\ \underline{b}(0)\ , \\ \underline{c}_1 & = & R_1^\top(0)\ \underline{c}(0)\ , \end{array}$$

One can lock any rotation except about the joint axis by demanding

$$\begin{array}{rcl} R_1(t)\underline{b}_1 \cdot R_2(t)\underline{a}_2 & = & 0\ , \\ R_1(t)\underline{c}_1 \cdot R_2(t)\underline{a}_2 & = & 0\ , \end{array} \forall t \geq 0\ .$$

The algebraic equation are therefore given by

$$\begin{array}{rcl} \underline{\Phi}\ :\ \mathbb{R}^{12} & \to & \mathbb{R}^5\ , \\ \underline{x} & \mapsto & \left[\begin{array}{c} \underline{x}_{\mathrm{t},2}(t) + R_2(t)\ \underline{p}_2 - \underline{x}_{\mathrm{t},1}(t) - R_1(t)\ \underline{p}_1 \\ R_1(t)\underline{b}_1 \cdot R_2(t)\underline{a}_2 \\ R_1(t)\underline{c}_1 \cdot R_2(t)\underline{a}_2 \end{array} \right]\ , \\ \underline{\Phi}(\underline{x}) & = & \underline{0}\ ,\ \forall t \geq 0\ . \end{array}$$

The manifold of admissible states for each body with respect to the other body is a circle in the plain perpendicular to $\underline{a}$ and with P as its middle point.

The respective implicit constraint matrix is obtained by taking the derivative of $\underline{\Phi}$ with respect to t. For the translational lock one obtains

$$\left[-I\ ,\ \widetilde{R_1(t)\ \underline{p}_1}\ ,\ I\ ,\ -\widetilde{R_2(t)\ \underline{p}_2} \right]\ \underline{v}(t) = 0\ .$$

In order to obtain this form, the equality

$$\underline{a} \times \underline{b} = -\underline{b} \times \underline{a}$$

for two vectors $\underline{a}, \underline{b} \in \mathbb{R}^3$ was used. The operator $\widetilde{\cdot}$ denotes the skew-symmetric matrix, which represents the outer product with a vector, i.e

$$\underline{a} \times \underline{b} = \widetilde{\underline{a}}\ \underline{b}\ .$$

For the rotational constraints it holds

$$\begin{array}{rcl} \dfrac{\mathrm{d}}{\mathrm{dt}}\left(R_1(t)\underline{b}_1 \cdot R_2(t)\underline{a}_2\right) & = & \dfrac{\mathrm{d}}{\mathrm{dt}}\left(R_1(t)\underline{b}_1\right) \cdot R_2(t)\underline{a}_2 + R_1(t)\underline{b}_1 \cdot \dfrac{\mathrm{d}}{\mathrm{dt}}\left(R_2(t)\underline{a}_2\right) \\ & = & \left(\underline{\omega}_1(t) \times R_1(t)\underline{b}_1\right) \cdot R_2(t)\underline{a}_2 + R_1(t)\underline{b}_1 \cdot \left(\underline{\omega}_2(t) \times R_2(t)\underline{a}_2\right)\ . \end{array}$$

With the equality

$$\underline{a} \cdot (\underline{b} \times \underline{c}) = \underline{c} \cdot (\underline{a} \times \underline{b}) \ , \ \forall \underline{a}, \underline{b}, \underline{c} \in \mathbb{R}^3 \ ,$$

it holds

$$\left[\underline{0}^\top \ , \ (R_1(t)\underline{b}_1)^\top \cdot \widetilde{R_2(t)\underline{a}_2} \ , \ \underline{0}^\top \ , \ -(R_1(t)\underline{b}_1)^\top \cdot \widetilde{R_2(t)\underline{a}_2} \right] \ \underline{v}(t) = 0 \ .$$

This holds analogously for the second rotational constraint with the vector $\underline{c}_1$. In total, the implicit constraint matrix is

$$G(\underline{x}) = \begin{bmatrix} -I & \widetilde{R_1(t)\ \underline{p}_1} & I & -\widetilde{R_2(t)\ \underline{p}_2} \\ \underline{0}^\top & (R_1(t)\underline{b}_1)^\top \cdot \widetilde{R_2(t)\underline{a}_2} & \underline{0}^\top & -(R_1(t)\underline{b}_1)^\top \cdot \widetilde{R_2(t)\underline{a}_2} \\ \underline{0}^\top & (R_1(t)\underline{c}_1)^\top \cdot \widetilde{R_2(t)\underline{a}_2} & \underline{0}^\top & -(R_1(t)\underline{c}_1)^\top \cdot \widetilde{R_2(t)\underline{a}_2} \end{bmatrix} \in \mathbb{R}^{5\times 6} \ .$$

A.2. Spherical joint

The spherical joint is very much like the revolute joint. The only difference is that any rotation with respect to the point of articulation is allowed. Therefore the two rotational constraints are omitted and $\underline{\Phi}$ is

$$\begin{aligned} \underline{\Phi} \ : \ \mathbb{R}^{12} &\ \rightarrow\ \mathbb{R}^3 \ , \\ \underline{x} &\ \mapsto\ \left[\underline{x}_{\mathrm{t},2} + R_2(t)\ \underline{p}_2 - \left(\underline{x}_{\mathrm{t},1} + R_1(t)\ \underline{p}_1 \right) \right] \ , \\ \underline{\Phi}(\underline{x}) &\ =\ \underline{0} \ , \ \forall t \geq 0 \ . \end{aligned}$$

The manifold of admissible states for each body with respect to the other body is a sphere surface with P as its middle point. The implicit constraint matrix $G(\underline{x}(t))$ is given by the respective rows of the matrix of a revolute joint. The degree of freedom is 3.

A.3. Prismatic joint

The prismatic joint has a single degree of freedom, like the revolute joint. The rotations are locked though and the relative movement is a translation along the joint axis $\underline{a}(t)$.

The rotational lock is imposed by demanding

$$\underline{w}_1(t) - \underline{w}_2(t) - \underline{w}_0 = \underline{0} \ , \forall t \geq 0 \ ,$$

where $\underline{w}_0 = \underline{w}_1(0) - \underline{w}_2(0)$ is a constant offset registered at $t = 0$.

Let again P be the point of articulation. The coordinates in the body fixed frame are again calculated by

$$\underline{p}_i = R_i^\top(0) \left[\underline{x}_P(0) - \underline{x}_{\mathrm{t},i}(0) \right] \ , \ i \in \{1, 2\}.$$

At time $t = 0$ it holds

$$\underline{x}_{\mathrm{t},1}(0) + R_1(0)\ \underline{p}_1 = \underline{x}_{\mathrm{t},2}(0) + R_2(0)\ \underline{p}_2 \ .$$

To assure a relative translation parallel to an axis $\underline{a}$, one has to assure the parallelism of

$$\Big[\underline{x}_{\mathrm{t},1}(t) + R_1(t)\ \underline{p}_1 - \underline{x}_{\mathrm{t},2}(t) - R_2(t)\ \underline{p}_2\Big] \parallel\ \underline{a}(t)\ , \forall t \geq 0\ ,$$

or the orthogonality to the plane orthogonal to $\underline{a}(t)$. As for the revolute joint, let this plane be spanned by $\{R_1(t)\underline{b}_1,\ R_1(t)\underline{c}_1\}$. The orthogonality criterion yields two scalar constraint equations

$$\left.\begin{array}{rcl} \Big[\underline{x}_{\mathrm{t},1}(t) + R_1(t)\ \underline{p}_1 - \underline{x}_{\mathrm{t},2}(t) - R_2(t)\ \underline{p}_2\Big] \cdot R_1(t)\underline{b}_1 & = & 0\ , \\ \Big[\underline{x}_{\mathrm{t},1}(t) + R_1(t)\ \underline{p}_1 - \underline{x}_{\mathrm{t},2}(t) - R_2(t)\ \underline{p}_2\Big] \cdot R_1(t)\underline{c}_1 & = & 0\ , \end{array}\right. \forall t \geq 0\ .$$

The implicit constraints are therefore given by

$$\begin{array}{rcl} \underline{\Phi}\ :\ \mathbb{R}^{12} & \to & \mathbb{R}^5\ , \\ \underline{x} & \mapsto & \begin{bmatrix} \underline{w}_1(t) - \underline{w}_2(t) - \underline{w}_0 \\ \Big[\underline{x}_{\mathrm{t},1}(t) + R_1(t)\ \underline{p}_1 - \underline{x}_{\mathrm{t},2}(t) - R_2(t)\ \underline{p}_2\Big] \cdot R_1(t)\underline{b}_1 \\ \Big[\underline{x}_{\mathrm{t},1}(t) + R_1(t)\ \underline{p}_1 - \underline{x}_{\mathrm{t},2}(t) - R_2(t)\ \underline{p}_2\Big] \cdot R_1(t)\underline{c}_1 \end{bmatrix}\ , \\ \underline{\Phi}(\underline{x}) & = & \underline{0}\ ,\ \forall t \geq 0\ . \end{array}$$

The manifold of admissible states is a one-dimensional, straight line at time t in direction $\underline{a}(t)$.

The implicit constraint matrix can be calculated using the same rules as for the revolute joint. The only new step is the use of the Dynamic Kardan Equation 1.2, since the derivatives of $\underline{w}_i(t)$ appear directly. The technical steps of the differentiation are omitted now. It holds

$$\begin{array}{rcl} G(\underline{x}) & = & \left[\begin{array}{ccc} & K_1(t) & \\ (R_1(t)\underline{b}_1)^\top & (R_1(t)\underline{b}_1 \times \underline{d}(t))^\top & \dots \\ (R_1(t)\underline{c}_1)^\top & (R_1(t)\underline{c}_1 \times \underline{d}(t))^\top & \end{array}\right. \\ & & \left.\begin{array}{ccc} & & -K_2(t) \\ \dots & -(R_1(t)\underline{b}_1)^\top & -\Big(R_2(t)\underline{p}_2 \times R_1(t)\underline{b}_1\Big)^\top \\ & -(R_1(t)\underline{c}_1)^\top & -\Big(R_2(t)\underline{p}_2 \times R_1(t)\underline{c}_1\Big)^\top \end{array}\right] \in \mathbb{R}^{5\times 6}\ , \end{array}$$

where

$$\underline{d}(t) = \underline{x}_{\mathrm{t},1}(t) - \underline{x}_{\mathrm{t},2}(t) - R_2(t)\underline{p}_2\ .$$

B. Numerical and analytical treatment of the 1-D Yukawa equation

Consider the second order differential equation

$$-\rho_1 u''(t) + \rho_0 u(t) = f(t) \ , \ t \in E := (t_0, t_1) \ , \ \rho_0, \rho_1 > 0 \ , \tag{B.1}$$

with arbitrary boundary conditions for now. Let $u(t)$ be an element of the Sobolev space $\mathcal{H}^1(E)$ and let $v(t) \in \mathcal{H}^1(E)$ be an arbitrary test function. It holds

$$\begin{aligned} -\rho_1 \int_{t_0}^{t_1} u''(t)\ v(t)\ \mathrm{dt} + \rho_0 \int_{t_0}^{t_1} u(t)\ v(t)\ \mathrm{dt} &= \int_{t_0}^{t_1} f(t)\ v(t)\ \mathrm{dt} \ , \\ \rho_1 \int_{t_0}^{t_1} u'(t)\ v'(t)\ \mathrm{dt} - \rho_1 \left[u'(t)\ v(t)\right]_{t_0}^{t_1} + \rho_0 \int_{t_0}^{t_1} u(t)\ v(t)\ \mathrm{dt} &= \int_{t_0}^{t_1} f(t)\ v(t)\ \mathrm{dt} \ . \end{aligned} \tag{B.2}$$

Define the bilinear form

$$\begin{aligned} a(u,v) : \mathcal{H}^1(E) \times \mathcal{H}^1(E) &\to \mathbb{R} \ , \\ (u,v) &\mapsto \rho_1 \int_{t_0}^{t_1} u'(t)\ v'(t)\ \mathrm{dt} + \rho_0 \int_{t_0}^{t_1} u(t)\ v(t)\ \mathrm{dt} \ . \end{aligned} \tag{B.3}$$

$a(u,v)$ is bounded, since

$$\begin{aligned} |a(u,v)| &\leq \max\{\rho_0,\rho_1\} \left(\|u'\|_{\mathcal{L}^2(E)}\|v'\|_{\mathcal{L}^2(E)} + \|u\|_{\mathcal{L}^2(E)}\|v\|_{\mathcal{L}^2(E)}\right) \\ &\leq \max\{\rho_0,\rho_1\} \left(\|u'\|_{\mathcal{L}^2(E)} + \|u\|_{\mathcal{L}^2(E)}\right) \left(\|v'\|_{\mathcal{L}^2(E)} + \|v\|_{\mathcal{L}^2(E)}\right) \\ &= \max\{\rho_0,\rho_1\} \|u\|_{\mathcal{H}^1(E)} \|v\|_{\mathcal{H}^1(E)} \ , \end{aligned}$$

and coercive, since

$$|a(u,u)| \geq \min\{\rho_0,\rho_1\} \|u\|_{\mathcal{H}^1(E)} \ .$$

The functional

$$F(v) := \int_{t_0}^{t_1} f(t)\ v(t)\ \mathrm{dt} \tag{B.4}$$

is likewise linear and bounded, if the function $f(t)$ is bounded. After defining the boundary conditions and, if necessary, restricting the trial and test space, the *Lax-Milgram lemma* assures unique solvability. For a finite-dimensional approximation

$u_h(t)$, *Céa's lemma* yields the quasi-optimality of the approximation

$$\|u - u_h\|_{\mathcal{H}^1(E)} \leq \frac{\max\{\rho_0, \rho_1\}}{\min\{\rho_0, \rho_1\}} \, v_h \overset{\inf}{\in} V_h \, \|u - v_h\|_{\mathcal{H}^1(E)} \ ,$$

where V_h is the respective discrete test space. An optimal error coefficient is therefore reached if $\rho_0 = \rho_1$.

B.1. Discretization with second-order B-Splines

For the interval $E_k = [t_k, t_{k+1}]$, with $h_k = t_{k+1} - t_k$, consider the nodes in Figure B.1. The interval is extended by $\frac{h_k}{4}$ in both directions in order to include more splines, such that non-zero values are possible at the interval ends. There are 9 nodes in total and they are enumerated from left to right, i.e. $t_0 = t_k - \frac{h_k}{4}$ to $t_8 = t_{k+1} + \frac{h_k}{4}$

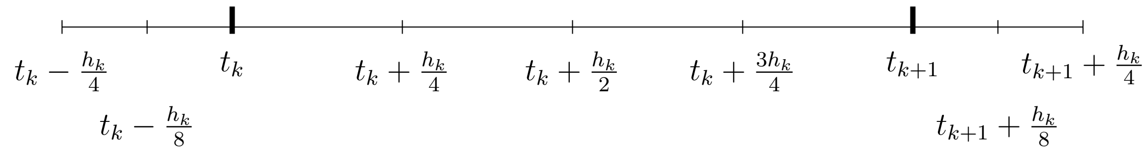

Figure B.1.: Interval discretization.

Zero-order B-splines are defined by

$$S_{i,0;h_k} = \begin{cases} 1 & ,t \in [t_i \ t_{i+1}) \ , \\ 0 & , \text{ else,} \end{cases} \tag{B.5}$$

for $i \in \{0, \dots, 7\}$. There are 8 splines, one for each subinterval and together they form a decomposition of unity on the extended interval.

Second-order B-splines can be calculated by using the recursion formula [14, Def. 11.14 and following], i.e.

$$S_{i,k;h_k}(t) = \frac{t - t_i}{t_{i+k} - t_i} \ S_{i,k-1;h_k} + \frac{t_{i+k+1} - t}{t_{i+k+1} - t_{i+1}} \ S_{i+1,k-1;h_k}(t) \ . \tag{B.6}$$

Figure B.2 shows the in total 6 functions, which are second-order polynomials on each subinterval.

It can be shown, that the derivatives of the splines fulfil the recursion given by

$$\frac{\mathrm{d}}{\mathrm{dt}} S_{i,k;h_k}(t) = \frac{k}{t_{i+k} - t_i} S_{i,k-1;h_k} - \frac{k}{t_{i+k+1} - t_{i+1}} S_{i+1,k-1;h}(t) \ . \tag{B.7}$$

As preparation for a more efficient, consecutive *FE method*, a transformation of the splines onto a normed interval is necessary.

It is evident by insertion, that a translation of the interval along the real axis does not change the shape of the spline functions. The same set of B-Splines is obtained on the interval given in Figure (B.3).

The set of nodes

$$K := \{0, \frac{1}{8}, \frac{1}{4}, \frac{1}{2}, \frac{3}{4}, 1, \frac{5}{4}, \frac{11}{8}, \frac{3}{2}\} \ , \tag{B.8}$$

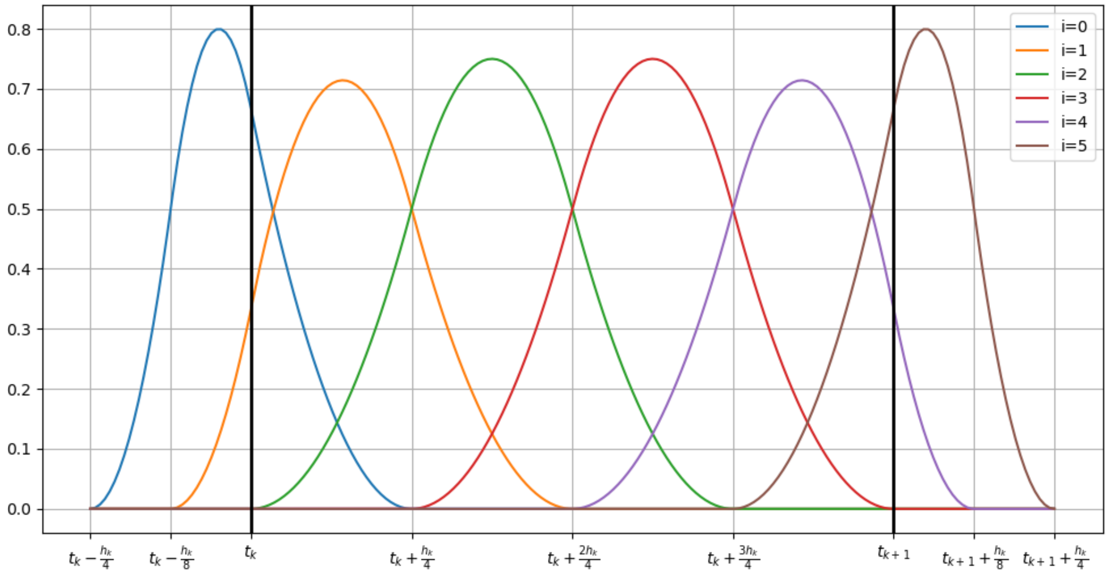

Figure B.2.: Second-order B-Splines on the the extended interval.

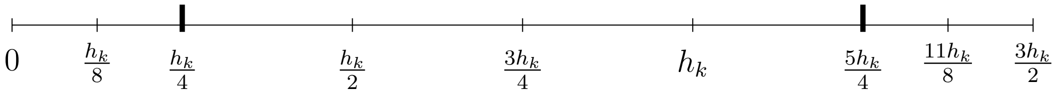

Figure B.3.: Interval discretization.

can span any such interval by scaling. Let $S_{i,2}(t)$ denote the second-order B-Splines based on the set K and let $S_{i,2;h_k}(t)$ denote those based on the scaled nodes. Using the recursion formula (B.6) it can be shown by insertion that

$$S_{i,2;h_k}(h_k\ t) = S_{i,2}(t)\ . \tag{B.9}$$

Using (B.7) and (B.9) it can be shown for the derivatives, that

$$S'_{i,2;h_k}(h_k\ t) = \frac{1}{h_k} S'_{i,2}(t)\ . \tag{B.10}$$

B.2. The homogeneous Neumann problem

Consider equation (B.1) on the shifted interval $E_k = \left(\frac{h_k}{4}, \frac{5h_k}{4}\right)$ with homogeneous Neumann boundary values, i.e.

$$u'(\frac{h_k}{4}) = u'(\frac{5h_k}{4}) = 0\ . \tag{B.11}$$

The boundary terms in the variational formulation (B.2) can be dropped now. This leads to

$$\rho_1 \int\limits_{\frac{h_k}{4}}^{\frac{5h_k}{4}} u'(t)\ v'(t)\ \mathrm{dt} + \rho_0 \int\limits_{\frac{h_k}{4}}^{\frac{5h_k}{4}} u(t)\ v(t)\ \mathrm{dt} = \int\limits_{\frac{h_k}{4}}^{\frac{5h_k}{4}} f(t)\ v(t)\ \mathrm{dt}\ , \tag{B.12}$$

where $u, v \in \mathcal{H}^1(E_k)$. Consider the space

$$S^{h_k} = \mathrm{span}\{S_{i,2;h_k}(t)\}_{i=0}^{5} \subset \mathcal{H}^1(E_k) \tag{B.13}$$

as trial and test space, where the splines are restricted to the respective subintervals. Let $u_{h_k}(t) \in S^{h_k}$ be the discrete trial function represented by

$$u_{h_k}(t) = \sum_{j=0}^{5} u_j \; S_{j,2;h_k}(t) \ , \ u_j \in \mathbb{R} \ . \tag{B.14}$$

For the test function $S_{i,2;h_k}(t)$, $i \in \{0, \dots, 5\}$, it holds

$$a(u_{h_k}, S_{i,2;h_k}) = \sum_{j=0}^{5} u_j \; a(S_{j,2;h_k}, S_{i,2;h_k}) = F(S_{i,2;h_k})$$

Considering this equation for each $i \in \{0, \dots, 5\}$ leads to the solvable FE system

$$A_{h_k} \; \underline{u} = \underline{f}_{h_k} \ , \tag{B.15}$$

where $A \in \mathbb{R}^{6\times 6}$ and $\underline{f} \in \mathbb{R}^6$. Their entries are calculated by

$$\begin{aligned} A_{i,j;h_k} &= a(S_{j,2;h_k}, S_{i,2;h_k}) \ , \\ f_{i;h_k} &= F(S_{i,2;h_k}) \ . \end{aligned}$$

The matrix A_{h_k} is symmetric, since the bilinear from a is symmetric too. Figure B.2 shows further, that the splines have an overlapping domain only with the next 2 and previous 2 splines in their order. Therefore A_{h_k} is also a banded matrix with band width 5 and it is necessary to calculate only 15 out of 36 entries. A single entry is given by

$$a(S_{j,2;h_k}, S_{i,2;h_k}) = \rho_1 \int\limits_{\frac{h_k}{4}}^{\frac{5h_k}{4}} S'_{j,2;h_k}(\widetilde{t}) \; S'_{i,2;h_k}(\widetilde{t}) \; \mathrm{d}\widetilde{t} + \rho_0 \int\limits_{\frac{h_k}{4}}^{\frac{5h_k}{4}} S_{j,2;h_k}(\widetilde{t}) \; S_{i,2;h_k}(\widetilde{t}) \; \mathrm{d}\widetilde{t} \ .$$

With the interval scaling $\widetilde{t} = h_k t$, the rule of integration by substitution and the relations (B.9) and (B.10) it holds further

$$\begin{aligned} A_{i,j;h_k} &= \rho_1 \int\limits_{\frac{h_k}{4}}^{\frac{5h_k}{4}} S'_{j,2;h_k}(\widetilde{t}) \; S'_{i,2;h_k}(\widetilde{t}) \; \mathrm{d}\widetilde{t} + \rho_0 \int\limits_{\frac{h_k}{4}}^{\frac{5h_k}{4}} S_{j,2;h_k}(\widetilde{t}) \; S_{i,2;h_k}(\widetilde{t}) \; \mathrm{d}\widetilde{t} \\ &= \rho_1 \int\limits_{\frac{1}{4}}^{\frac{5}{4}} S'_{j,2;h_k}(h_k t) \; S'_{i,2;h_k}(h_k t) \; h_k \mathrm{d}t + \rho_0 \int\limits_{\frac{1}{4}}^{\frac{5}{4}} S_{j,2;h_k}(h_k t) \; S_{i,2;h_k}(h_k t) \; h_k \mathrm{d}t \\ &= \rho_1 \int\limits_{\frac{1}{4}}^{\frac{5}{4}} \frac{1}{h_k^2} S'_{j,2}(t) \; S'_{i,2}(t) \; h_k \mathrm{d}t + \rho_0 \int\limits_{\frac{1}{4}}^{\frac{5}{4}} S_{j,2}(t) \; S_{i,2}(t) \; h_k \mathrm{d}t \\ &= \rho_1 \frac{1}{h_k} \int\limits_{\frac{1}{4}}^{\frac{5}{4}} S'_{j,2}(t) \; S'_{i,2}(t) \; \mathrm{d}t + \rho_0 \; h_k \int\limits_{\frac{1}{4}}^{\frac{5}{4}} S_{j,2}(t) \; S_{i,2}(t) \; \mathrm{d}t \\ &=: \rho_1 \frac{1}{h_k} \; B_{i,j} + \rho_0 \; h_k \; C_{i,j} \ . \end{aligned}$$

The matrix A_{h_k} can therefore be split into two parts

$$A_{h_k} = \rho_1 \frac{1}{h_k}\ B + \rho_0\ h_k\ C\ , \tag{B.16}$$

where B and C are constant matrices independent of h_k. This simplifies the calculation of A_{h_k} for each h_k significantly, since B and C have to be calculated only once.

B.2.1. The analytic approach and the fundamental solution

The task is to find $u(t)$ such that

$$\begin{aligned} L\left[u\right](t) &= -\rho_1 u''(t) + \rho_0 u(t) = f(t)\ , \\ u'(t_0) &= u'(t_1) = 0\ . \end{aligned} \tag{B.17}$$

Choose test functions $v(t) \in \mathcal{H}^1(t_0, t_1)$, multiply the left-hand side of the equation with them and integrate by parts

$$\begin{aligned} \int\limits_{t_0}^{t_1} L\left[u\right]\ v\ \mathrm{dt} &= \int\limits_{t_0}^{t_1} \rho_1 u'\ v' + \rho_0 u\ v\ \mathrm{dt} - \left[\rho_1 u'\ v\right]_{t_0}^{t_1} \\ &= \int\limits_{t_0}^{t_1} -\rho_1 u\ v'' + \rho_0 u\ v\ \mathrm{dt} - \left[\rho_1 u'\ v\right]_{t_0}^{t_1} + \left[\rho_1 u\ v'\right]_{t_0}^{t_1}\ , \end{aligned}$$

$$\int\limits_{t_0}^{t_1} L\left[u\right]\ v\ \mathrm{dt}\ +\ \left[\rho_1 u'\ v\right]_{t_0}^{t_1} = \int\limits_{t_0}^{t_1} L^*\left[v\right]\ u\ \mathrm{dt} + \left[\rho_1 u\ v'\right]_{t_0}^{t_1}\ ,$$

$$\int\limits_{t_0}^{t_1} f\ v\ \mathrm{dt}\ +\ \left[\rho_1 u'\ v\right]_{t_0}^{t_1} = \int\limits_{t_0}^{t_1} L^*\left[v\right]\ u\ \mathrm{dt} + \left[\rho_1 u\ v'\right]_{t_0}^{t_1}\ , \tag{B.18}$$

where $L = L^*$ is self-adjoint.

Let $w_1(t)$ and $w_2(t)$ be the fundamental solutions of $L^*\left[v\right] = 0$. The test functions fulfil $L^*\left[v\right] = 0$, since they are a linear combination of those solutions.

In order to find an analytical solution, we split the interval such that $t_0 < s < t_1$.

First interval: $E_1 = [t_0, s\ )$

Define

$$v_0(t, s) = c_1^0(s)\ w_1(t) + c_2^0(s)\ w_2(t)\ ,$$

for $\widehat{t} \in E_1$, and let it fulfil the initial condition

$$\frac{\mathrm{d}}{\mathrm{dt}} v_0(t, s)|_{t=t_0} = 0\ .$$

Using v_0 as a test function in Equation (B.18) with the limits of E_1 leads to

$$\int\limits_{t_0}^{t} f(s)\ v_0(t, s)\ \mathrm{ds} + \rho_1 u'(t)\ v_0(t, t) = \rho_1 u(t)\ \frac{\mathrm{d}}{\mathrm{dt}} v_0(t, s)|_{s=t}\ . \tag{B.19}$$

Second interval: $E_2 = (s, t_1\ ]$
Define

$$v_1(t,s) = c_1^1(s)\ w_1(t) + c_2^1(s)\ w_2(t)\ ,$$

for $\widehat{t} \in E_2$, and let it fulfil the terminal condition

$$\frac{\mathrm{d}}{\mathrm{dt}} v_1(t,s)|_{t=t_1} = 0\ .$$

Using v_1 as a test function in Equation (B.18) with the limits of E_2 leads to

$$\int\limits_{t}^{t_1} f(s)\ v_1(t,s)\ \mathrm{ds} - \rho_1 u'(t)\ v_1(t,t) = -\rho_1 u(t)\ \frac{\mathrm{d}}{\mathrm{dt}} v_1(t,s)|_{s=t}\ . \qquad \text{(B.20)}$$

Adding (B.20) to (B.19) leads to

$$\begin{aligned}\int\limits_{t_0}^{t} f(s)\ v_0(t,s)\ \mathrm{ds}\ \ &+ \int\limits_{t}^{t_1} f(s)\ v_1(t,s)\ \mathrm{ds} + \rho_1 u'(t)\ \ [v_0(t,t) - v_1(t,t)] = \\ &= \rho_1 u(t)\ \left[\frac{\mathrm{d}}{\mathrm{dt}} v_0(t,s)|_{s=t} - \frac{\mathrm{d}}{\mathrm{dt}} v_1(t,s)|_{s=t}\right]\ .\end{aligned}$$

Assuming

$$\begin{aligned} v_0(t,t) &= v_1(t,t)\ , && \text{(B.21)} \\ \frac{\mathrm{d}}{\mathrm{dt}} v_0(t,s)|_{t=s} - \frac{\mathrm{d}}{\mathrm{dt}} v_1(t,s)|_{t=s} &= \frac{1}{\rho_1}\ , && \text{(B.22)} \end{aligned}$$

one obtains

$$u(t) = \int\limits_{t_0}^{t_1} f(s)\ G(t,s)\ \mathrm{ds}\ , \qquad \text{(B.23)}$$

where

$$G(t,s) := \begin{cases} v_0(t,s) & t \in E_1\ , \\ v_1(t,s) & t \in E_2\ , \end{cases} \qquad \text{(B.24)}$$

is called *Green function.* In order to find v_0 and v_1, consider the equation for $t \neq s$

$$\begin{aligned} L^*[v] &= 0\ , \\ -v''(t) + \frac{\rho_0}{\rho_1} v(t) &= 0\ . \end{aligned}$$

With $r^2 := \dfrac{\rho_0}{\rho_1}$, the fundamental solutions are given by

$$\begin{aligned} w_1(t) &= e^{rt}\ , \\ w_2(t) &= e^{-rt}\ . \end{aligned} \qquad \text{(B.25)}$$

By using (B.21), (B.22) and the boundary conditions for v_0 and v_1, the coefficients $c_1^0(s)$, $c_2^0(s)$, $c_1^1(s)$ and $c_2^1(s)$ can be obtained. The boundary conditions

$$\begin{aligned} 0 = \frac{\mathrm{d}}{\mathrm{dt}} v_0(t,s)|_{t=t_0} &= r\ c_1^0(s) w_1(t_0) - r c_2^0(s) w_2(t_0)\ , \\ 0 = \frac{\mathrm{d}}{\mathrm{dt}} v_1(t,s)|_{t=t_1} &= r\ c_1^1(s) w_1(t_1) - r c_2^1(s) w_2(t_1)\ , \end{aligned}$$

lead to the equations

$$\begin{aligned} c_2^0(s) &= e^{2rt_0} c_1^0(s)\ , && \text{(B.26)} \\ c_2^1(s) &= e^{2rt_1} c_1^1(s)\ , && \text{(B.27)} \end{aligned}$$

and the assumptions (B.21) and (B.22) yield

$$c_1^0(s)\ w_1(s) + c_2^0(t)\ w_2(s) = c_1^1(s)\ w_1(s) + c_2^1(s)\ w_2(s) \qquad \text{(B.28)}$$

$$c_1^0(t)\ w_1(s) - c_2^0(t)\ w_2(s) - c_1^1(s)\ w_1(s) + c_2^1(s)\ w_2(s) = \frac{1}{\rho_1\ r} \qquad \text{(B.29)}$$

Inserting (B.26) and (B.27) into (B.28) and (B.29) and using the definition of the fundamental solutions leads to

$$\begin{aligned} c_1^0(s)\left[e^{rs} + e^{r(2t_0-s)}\right] &= c_1^1(s)\left[e^{rs} + e^{r(2t_1-s)}\right] && \text{(B.30)} \\ c_1^0(s)\left[e^{rs} - e^{r(2t_0-s)}\right] - c_1^1\left[e^{rs} - e^{r(2t_1-s)}\right] &= \frac{1}{\rho_1\ r} && \text{(B.31)} \end{aligned}$$

Substituting c_1^1 in (B.31) with the help of (B.30) leads to

$$c_1^0(s) = \frac{1}{\rho_1\ r} \frac{1}{e^{rs} - e^{r(2t_0-s)} - \left[e^{rs} + e^{r(2t_0-s)}\right] \dfrac{e^{rs} - e^{r(2t_1-s)}}{e^{rs} + e^{r(2t_1-s)}}} \qquad \text{(B.32)}$$

Using (B.26), (B.27) and (B.30) leads finally to

$$G(t,s) := \begin{cases} c_1^0(s)\left[e^{rt} + e^{r(2t_0-t)}\right] & t \in E_1\ , \\ c_1^0(s) \dfrac{e^{rs} + e^{r(2t_0-s)}}{e^{rs} + e^{r(2t_1-s)}} \left[e^{rt} + e^{r(2t_1-t))}\right] & t \in E_2\ . \end{cases} \qquad \text{(B.33)}$$

Since the Green functions turns out to be very complex, the integral (B.23) has to be approximated numerically. Due to this circumstance, one can solve equation (B.17) numerically as seen in the previous section. The difference in efficiency is for small intervals and small FE systems negligible.

B.3. The mixed boundary values problem

In this section mixed boundary values for (B.1) are considered, namely a Dirichlet condition as initial value and a Neumann condition as terminal value

$$u(\frac{h_k}{4}) = u_d \ , \ u'(\frac{5h_k}{4}) = 0 \ . \tag{B.34}$$

In contrast to the previous section, the boundary terms in the variational formulation (B.2) have to be taken care of. Since $u'(\frac{h_k}{4})$ is unknown, restrict the test space to

$$\mathcal{H}^1_{0,}(E_k) = \{v(t) \in \mathcal{H}^1(E_k) \mid v(\frac{h_k}{4}) = 0\} \subset \mathcal{H}^1 \ . \tag{B.35}$$

In order to take the Dirichlet data into account, decompose the solution into two parts

$$u(t) = u_0(t) + u_D(t) \ ,$$

where $u_0(t) \in \mathcal{H}^1_{0,}(E_k)$ is the solution to the problem with homogeneous Dirichlet data and $u_D(t)$ is an extension of the boundary value onto E_k. This leads to the following variational equation

$$\begin{aligned} a(u,v) &= a(u_0,v) + a(u_D,v) = F(v) \ , \\ a(u_0,v) &= \widetilde{F}(v) := F(v) - a(u_D,v) \ , \end{aligned} \tag{B.36}$$

where $u_0, v \in \mathcal{H}^1_{0,}(E_k)$.

When using the same discretization as in Sections B.1 and B.2, it is possible to split the 6 splines into two groups. $S_{0,2;h_k}(t)$ and $S_{1,2;h_k}(t)$ can be used to extend the Dirichlet data onto E_k. Like for the Neumann problem, the splines are restricted to the subintervals inside $\left[\frac{h_k}{4}, \frac{5hk}{4}\right]$. $u_D(t)$ is now of the form

$$u_D(t) = c_0 \ S_{0,2;h_k}(t) + c_1 \ S_{1,2;h_k}(t) \ . \tag{B.37}$$

Setting $c_1 = u_d$ and considering the interpolation condition

$$u_d = c_0 \ S_{0,2;h_k}(\frac{h_k}{4}) + c_1 \ S_{1,2;h_k}(\frac{h_k}{4}) \ ,$$

yields

$$c_0 = u_d \frac{1 - S_{1,2;h_k}(\frac{h_k}{4})}{S_{0,2;h_k}(\frac{h_k}{4})} \ .$$

The remaining 4 splines $\{S_{i,2;h_k}(t)\}_{i=2}^5$ span a finite dimensional subspace of $\mathcal{H}^1_{0,}(E_k)$ and can be used to approximate the solution of (B.36).

The discrete FE system

$$\hat{A}_{h_k}\underline{u} = \underline{\hat{f}}_{h_k} \tag{B.38}$$

consists of parts of the Neumann FE system (B.15). Keeping in mind, that the first two splines are excluded from the trial and test spaces, it holds

$$\hat{A}_{i,j;h_k} = A_{i+2,j+2;h_k} \ , \ i,j \in \{0,\dots,3\} \ , \tag{B.39}$$

where $A_{i,j}$ is calculated as in Section B.2. Since the Dirichlet extension is of the form (B.37), the values $a(u_D, S_{i,2;h_k})$ are also calculated with the help of $A_{i,j;h_k}$ and it holds

$$\hat{f}_{i;h_k} = f_{i;h_k} - c_0 \ A_{i+2,0;h_k} - c_1 \ A_{i+2,1;h_k} \ , \ i \in \{0,\dots,3\} \ . \tag{B.40}$$

System (B.38) is in total a solvable system of 4 linear equations.

Bibliography

[1] R. Altmann and J. Heiland. Simulation of multibody systems with servo constraints through optimal control. *Multibody Syst Dyn*, 40:75–98, 2017.

[2] M. Arnold, B. Burgermeister, and B. Esterl. DAE time integration for real-time applications in multi-body dynamics. *ZAMM Journal of Applied Mathematics and Mechanics*, 86:759–771, 2006.

[3] J. Baumgarte. Stabilization of constraints and integrals of motion in dynamical systems. *Computer Methods in Applied Mechanics and Engineering*, 1:1–16, 1972.

[4] W. Blajer. The use of servo-constraints in the inverse dynamics analysis of underactuated multibody systems. *Journal of Computational and Nonlinear Dynamics*, 9:041008, 2014.

[5] K. Brenan, S. Campbell, and L. Petzold. *Numerical Solution of Initial-Value problems in Differential-Algebraic Equations.* SIAM, Philadelphia, 1996.

[6] A. Bryson and Y. Ho. *Applied Optimal Control: optimization, estimation, and control.* Hemisphere Publishing Corporation, New York, 1975.

[7] B. Esterl. *Modulare echtzeitfähige Simulation des Fahrzeug-Mehrkörpersystems.* Dissertation, Faculty of Mechanical Engineering and Economic Sciences, Graz University of Technology, 2011.

[8] E. Hairer, M. Roche, and C. Lubich. *The Numerical Solution of Differential-Algebraic Systems by Runge-Kutta Methods.* Springer, Berlin-Heidelberg, 1989.

[9] E. Hairer and G. Wanner. *Solving Ordinary Differential Equations II.* Springer, Berlin-Heidelberg, 1996.

[10] A. Kecskemethy. *Objektorientierte Modellierung der Dynamik von Mehrkörpersystemen mit Hilfe von Übertragungselementen.* Dissertation, Universities of Stuttgart and Duisburg, 1993.

[11] C. Lanczos. *The variational principles of mechanics.* University of Toronto Press, Toronto and Buffalo, 1970.

[12] V. Lipovac. *Modular, computer-based multibody systems.* Seminar, Institute for Applied Mathematics, Graz University of Technology, 2019.

[13] V. Lipovac. *Numerical treatment of open multibody systems.* Project, Institute for Applied Mathematics, Graz University of Technology, 2019.

[14] R. Schaback and H. Wendland. *Numerische Mathematik.* Springer, Berlin - Heidelberg, 2005.

[15] W. Schiehlen. *Technische Dynamik.* Springer Vieweg, Wiesbaden, 2017.

[16] D. Schramm, M. Hiller, and R. Bardini. *Modellbildung und Simulation der Dynamik von Kraftfahrzeugen.* Springer Vieweg, Berlin - Heidelberg, 2018.

[17] A. Shabana and H. Carsten. *Einführung in die Mehrkörpersimulation.* John Wiley and Sons, New Jersey, 2016.

[18] K. Strehmel et al. *Numerik gewöhnlicher Differentialgleichungen.* Springer Spektrum, Wiesbaden, 2012.

[19] J. Wallner and J. Behrndt. *Advanced Analysis.* Lecture, Graz University of Technology, 2017.

[20] C. Woernle. *Mehrkörpersysteme.* Springer, Berlin-Heidelberg, 2011.

Affidavit

I declare that I have authored this thesis independently, that I have not used other than the declared sources/resources, and that I have explicitely indicated all material which has been quoted either literally or by content from the sources used. The text document uploaded to TUGRAZonline is identical to the present master‘s thesis.

Date

Signature